A Template Tutorial: Panels, Families, Clones, Winners and Losers

C. A. Felippa

Publication CIMNE Nº-219, September 2002

A Template Tutorial: Panels, Families, Clones, Winners and Losers

C.A. Felippa

Publication CIMNE Nº-219, September 2002

International Center for Numerical Methods in Engineering
Gran Capitán s/n, 08034 Barcelona, Spain

TABLE OF CONTENTS

A Template Tutorial: Panels, Families, Clones, Winners and Losers

CARLOS A. FELIPPA

Department of Aerospace Engineering Sciences
and Center for Aerospace Structures
University of Colorado
Boulder, Colorado 80309-0429, USA

Abstract

The article has a dual historical and educational theme. It is a tutorial on finite element templates for two-dimensional structural problems. The exposition focuses on the four-node plane stress element of flat rectangular geometry, called here the "rectangular panel" for brevity. This is one of the two oldest two-dimensional structural elements, soon to reach its gold anniversary. On the other hand the concept of finite element templates is a recent development. Interweaving the old and the new throws historical perspective into the "golden age" of discovery of finite elements. Templates provide a framework in which diverse element development methods can be fitted, compared and traced back to the sources. On the technical side templates have the virtue of facilitating the unified implementation of element families as well as the construction of custom elements. As an illustration of customization power, the Appendix presents the construction of a four noded bending optimal trapezoid that has eluded FEM investigators for several decades.

El agua es como un espejo en que desfilan las imágenes del pasado.
Ricardo Güiraldes, Don Segundo Sombra (1926)

Keywords: finite elements; history; templates; instances; clones; inplane bending; optimality; quadrilateral; membrane; plane stress; patch test; distortion sensitivity

1. INTRODUCTION

This article has a dual theme: historical and educational. To serve the latter, the exposition is written as a tutorial article on two-dimensional finite element templates. Part of this material is extracted from an advanced FEM course. Templates are parametrized algebraic forms that provide a continuum of consistent and stable finite element models of a given type and node/freedom configuration. Template instances produced by setting values to parameters furnish specific elements. If the template embodies all possible consistent and stable elements of a given type, it is called universal.

Befitting the tutorial aim, the exposition centers on the simplest 2D element that possesses a nontrivial template: the four-node plane stress element of flat rectangular geometry. [The three-node linear triangle is simpler but its template is trivial.] This is called the *rectangular panel* for brevity.

The rectangular panel is interesting from both historical and instructional viewpoints because:

1. It is one of the two oldest continuum mechanical elements, the other being the linear triangle [1].
2. Along with its plane strain and axisymmetric cousins, it is the configuration treated by most new methods since the birth of finite elements. Thus it provides an *in-vivo* specimen of FEM evolution over the past 50 years.
3. It is amenable to complete analytical development, even for anisotropic material law. This makes the element particularly suitable for homework and project assignments.
4. Analytical forms make the concept of template signatures and clones highly visible to students.

The paper is organized as follows. Section 2 outlines element formulations from 1950 to date. Section 3 introduces the focus problem. Sections 4–6 follow up on the historical theme by developing stress, strain and displacement-based models for the rectangular panel.

The concept of template is introduced in Section 7 by calling attention to a common structure lurking behind the stiffness expressions of stress, strain and displacement elements. Template terminology follows as consequence of this idea: families, signatures, instances and clones. The role of higher order patch tests in optimality is illustrated in Chapters 8–9. The SRI scheme is worked out in Section 10 to show that templates naturally lead to correct splittings of the elasticity law. The concept of element families is illustrated in Section 11 using stress hybrid and displacement bubbles as examples. Section 11 provides numerical examples and Section 12 discussion and conclusions. The Appendix collects templates for more general geometries to give a glimpse into the unifying power of this concept for constructing custom elements.

2. HISTORICAL SKETCH

This section summarizes the history of structural finite elements since 1950 to date. It functions as a hub for dispersed historical references. Readers uninterested in historical aspects should skip directly to Section 3.

For exposition convenience, structural "finitelementology" may be divided into fourth generations that span 10 to 15 years each. There are no sharp intergenerational breaks but noticeable change of emphasis. The following summary does not cover the conjoint evolution of Matrix Structural Analysis into the Direct Stiffness Method from 1934 through 1970. This was the subject of a separate essay [3].

2.1. G1: The Pioneers

The 1956 paper by Turner, Clough, Martin and Topp [1], henceforth abbreviated to TCMT, is recognized as the start of the current FEM, as used in the overwhelming majority of commercial codes. Along with Argyris' serial [2] they prototype the first generation, which spans 1950 through 1962. A panoramic picture of this period is available in two textbooks [4,5]. Przemieniecki's text is still reprinted by Dover. The survey by Gallagher [6] was influential but is now difficult to access outside libraries.

The pioneers were structural engineers, schooled in classical mechanics. They followed a century of tradition in regarding structural elements as a device to transmit forces. This "element as force transducer" was the standard view in pre-computer structural analysis. It explains the use of flux assumptions to derive stiffness equations. Element developers worked in, or interacted closely with, the aircraft industry. (One reason is that only large aerospace companies were then able to afford mainframe computers.) Accordingly they focused on thin structures built up with bars, ribs, spars, stiffeners and panels. Although the Classical Force method dominated stress analysis during the 1950s, stiffness methods were kept alive by use in dynamics.

2.2. G2: The Golden Age

The next period spans the golden age of FEM: 1962–1972. This is the "variational generation." Melosh [7] showed that conforming displacement models are a form of Rayleigh-Ritz based on the minimum potential energy principle. This influential paper marks the confluence of three lines of research: Argyris' dual formulation of energy methods [2], the Direct Stiffness Method (DSM) of Turner [8–10], and early ideas of interelement compatibility as basis for error bounding and convergence [11,12]. G1 workers thought of finite elements as idealizations of structural components. From 1962 onward a two-step interpretation emerges: discrete elements approximate continuum models, which in turn approximate real structures.

By the early 1960s FEM begins to expand into Civil Engineering through Clough's Boeing-Berkeley connection [13] and had been named [14,15]. Reading de Veubeke's famous article [16] side by side with

TCMT [1] one can sense the ongoing change in perspective opened up by the variational framework. The first book devoted to FEM appears in 1967 [17]. Applications to nonstructural problems start by 1965 [18].

From 1962 onwards the displacement formulation dominates. This was given a big boost by the invention of the isoparametric formulation and related tools (numerical integration, fitted coordinates, shape functions, patch test) by Irons and coworkers [19–23]. Low order displacement models often exhibit disappointing performance. Thus there was a frenzy to develop higher order elements. Other variational formulations, notably hybrids [24–27], mixed [28,29] and equilibrium models [16] emerged. G2 can be viewed as closed by the monograph of Strang and Fix [30], the first book to focus on the mathematical foundations.

2.3. G3: Consolidation

The post-Vietnam economic doldrums are mirrored during this post-1972 period. Gone is the youthful exuberance of the golden age. This is consolidation time. Substantial effort is put into improving the stock of G2 displacement elements by tools initially labeled "variational crimes" [31], but later justified. A comprehensive exposition may be found in Hughes' textbook [32]. Hybrid and mixed formulations record steady progress [33]. Assumed strain formulations appear [34]. A booming activity in error estimation and mesh adaptivity is fostered by better understanding of the mathematical foundations [35].

Commercial FEM codes gradually gain importance. They provide a reality check on what works in the real world and what doesn't. By the mid-1980s there was gathering evidence that complex and high order elements were commercial flops. Exotic gadgetry interweaved amidst millions of lines of code easily breaks down in new releases. Complexity is particularly dangerous in nonlinear and dynamic analyses conducted by novice users. A trend back toward simplicity starts [36,37].

2.4. G4: Back to Basics

The fourth generation begins by the early 1980s. More approaches come on the scene, notably the Free Formulation [38,39], orthogonal hourglass control [40], Assumed Natural Strain methods [41–44], stress hybrid models in natural coordinates [45–47], as well as derivatives: ANDES [48,49], EAS [50,51] and others. Although technically diverse the G4 approaches share two common objectives:

(i) Elements must fit into DSM-based programs since that includes the vast majority of production codes, commercial or otherwise.

(ii) Elements are kept simple but should provide answers of engineering accuracy with relatively coarse meshes. These were collectively labeled "high performance elements" in 1989 [52].

"Things are always at their best in the beginning," said Pascal. Indeed. By now FEM looks like an aggregate of largely disconnected methods and recipes. Sections 4-6 look at three disparate components of this edifice to set up the subsequent exhibition of common features by templates.

3. PROBLEM DESCRIPTION

3.1. Governing Equations

Consider the thin homogeneous plate in plane stress sketched in Figure 1. The inplane displacements are $\{u_x, u_y\}$, the associated strains are $\{e_{xx}, e_{yy}, e_{xy}\}$ and the inplane (membrane) stresses are $\{\sigma_{xx}, \sigma_{yy}, \sigma_{xy}\}$. Prescribed inplane body forces are $\{b_x, b_y\}$, but they will be set to zero in derivations of equilibrium elements. Prescribed displacements and surface tractions are denoted by $\{\hat{u}_x, \hat{u}_y\}$ and $\{\hat{t}_x, \hat{t}_y\}$ respectively. All fields are considered uniform through the thickness h. The governing plane-stress elasticity equations

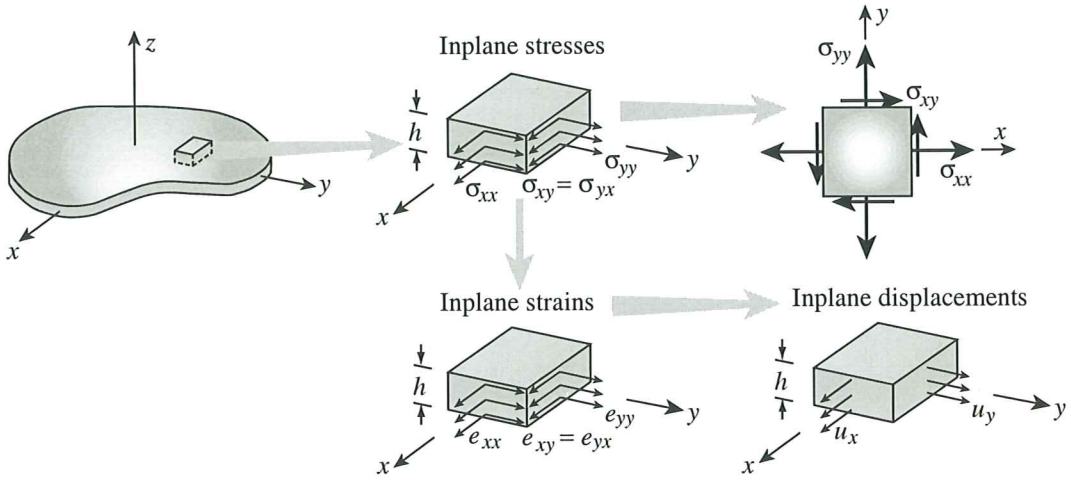

Figure 1. A thin plate in plane stress, illustrating notation.

are

$$\begin{bmatrix} e_{xx} \\ e_{yy} \\ 2e_{xy} \end{bmatrix} = \begin{bmatrix} \partial/\partial x & 0 \\ 0 & \partial/\partial y \\ \partial/\partial y & \partial/\partial x \end{bmatrix} \begin{bmatrix} u_x \\ u_y \end{bmatrix}, \qquad \begin{bmatrix} \sigma_{xx} \\ \sigma_{yy} \\ \sigma_{xy} \end{bmatrix} = \begin{bmatrix} E_{11} & E_{12} & E_{13} \\ E_{12} & E_{22} & E_{23} \\ E_{13} & E_{23} & E_{33} \end{bmatrix} \begin{bmatrix} e_{xx} \\ e_{yy} \\ 2e_{xy} \end{bmatrix},$$
$$\begin{bmatrix} \partial/\partial x & 0 & \partial/\partial y \\ 0 & \partial/\partial y & \partial/\partial x \end{bmatrix} \begin{bmatrix} \sigma_{xx} \\ \sigma_{yy} \\ \sigma_{xy} \end{bmatrix} + \begin{bmatrix} b_x \\ b_y \end{bmatrix} = \begin{bmatrix} 0 \\ 0 \end{bmatrix}. \tag{1}$$

The compact matrix version of (1) is

$$\mathbf{e} = \mathbf{D}\mathbf{u}, \qquad \sigma = \mathbf{E}\mathbf{e}, \qquad \mathbf{D}^T\sigma + \mathbf{b} = \mathbf{0}, \tag{2}$$

in which $\mathbf{E}$ is the plane stress elasticity matrix. The inverse of $\sigma = \mathbf{E}\mathbf{e}$ is

$$\begin{bmatrix} e_{xx} \\ e_{yy} \\ 2e_{xy} \end{bmatrix} = \begin{bmatrix} C_{11} & C_{12} & C_{13} \\ C_{12} & C_{22} & C_{23} \\ C_{13} & C_{23} & C_{33} \end{bmatrix} \begin{bmatrix} \sigma_{xx} \\ \sigma_{yy} \\ \sigma_{xy} \end{bmatrix}, \quad \text{or} \quad \mathbf{e} = \mathbf{C}\sigma, \tag{3}$$

where $\mathbf{C} = \mathbf{E}^{-1}$ is the matrix of elastic compliances.

3.2. The Rectangular Panel

The focus of this article, called the "rectangular panel," is shown in Figure 2. For an individual element the side-aligned local axes are also denoted as $\{x, y\}$ for brevity. The inplane dimensions are a and $b = a/\gamma$, where $\gamma = a/b$ is the aspect ratio. The thickness and elastic properties are constant over the element. The element has 4 corner nodes and 8 external (connective) degrees of freedom. The node displacement and force vectors are configured as

$$\mathbf{u} = [\, u_{x1} \quad u_{y1} \quad u_{x2} \quad u_{y2} \quad u_{x3} \quad u_{y3} \quad u_{x4} \quad u_{y4} \,]^T, \tag{4}$$

$$\mathbf{f} = [\, f_{x1} \quad f_{y1} \quad f_{x2} \quad f_{y2} \quad f_{x3} \quad f_{y3} \quad f_{x4} \quad f_{y4} \,]^T. \tag{5}$$

As noted in the Introduction most of the FEM formulation methods chronicled in Section 2 have been tried on this configuration as well as its plane strain and axisymmetric cousins. The reason for this popularity is that the rectangular panel is the *simplest multidimensional element that can be improved.* (The three-node linear triangle is simpler but cannot be improved.)

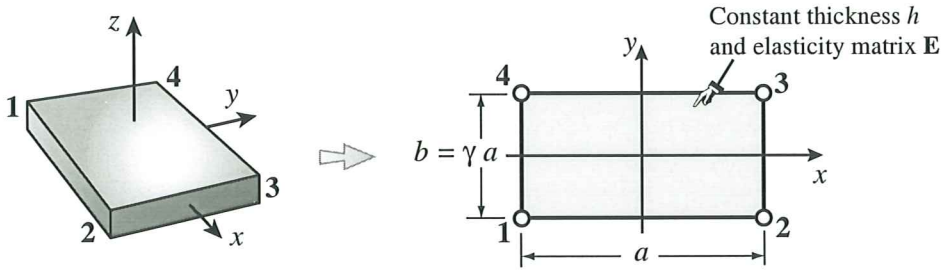

Figure 2. The rectangular panel.

In keeping with the expository theme, the next three sections derive the rectangular panel stiffness from stress, strain and displacement assumptions, respectively. Mirroring history, the derivation of stress and strain models follows the matrix-based direct elasticity approach used by the first generation, as summarized in Gallagher's review [6].

Ironically, the direct derivation will give optimal or near-optimal elements with no sweat whereas the variationally derived displacement model needs tweaking (e.g., by SRI) to become useful.

4. THE STRESS ELEMENT

TCMT [1] is the starting point. In a historical summary Clough [13] remarks that the paper belatedly reports work performed at Boeing's Commercial Airplane Division in 1952-53 (indeed [1, p. 805] states that the material was presented at the 22nd Annual Meeting of IAS, held on January 25–29, 1954.) In addition to bars, beams and spars, TCMT presents two plane stress elements for modeling wing cover plates: the three-node triangle and the four-node flat rectangular panel. Quadrilateral panels of arbitrary geometry, not necessarily flat, were constructed as assemblies of four triangles.

Readers perusing that article for the first time have a surprise in store. The stiffness properties of both panel elements are derived from stress assumptions, rather than displacements, as became popular in the second generation. More precisely, simple patterns of interelement boundary tractions (a.k.a. stress flux modes) that satisfy internal equilibrium are taken as starting point. Twenty years later and apparently unaware of TCMT, Fraeijs de Veubeke [53] systematically extended the same idea in a variational setting, to produce what he called diffusive equilibrium elements. These are designed to weakly enforce interelement flux conservation. The comedy continues: twenty year later mathematicians rediscovered flux elements, now renamed as "Discontinuous Galerkin Methods," blessfully unaware of previous work.

The derivation below largely follows Chapter 3 of Gallagher [6], who presents a step by step procedure for what he calls the "equivalent force" approach. The main extension provided here is allowing anisotropy.

4.1. The 5-Parameter Stress Field

Since TCMT the appropriate stress field for the rectangular panel is known to be [6, p. 19]

$$\sigma_{xx} = \mu_1 + \mu_4 \frac{y}{b}, \qquad \sigma_{yy} = \mu_2 + \mu_5 \frac{x}{a}, \qquad \sigma_{xy} = \mu_3. \tag{6}$$

The five μ_i are stress-amplitude parameters with dimension of stress. They are collected in the 5-vector

$$\boldsymbol{\mu} = [\,\mu_1 \quad \mu_2 \quad \mu_3 \quad \mu_4 \quad \mu_5\,]^T. \tag{7}$$

The field (6) satisfies the internal equilibrium equations $(1)_3$ under zero body forces. Evaluation over element sides produces the traction flux patterns of Figure 3, copied verbatim from TCMT. Why five? "These load states are seen to represent uniform and linearly varying stresses plus constant shear, along

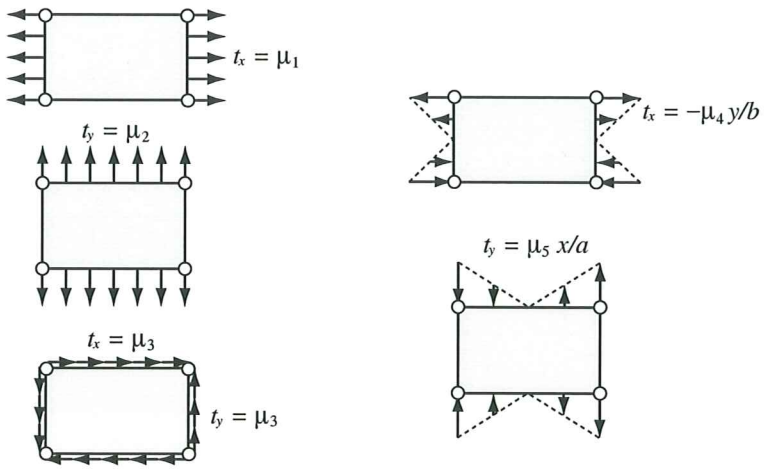

Figure 3. Nonzero interelement boundary tractions associated with the stress parameters μ_i in (7). After [1, p. 812], in which these five patterns are called "load states."

the plate edges. Later it will be seen that the number of load states must be $2n - 3$, where n = number of nodes." [1, p. 813].

To establish connection to node displacements, $\boldsymbol{\mu}$ is extended as

$$\boldsymbol{\mu}_+ = [\,\mu_1 \quad \mu_2 \quad \mu_3 \quad \mu_4 \quad \mu_5 \quad \mu_6 \quad \mu_7 \quad \mu_8\,]^T \tag{8}$$

This array contains three dimensionless coefficients: μ_6, μ_7 and μ_8, which define amplitudes of the three element rigid body modes (RBMs):

$$\text{RBM\#1: } u_x = \mu_6 a,\ u_y = 0, \quad \text{RBM\#2: } u_x = 0,\ u_y = \mu_7 b, \quad \text{RBM\#3: } u_x = -\mu_8 y,\ u_y = \mu_8 x, \tag{9}$$

These modes produce zero stress. The foregoing relations may be recast in matrix form:

$$\boldsymbol{\sigma} = \mathbf{N}\boldsymbol{\mu} = \mathbf{N}_+\boldsymbol{\mu}_+, \quad \mathbf{N} = \begin{bmatrix} 1 & 0 & 0 & \frac{y}{b} & 0 \\ 0 & 1 & 0 & 0 & \frac{x}{a} \\ 0 & 0 & 1 & 0 & 0 \end{bmatrix}, \quad \mathbf{N}_+ = \begin{bmatrix} 1 & 0 & 0 & \frac{y}{b} & 0 & 0 & 0 & 0 \\ 0 & 1 & 0 & 0 & \frac{x}{a} & 0 & 0 & 0 \\ 0 & 0 & 1 & 0 & 0 & 0 & 0 & 0 \end{bmatrix}. \tag{10}$$

The boundary traction patterns of Figure 3 are converted to node forces by statics. This yields

$$\mathbf{f} = \mathbf{A}\,\boldsymbol{\mu}, \qquad \mathbf{A}^T = \tfrac{1}{2}h \begin{bmatrix} -b & 0 & b & 0 & b & 0 & -b & 0 \\ 0 & -a & 0 & -a & 0 & a & 0 & a \\ -a & -b & -a & b & a & b & a & -b \\ \frac{1}{6}b & 0 & -\frac{1}{6}b & 0 & \frac{1}{6}b & 0 & -\frac{1}{6}b & 0 \\ 0 & \frac{1}{6}a & 0 & -\frac{1}{6}a & 0 & \frac{1}{6}a & 0 & -\frac{1}{6}a \end{bmatrix}. \tag{11}$$

Matrix $\mathbf{A}$ is the equilibrium matrix, also called the leverage matrix in the early FEM literature. When restricted to the constant stress states (the first three columns of $\mathbf{A}$), it is called a force-lumping matrix and denoted by $\mathbf{L}$ in the Free Formulation of Bergan [38,39,54–60].

4.2. The Generalized Stiffness

Integrating the complementary energy density $\mathcal{U}^* = \frac{1}{2}\boldsymbol{\sigma}^T\mathbf{C}\boldsymbol{\sigma}$ over the element volume V and identifying $U^* = \int_{V^e}\mathcal{U}^*\,dV$ with $\frac{1}{2}\boldsymbol{\mu}^T\mathbf{F}_\mu\boldsymbol{\mu}$ yields the 5×5 flexibility matrix $\mathbf{F}_\mu$ in terms of the stress parameters.

Its inverse is the generalized stiffness matrix $\mathbf{S}_\mu = \mathbf{F}_\mu^{-1}$:

$$\mathbf{F}_\mu = V\begin{bmatrix} C_{11} & C_{12} & C_{13} & 0 & 0 \\ C_{12} & C_{22} & C_{23} & 0 & 0 \\ C_{13} & C_{23} & C_{33} & 0 & 0 \\ 0 & 0 & 0 & \frac{1}{12}C_{11} & 0 \\ 0 & 0 & 0 & 0 & \frac{1}{12}C_{22} \end{bmatrix}, \quad \mathbf{S}_\mu = \frac{1}{V}\begin{bmatrix} E_{11} & E_{12} & E_{13} & 0 & 0 \\ E_{12} & E_{22} & E_{23} & 0 & 0 \\ E_{13} & E_{23} & E_{33} & 0 & 0 \\ 0 & 0 & 0 & 12C_{11}^{-1} & 0 \\ 0 & 0 & 0 & 0 & 12C_{22}^{-1} \end{bmatrix}, \quad (12)$$

in which $V = abh$ is the volume of the element.

4.3. The Physical Stiffness

Integration of the slave strain field $\mathbf{e} = \mathbf{E}^{-1}\boldsymbol{\sigma} = \mathbf{C}\mathbf{N}_+\boldsymbol{\mu}_+$ produces the displacement field

$$\begin{aligned} u_x(x,y) &= \mu_6 a + \tfrac{1}{8}\omega_6 + (\mu_1 C_{11} + \mu_2 C_{12} + \mu_3 C_{13})x + (\tfrac{1}{2}(\mu_1 C_{13} + \mu_2 C_{23} + \mu_3 C_{33}) - \mu_8)y \\ &\quad + \tfrac{1}{2}(\mu_5/a)C_{12}x^2 + (\mu_4/b)C_{11}xy + \tfrac{1}{2}\big((\mu_4/b)C_{13} - (\mu_5/a)C_{22}\big)y^2, \\ u_y(x,y) &= \mu_7 b + \tfrac{1}{8}\omega_7 + (\tfrac{1}{2}(\mu_1 C_{13} + \mu_2 C_{23} + \mu_3 C_{33}) + \mu_8)x + (\mu_1 C_{12} + \mu_2 C_{22} + \mu_3 C_{23})y \\ &\quad + \tfrac{1}{2}\big((\mu_5/a)C_{23} - (\mu_4/b)C_{11}\big)x^2 + (\mu_5/a)C_{22}xy + \tfrac{1}{2}(\mu_4/b)C_{12}y^2. \end{aligned} \quad (13)$$

with $\omega_6 = -b^2C_{13}\mu_4/b + (b^2C_{22} - a^2C_{12})(\mu_5/a)$ and $\omega_7 = (a^2C_{11} - b^2C_{12})(\mu_4/b) - a^2C_{23}\mu_5/a$. The constant terms in u_x and u_y, which do not affect strains and stresses, have been adjusted to get relatively simple terms in columns 4 through 8 of the matrix $\mathbf{T}_+$ below. Physically, (13) aligns the bending deformation patterns along the $\{x, y\}$ axes. Evaluating (13) at the nodes we obtain the matrix that connects node displacements to stress parameters: $\mathbf{u} = \mathbf{T}_+\boldsymbol{\mu}_+$, where

$$\mathbf{T}_+ = \tfrac{1}{4}\begin{bmatrix} -2aC_{11} - bC_{13} & -2aC_{12} - bC_{23} & -2aC_{13} - bC_{33} & aC_{11} & 0 & 4a & 0 & 2b \\ -2bC_{12} - aC_{13} & -2bC_{22} - aC_{23} & -2bC_{23} - aC_{33} & 0 & bC_{22} & 0 & 4b & -2a \\ 2aC_{11} - bC_{13} & 2aC_{12} - bC_{23} & 2aC_{13} - bC_{33} & -aC_{11} & 0 & 4a & 0 & 2b \\ -2bC_{12} + aC_{13} & -2bC_{22} + aC_{23} & -2bC_{23} + aC_{33} & 0 & -bC_{22} & 0 & 4b & 2a \\ 2aC_{11} + bC_{13} & 2aC_{12} + bC_{23} & 2aC_{13} + bC_{33} & aC_{11} & 0 & 4a & 0 & -2b \\ 2bC_{12} + aC_{13} & 2bC_{22} + aC_{23} & 2bC_{23} + aC_{33} & 0 & bC_{22} & 0 & 4b & 2a \\ -2aC_{11} + bC_{13} & -2aC_{12} + bC_{23} & -2aC_{13} + bC_{33} & -aC_{11} & 0 & 4a & 0 & -2b \\ 2bC_{12} - aC_{13} & 2bC_{22} - aC_{23} & 2bC_{23} - aC_{33} & 0 & -bC_{22} & 0 & 4b & -2a \end{bmatrix} \quad (14)$$

The determinant of $\mathbf{T}_+$ is $a^4b^4C_{11}C_{22}\det(\mathbf{C})$, so $\mathbf{T}_+$ is invertible if $a \neq 0$, $b \neq 0$, $C_{11} \neq 0$, $C_{22} \neq 0$ and $\mathbf{C}$ is nonsingular. Inversion yields $\boldsymbol{\mu}_+ = \mathbf{U}_+\mathbf{u}$, where

$$\mathbf{U}_+ = \mathbf{T}_+^{-1} = \frac{1}{ab}\begin{bmatrix} U_{11} & U_{12} & U_{13} & U_{14} & U_{15} & U_{16} & U_{17} & U_{18} \\ U_{21} & U_{22} & U_{23} & U_{24} & U_{25} & U_{26} & U_{27} & U_{28} \\ U_{31} & U_{32} & U_{33} & U_{34} & U_{35} & U_{36} & U_{37} & U_{38} \\ bC_{11}^{-1} & 0 & -bC_{11}^{-1} & 0 & bC_{11}^{-1} & 0 & -bC_{11}^{-1} & 0 \\ 0 & aC_{22}^{-1} & 0 & -aC_{22}^{-1} & 0 & aC_{22}^{-1} & 0 & -aC_{22}^{-1} \\ \frac{1}{4}b & 0 & \frac{1}{4}b & 0 & \frac{1}{4}b & 0 & \frac{1}{4}b & 0 \\ 0 & \frac{1}{4}a & 0 & \frac{1}{4}a & 0 & \frac{1}{4}a & 0 & \frac{1}{4}a \\ \frac{1}{4}a & -\frac{1}{4}b & \frac{1}{4}a & \frac{1}{4}b & -\frac{1}{4}a & \frac{1}{4}b & -\frac{1}{4}a & -\frac{1}{4}b \end{bmatrix}, \quad (15)$$

in which $U_{11} = -\frac{1}{2}(bE_{11}+aE_{13})$, $U_{12} = -\frac{1}{2}(aE_{12}+bE_{13})$, $U_{13} = \frac{1}{2}(bE_{11}-aE_{13})$, $U_{14} = -\frac{1}{2}(aE_{12}-bE_{13})$, $U_{15} = \frac{1}{2}(bE_{11}+aE_{13})$, $U_{16} = \frac{1}{2}(aE_{12}+bE_{13})$, $U_{17} = -\frac{1}{2}(bE_{11}-aE_{13})$, $U_{18} = \frac{1}{2}(aE_{12}-bE_{13})$, $U_{21} = -\frac{1}{2}(bE_{12}+aE_{23})$, $U_{22} = -\frac{1}{2}(aE_{22}+bE_{23})$, $U_{23} = \frac{1}{2}(bE_{12}-aE_{23})$, $U_{24} = -\frac{1}{2}(aE_{22}-bE_{23})$, $U_{25} = \frac{1}{2}(bE_{12}+aE_{23})$, $U_{26} = \frac{1}{2}(aE_{22}+bE_{23})$, $U_{27} = -\frac{1}{2}(bE_{12}-aE_{23})$, $U_{28} =$

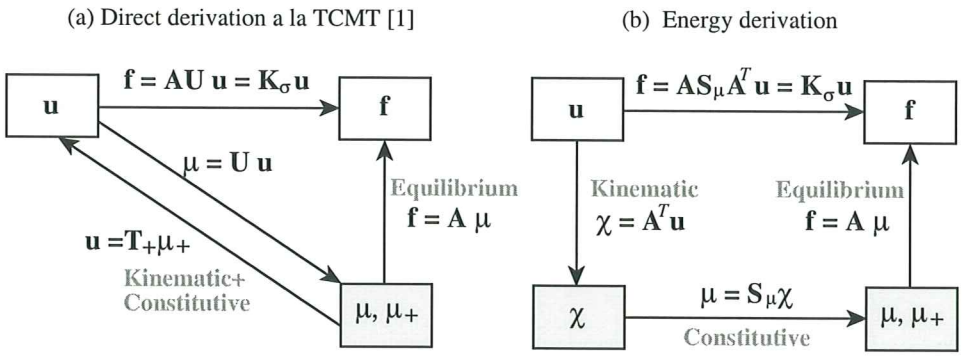

Figure 4. Derivation of the stress-assumed rectangular panel stiffness. Left side shows derivation bypassing energy methods.

$\frac{1}{2}(aE_{22}-bE_{23})$, $U_{31} = -\frac{1}{2}(bE_{13}+aE_{33})$, $U_{32} = -\frac{1}{2}(aE_{23}+bE_{33})$, $U_{33} = \frac{1}{2}(bE_{13}-aE_{33})$, $U_{34} = -\frac{1}{2}(aE_{23}-bE_{33})$, $U_{35} = \frac{1}{2}(bE_{13}+aE_{33})$, $U_{36} = \frac{1}{2}(aE_{23}+bE_{33})$, $U_{37} = -\frac{1}{2}(bE_{13}-aE_{33})$ and $U_{38} = \frac{1}{2}(aE_{23}-bE_{33})$. The stress-displacement matrix $\mathbf{U}$ that relates stress parameters to displacements: $\boldsymbol{\mu} = \mathbf{U}\,\mathbf{u}$, is obtained by extracting the first five rows of $\mathbf{U}_+$:

$$\mathbf{U} = \frac{1}{ab}\begin{bmatrix} U_{11} & U_{12} & U_{13} & U_{14} & U_{15} & U_{16} & U_{17} & U_{18} \\ U_{21} & U_{22} & U_{23} & U_{24} & U_{25} & U_{26} & U_{27} & U_{28} \\ U_{31} & U_{32} & U_{33} & U_{34} & U_{35} & U_{36} & U_{37} & U_{38} \\ bC_{11}^{-1} & 0 & -bC_{11}^{-1} & 0 & bC_{11}^{-1} & 0 & -bC_{11}^{-1} & 0 \\ 0 & aC_{22}^{-1} & 0 & -aC_{22}^{-1} & 0 & aC_{22}^{-1} & 0 & -aC_{22}^{-1} \end{bmatrix} = \mathbf{S}_\mu\,\mathbf{A}^T. \quad (16)$$

The relation $\mathbf{U} = \mathbf{S}_\mu\mathbf{A}^T$ can be checked directly. For this element it can be proven to hold by energy methods, but that was not obvious in 1952. It must have been a relief when the element stiffness came out symmetric. As Gallagher remarks [6, p. 22] symmetry is the exception rather than the rule for more complicated configurations. That difficulty proved a big boost for the energy and variational methods of the second generation.

The physical stiffness $\mathbf{K}_\sigma$ relates $\mathbf{f} = \mathbf{K}_\sigma\,\mathbf{u}$, where the σ subscript flags the stress element. Combining $\mathbf{f} = \mathbf{A}\,\boldsymbol{\mu}$ and $\boldsymbol{\mu} = \mathbf{U}\,\mathbf{u} = \mathbf{S}_\mu\,\mathbf{A}^T\,\mathbf{u}$ yields

$$\mathbf{K}_\sigma = \mathbf{A}\,\mathbf{U} = \mathbf{A}\,\mathbf{S}_\mu\,\mathbf{A}^T. \quad (17)$$

Figure 4 summarizes the foregoing derivation steps. Note that one can bypass the calculation of the generalized stiffness $\mathbf{S}_\mu$ if so desired, as diagrammed on the left of that figure. This is convenient for presentation to students without a background on energy methods.

Note that the displacement field (13) contains quadratic terms if μ_4 or μ_5 are nonzero. Hence the element is nonconforming. This is acknowledged but dismissed as innocuous in TCMT [1, p. 814].

5. THE STRAIN ELEMENT

A strain-assumed element can be developed through an entirely analogous procedure. The counterpart of (6) is

$$e_{xx} = \chi_1 + \chi_4\,\frac{y}{b}, \qquad e_{yy} = \chi_2 + \chi_5\,\frac{x}{a}, \qquad 2e_{xy} = \chi_3. \quad (18)$$

where the χ_i are dimensionless strain-amplitude parameters. They are collected in the 5-vector

$$\boldsymbol{\chi} = [\,\chi_1 \quad \chi_2 \quad \chi_3 \quad \chi_4 \quad \chi_5\,]^T. \quad (19)$$

An extended vector is constructed by appending the RBM amplitudes

$$\chi_+ = [\,\chi_1 \quad \chi_2 \quad \chi_3 \quad \chi_4 \quad \chi_5 \quad \chi_6 \quad \chi_7 \quad \chi_8\,]^T. \tag{20}$$

in which χ_6, χ_7 and χ_8 are defined a a manner similar to (9). Note that $\mathbf{e} = \mathbf{N}\chi = \mathbf{N}_+\chi_+$ where $\mathbf{N}$ and $\mathbf{N}_+$ are defined in (10). Integrating the strains yields the displacement field

$$\begin{aligned} u_x(x,y) &= \chi_6 + \chi_8 y + (\chi_1 + \chi_4/b)xy - \tfrac{1}{2}(\chi_5/a)y^2, \\ u_y(x,y) &= \chi_7 + (\chi_3 - \chi_8)x + \chi_2 y - \tfrac{1}{2}(\chi_4/b)x^2 + (\chi_5/a)xy. \end{aligned} \tag{21}$$

Evaluating at the nodes and inverting yields $\chi_+ = \mathbf{B}_+\mathbf{u}$ where

$$\mathbf{B}_+ = \frac{1}{8ab}\begin{bmatrix} -4b & 0 & 4b & 0 & 4b & 0 & -4b & 0 \\ 0 & -4a & 0 & -4a & 0 & 4a & 0 & 4a \\ -4a & -4b & -4a & 4b & 4a & 4b & 4a & -4b \\ 8b & 0 & -8b & 0 & 8b & 0 & -8b & 0 \\ 0 & 8a & 0 & -8a & 0 & 8a & 0 & -8a \\ 2ab & b^2 & 2ab & -b^2 & 2ab & b^2 & 2ab & -b^2 \\ a^2 & 2ab & -a^2 & 2ab & a^2 & 2ab & -a^2 & 2ab \\ -4a & 0 & -4a & 0 & 4a & 0 & 4a & 0 \end{bmatrix} \tag{22}$$

from which we extract the first five rows to get the strain-displacement matrix relating $\chi = \mathbf{B}_\chi\mathbf{u}$:

$$\mathbf{B}_\chi = \frac{h}{2V}\begin{bmatrix} -b & 0 & b & 0 & b & 0 & -b & 0 \\ 0 & -a & 0 & -a & 0 & a & 0 & a \\ -a & -b & -a & b & a & b & a & -b \\ 2b & 0 & -2b & 0 & 2b & 0 & -2b & 0 \\ 0 & 2a & 0 & -2a & 0 & 2a & 0 & -2a \end{bmatrix} \tag{23}$$

For use below we note the following relation between the transformation matrices of the stress and strain elements

$$\mathbf{A}^T = V\,\mathbf{D}_A\,\mathbf{B}_\chi, \quad \mathbf{B}_\chi = \frac{1}{V}\mathbf{D}_A^{-1}\mathbf{A}^T, \quad \mathbf{D}_A = \begin{bmatrix} 1 & 0 & 0 & 0 & 0 \\ 0 & 1 & 0 & 0 & 0 \\ 0 & 0 & 1 & 0 & 0 \\ 0 & 0 & 0 & \frac{1}{12} & 0 \\ 0 & 0 & 0 & 0 & \frac{1}{12} \end{bmatrix} = \begin{bmatrix} \mathbf{I}_3 & \mathbf{0} \\ \mathbf{0} & \frac{1}{12}\mathbf{I}_2 \end{bmatrix} = \mathbf{D}_A^T. \tag{24}$$

From (11) the lumping of the slave stress field $\mathbf{E}\mathbf{e} = \mathbf{E}\mathbf{N}\chi$ to node forces can be worked out to be

$$\mathbf{f} = \mathbf{A}\mathbf{E}_+\chi = V\,\mathbf{B}_\chi^T\mathbf{D}_A\mathbf{E}_+\chi, \quad \text{with} \quad \mathbf{E}_+ = \begin{bmatrix} E_{11} & E_{12} & E_{13} & 0 & 0 \\ E_{12} & E_{22} & E_{23} & 0 & 0 \\ E_{13} & E_{23} & E_{33} & 0 & 0 \\ 0 & 0 & 0 & E_{11} & 0 \\ 0 & 0 & 0 & 0 & E_{22} \end{bmatrix} \tag{25}$$

Combining previous equations, the physical element stiffness is

$$\mathbf{K}_e = V\,\mathbf{B}_\chi^T\mathbf{D}_A\mathbf{E}_+\mathbf{B}_\chi = \mathbf{B}_\chi^T\mathbf{K}_\chi\mathbf{B}_\chi, \quad \text{with} \quad \mathbf{K}_\chi = V\,\mathbf{D}_A\mathbf{E}_+. \tag{26}$$

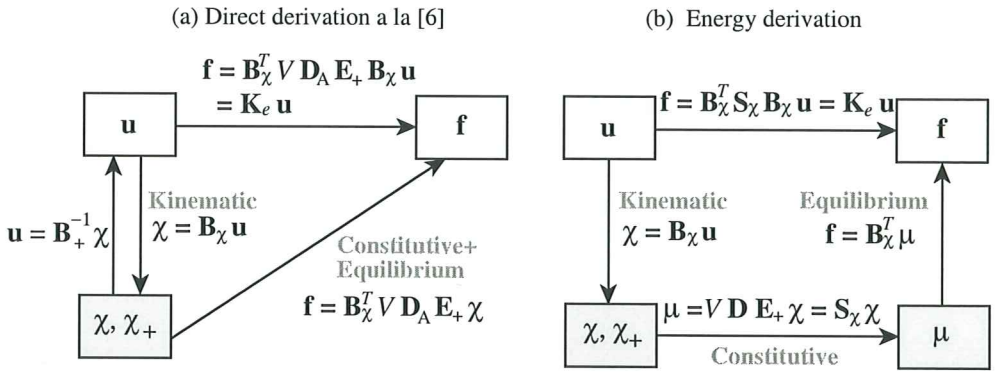

Figure 5. Derivation of the strain-assumed rectangular panel stiffness. Left diagram shows derivation bypassing energy methods.

Here $\mathbf{K}_\chi$ denotes the generalized stiffness in terms of $\boldsymbol{\chi}$. This matrix may be obtained also from standard energy arguments: the strain energy density is $\mathcal{U} = \frac{1}{2}\boldsymbol{\chi}^T\mathbf{E}\boldsymbol{\chi}$. Integrating over the element volume: $U = \int_{V^e} \mathcal{U}\, dV$ and identifying with $\frac{1}{2}\boldsymbol{\chi}^T\mathbf{K}_\chi\boldsymbol{\chi}$ gives

$$\mathbf{K}_\chi = V\,\mathbf{D}_A\mathbf{E}_+ = V\begin{bmatrix} E_{11} & E_{12} & E_{13} & 0 & 0 \\ E_{12} & E_{22} & E_{23} & 0 & 0 \\ E_{13} & E_{23} & E_{33} & 0 & 0 \\ 0 & 0 & 0 & \frac{1}{12}E_{11} & 0 \\ 0 & 0 & 0 & 0 & \frac{1}{12}E_{22} \end{bmatrix} \tag{27}$$

Figure 5 summarizes the foregoing derivation steps. The direct step from $\boldsymbol{\chi}$ to $\mathbf{f}$ on the left is more difficult to explain to students than the step from $\mathbf{u}$ to $\boldsymbol{\mu}$ in Figure 4. The energy based formulation shown on the right of Figure 5 tends to be more palatable.

6. THE CONFORMING DISPLACEMENT ELEMENT

This derivation of the assumed-displacement element starts from a conforming displacement field that enforces linear edge displacements. Using the matrix notation of [61, p. 227] for Irons' isoparametric formulation [23] specialized to the rectangle, the displacement field is bilinearly interpolated as

$$\begin{bmatrix} u_x(x,y) \\ u_y(x,y) \end{bmatrix} = \tfrac{1}{2}\begin{bmatrix} -a & 0 & a & 0 & a & 0 & -a & 0 \\ 0 & -b & 0 & -b & 0 & b & 0 & b \end{bmatrix}\begin{bmatrix} \frac{1}{4}(1-\xi)(1-\eta) \\ \frac{1}{4}(1+\xi)(1-\eta) \\ \frac{1}{4}(1+\xi)(1+\eta) \\ \frac{1}{4}(1-\xi)(1+\eta) \end{bmatrix}, \tag{28}$$

where $\xi = 2x/a$ and $\eta = 2y/b$ are the dimensionless quadrilateral coordinates. The derivation based on the minimum potential energy principle is standard textbook material and only the final result is presented here:

$$\mathbf{K}_u = \mathbf{B}_u^T\mathbf{K}_q\mathbf{B}_u, \quad \text{with} \quad \mathbf{K}_q = \frac{1}{V}\begin{bmatrix} E_{11} & E_{12} & E_{13} & 0 & 0 \\ E_{12} & E_{22} & E_{23} & 0 & 0 \\ E_{13} & E_{23} & E_{33} & 0 & 0 \\ 0 & 0 & 0 & Q_{11} & Q_{12} \\ 0 & 0 & 0 & Q_{12} & Q_{22} \end{bmatrix}, \tag{29}$$

in which $\mathbf{B}_u = \mathbf{A}^T$ as given by (11) and

$$Q_{11} = 12\frac{b^2E_{11} + a^2E_{33}}{ab^3h}, \quad Q_{12} = 12\left(\frac{E_{13}}{a^2h} + \frac{E_{23}}{b^2h}\right), \quad Q_{22} = 12\frac{a^2E_{22} + b^2E_{33}}{a^3bh} \tag{30}$$

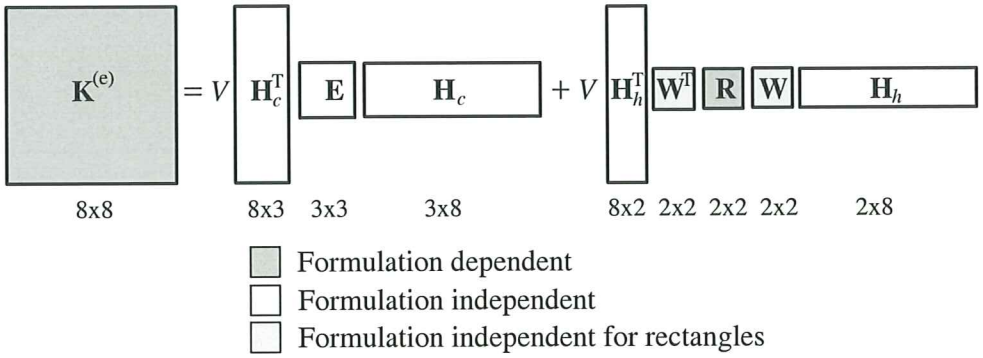

Figure 6. The template for the rectangular panel, illustrating formulation dependent and independent parts.

This model has a checkered history. It was first derived as a rectangular panel with edge reinforcements (omitted here) by Argyris in his 1954 *Aircraft Engineering* series [2, p. 49 in reprint]. He used bilinear displacement interpolation in Cartesian coordinates. After much flailing, a conforming generalization to arbitrary geometry was published in 1964 by Taig and Kerr [62] using quadrilateral-fitted coordinates called $\{\xi, \eta\}$ but running from 0 to 1. (Reference [62] cites an 1961 English Electric Aircraft internal report as original source but [23, p. 520] remarks that the work goes back to 1957.) Bruce Irons, who was aware of Taig's work while at Rolls Royce, created the seminal isoparametric family as a far-reaching extension upon moving to Swansea [19–22].

7. TEMPLATES

7.1. Stiffness Decomposition

The stiffnesses $\mathbf{K}_\sigma$, $\mathbf{K}_\sigma$ and $\mathbf{K}_u$ derived in the foregoing three Sections do not appear to have much in common. Indeed if one looks at just the matrix entries no pattern is readily seen. Closer examination reveals, however, that they are instances of the algebraic form

$$\mathbf{K} = \mathbf{K}_b + \mathbf{K}_h = V\,\mathbf{H}_c^T\mathbf{E}\mathbf{H}_c + V\,\mathbf{H}_h^T\mathbf{W}^T\mathbf{R}\mathbf{W}\mathbf{H}_h, \tag{31}$$

where $V = abh$ is the element volume and

$$\begin{aligned}
\mathbf{H}_c &= \frac{1}{2ab}\begin{bmatrix} -b & 0 & b & 0 & b & 0 & -b & 0 \\ 0 & -a & 0 & -a & 0 & a & 0 & a \\ -a & -b & -a & b & a & b & a & -b \end{bmatrix}, \\
\mathbf{H}_h &= \tfrac{1}{2}\begin{bmatrix} 1 & 0 & -1 & 0 & 1 & 0 & -1 & 0 \\ 0 & 1 & 0 & -1 & 0 & 1 & 0 & -1 \end{bmatrix}, \\
\mathbf{W} &= \begin{bmatrix} 1/a & 0 \\ 0 & 1/b \end{bmatrix}, \quad \mathbf{R} = \begin{bmatrix} R_{11} & R_{12} \\ R_{12} & R_{22} \end{bmatrix}.
\end{aligned} \tag{32}$$

Matrices $\mathbf{H}_c$ and $\mathbf{H}_h$ are the same for the three elements. Matrix $\mathbf{R}$ (a generalized bending rigidity) depends on the formulation. The transition matrix $\mathbf{W}$ is formulation independent for rectangular panels. For more complex geometries discussed in the Appendix, $\mathbf{W}$ may be formulation-adjusted to make $\mathbf{R}$ simpler.

For the stress, strain and displacement elements $\mathbf{R}$ is $\mathbf{R}_\sigma$, $\mathbf{R}_e$ and $\mathbf{R}_u$, respectively, where

$$\mathbf{R}_\sigma = \tfrac{1}{3}\begin{bmatrix} C_{11}^{-1} & 0 \\ 0 & C_{22}^{-1} \end{bmatrix}, \quad \mathbf{R}_e = \tfrac{1}{3}\begin{bmatrix} E_{11} & 0 \\ 0 & E_{22} \end{bmatrix}, \quad \mathbf{R}_u = \tfrac{1}{3}\begin{bmatrix} E_{11} + \dfrac{a^2E_{33}}{b^2} & \dfrac{bE_{13}}{a} + \dfrac{aE_{23}}{b} \\ \dfrac{bE_{13}}{a} + \dfrac{aE_{23}}{b} & E_{22} + \dfrac{b^2E_{33}}{a^2} \end{bmatrix}. \tag{33}$$

```
RectPanel4TemplateStiffness[{a_,b_},Emat_,Cmat_,h_,name_,Rlist_]:=
  Module[{V,found,Hc,Hh,W,Ke}, V=a*b*h;
  {WRW,found}=RectPanel4TemplateWRW[{a,b},Emat,Cmat,name,Rlist];
  If [Not[found], Print["Illegal elem name: ",name]; Abort[]];
  Hc={{-b,0,b,0,b,0,-b,0}, {0,-a,0,-a,0,a,0,a},
      {-a,-b,-a,b,a,b,a,-b}}/(2*a*b);
  Hh={{1,0,-1,0,1,0,-1,0},{0,1,0,-1,0,1,0,-1}}/2;
  Ke=V*Transpose[Hc].Emat.Hc+V*Transpose[Hh].WRW.Hh;
  Return[Simplify[Ke]]];

RectPanel4TemplateWRW[{a_,b_},Emat_,Cmat_,name_,Rlist_]:=
 Module[{R11,R12,R22,Rmat,E11,E12,E13,E22,E23,E33,
 found=False,C11,C22,C33,C12,C13,C23,Edet,Cdet,W,WRW},
  {{E11,E12,E13},{E12,E22,E23},{E13,E23,E33}}=Emat;
  If [Length[Cmat]<=0,
     Edet=E11*E22*E33+2*E12*E13*E23-E11*E23^2-E22*E13^2-E33*E12^2;
     C11=(E22*E33-E23^2)/Edet; C22=(E11*E33-E13^2)/Edet;
     C33=(E11*E22-E12^2)/Edet; C12=(E13*E23-E12*E33)/Edet;
     C13=(E12*E23-E13*E22)/Edet; C23=(E12*E13-E11*E23)/Edet,
     {{C11,C12,C13},{C12,C22,C23},{C13,C23,C33}}=Cmat,
     {{C11,C12,C13},{C12,C22,C23},{C13,C23,C33}}=Cmat];
  If [name=="Stress"||name=="QM6"||name=="Q6",
     R11=1/(3*C11); R22=1/(3*C22); R12=0; found=True];
  If [name=="Strain", R11=E11/3; R22=E22/3; R12=0; found=True];
  If [name=="Disp",  R11=(E11+E33*a^2/b^2)/3;
     R22=(E22+E33*b^2/a^2)/3; R12=(E13*b/a+E23*a/b)/3; found=True];
  If [name=="Arbitrary", {R11,R12,R22}=Rlist; found=True];
  W={{1/a,0},{0,1/b}}; Rmat={{R11,R12},{R12,R22}};
  WRW=Transpose[W].Rmat.W; Return[{WRW,found}]];
```

Figure 7. A *Mathematica* implementation of the rectangular panel template (31).

But actually we are not restricted to these. Other expressions for $\mathbf{R}$ would yield other $\mathbf{K}$. These are possible, although not necessarily useful, stiffnesses for the rectangular panel if $\mathbf{R}$ is symmetric and positive definite, and if its entries have physical dimensions of elastic moduli. Further if $E_{13} = E_{23} = 0$ we set $R_{12} = 0$. The key discovery is that the element formulation affects only part of the stiffness expression. See Figure 6.

7.2. Template Terminology

The algebraic form (31)-(32) is called a finite element stiffness template, or *template* for short.

Matrices $\mathbf{K}_b$ and $\mathbf{K}_h$ are called the basic and higher-order stiffness matrix, respectively, in accordance with the fundamental decomposition of the Free Formulation [38,39,54–60]. These matrices play different and complementary roles.

The basic stiffness $\mathbf{K}_b$ takes care of consistency and mixability. In the Free Formulation a restatement of (31) is preferred:

$$\mathbf{K}_b = V^{-1}\,\mathbf{L}\,\mathbf{E}\,\mathbf{L}^T, \tag{34}$$

where $\mathbf{L} = \mathbf{H}_c/V$ is called the force lumping matrix, or simply lumping matrix.

The higher order stiffness $\mathbf{K}_h$ is a *stabilization* term that provides the correct rank and may be adjusted for accuracy. This matrix is orthogonal to rigid body motions and constant strain states. To verify the claim for this template introduce the following 8×6 matrix, called the basic-mode matrix in the Free

Formulation:

$$\mathbf{G}_{rc} = \begin{bmatrix} 1 & 0 & y_1 & x_1 & 0 & y_1 \\ 0 & 1 & -x_1 & 0 & y_1 & x_1 \\ 1 & 0 & y_2 & x_2 & 0 & y_2 \\ 0 & 1 & -x_2 & 0 & y_2 & x_2 \\ 1 & 0 & y_3 & x_3 & 0 & y_3 \\ 0 & 1 & -x_3 & 0 & y_3 & x_3 \\ 1 & 0 & y_4 & x_4 & 0 & y_4 \\ 0 & 1 & -x_4 & 0 & y_4 & x_4 \end{bmatrix} = \frac{1}{2} \begin{bmatrix} 2 & 0 & -b & -a & 0 & -b \\ 0 & 2 & a & 0 & -b & -a \\ 2 & 0 & -b & a & 0 & -b \\ 0 & 2 & -a & 0 & -b & a \\ 2 & 0 & b & a & 0 & b \\ 0 & 2 & -a & 0 & b & a \\ 2 & 0 & b & -a & 0 & b \\ 0 & 2 & a & 0 & b & -a \end{bmatrix}. \tag{35}$$

The six columns of $\mathbf{G}_{rc}$ span the rigid body modes and constant strain states evaluated at the nodes (these bases are not orthonormalized as that property is not required here). It is readily checked that $\mathbf{H}_h\mathbf{G}_{rc} = \mathbf{0}$. Therefore those modes, and any linear combination thereof, are orthogonal to the higher order stiffness: $\mathbf{K}_h\mathbf{G}_{rc} = \mathbf{0}$. So the role of $\mathbf{H}_h$ is essentially that of a geometric *projector*.

A *Mathematica* implementation of (31) is shown in Figure 7, as module `RectPanel4TemplateStiffness`. The module arguments are the rectangle dimensions as list `{a,b}`, the 3 × 3 elasticity matrix as list `Emat={{E11,E12,E13},{E12,E22,E23},{E13,E23,E33}}`, the 3 × 3 compliance matrix as list `Cmat={{C11,C12,C13},{C12,C22,C23},{C13,C23,C33}}`, the thickness `h`, the name as one of `"Stress"` ,`"Strain"`, `"Disp"`, `"Q6"`, `"QM6"` or `"Arbitrary"`, and finally the list `Rlist={R11,R12,R22}`. The latter is used if the name is `"Arbitrary"`. This comes handy for finding the signature of known elements leaving the entries of `Rlist` symbolic and using the `Solve` command. If `Cmat` is supplied as the empty list `{ }`, the compliance matrix is calculated internally as inverse of `Emat`.

The module returns the 8 × 8 stiffness matrix `Ke` as function value. To get the basic stiffness $\mathbf{K}_b$ only, call with `name = "Arbitrary"` and `Rlist={0,0,0}`.

7.3. Requirements

An acceptable template fulfills four conditions: (C) consistency, (S) stability (correct rank), (I) observer invariance and (P) parametrization. These are discussed at length in other papers [69–75]. Conditions (C) and (S) are imposed to ensure convergence as the mesh size is reduced by enforcing *a priori* satisfaction of the Individual Element Test (IET) of Bergan and Hanssen [76,77]

Condition (P) means that the template contains free parameters or free matrix entries. In the case of (31), the simplest choice of parameters are the entries R_{11}, R_{12}, R_{22} themselves. To fulfill stability, $R_{11} > 0$, $R_{22} > 0$ and $R_{11}R_{22} - R_{12}^2 > 0$. Parametrization facilitates performance optimization as well as tuning elements, or combinations of elements, to fulfill specific needs.

Using the IET as departure point it is not difficult to show [78] that (31), under the stated restrictions on $\mathbf{R}$, includes all stiffnesses that satisfy the IET and stability. Observer invariance is a moot point for this element since $\{x, y\}$ are side aligned. As per the definition in the Introduction, (31) is an universal template.

7.4. Instances, Signatures, Clones

Setting the free parameters to specific values yields element instances. The set of free parameters is called the template *signature*, a term introduced in [73,74]. Borrowing terminology from biogenetics, the signature may be viewed as an "element DNA" that uniquely characterizes it as an individual entity. Elements derived by different techniques that share the same signature are called *clones*.

One of the "template services" is automatic identification of clones. If two elements fitting the template (31) share R_{11}, R_{12} and R_{22}, they are clones. Inasmuch as most FEM formulation schemes have been

Table 1. A Clone Gallery

Name	Description	Clones and sources
StressRP (a.k.a. BORP)	5-stress-mode element of Section 4	Direct derivation: TCMT [1], Gallagher [6] Pian 5-mode stress hybrid [25,27] Wilson-Taylor-Doherty-Ghaboussi Q6 [63] Taylor-Wilson-Beresford QM6 [64] Belytschko-Liu-Engelmann QBI [65] SRI of iso-P with **E** split as per (54)
StrainRP	5-strain-mode element of Section 5	MacNeal QUAD4 [36,66] SRI of iso-P with **E** split as per (56)
DispRP	Bilinear iso-P element of Section 6	Argyris [2] as edge stiffened rectangular panel Taig-Kerr [62] as specialized quadrilateral

Note 1: Many plane stress models listed above were derived for quadrilateral geometries, and a few as membrane component of shells. The right-hand-column classification only pertains to the rectangular panel specialization. For example, Q6 and QM6 differ for non-parallelogram shapes.
Note 2: Instances of the stress-hybrid and displacement-bubble-function "futile families" studied in Section 11 are omitted, as they lack practical value.
Note 3: Post-1990 clones (e.g. EAS [51]) omitted to save space. See [67] for a recent survey.

tried on the rectangular panel, it should come as no surprise that there are many clones, particularly of the stress element. Those presented before 1990 are collected in Table 1. For example, the incompatible mode element Q6 of Wilson et al. [63] is a clone of StressRP. The version QM6 of Taylor et al. [64], which passes the patch test for arbitrary geometries, reduces to Q6 for rectangular and parallelogram shapes. Even for this simple geometry recognition of some of the coalescences took a long time, as recently narrated in [68].

8. FINDING THE BEST

An universal template is nice to have. But an obvious question arises: among the infinity of elements that it can generate, is there a best one? By construction all instances verify exactly the IET for rigid body modes and uniform strain states. Hence the optimality criterion must rely on higher order patch tests.

8.1. The Bending Tests

The obvious tests involve response to in-plane bending along the side directions. This leads to comparisons in the form of energy ratios. These have been used since 1984 to tune up the higher order stiffness of triangular elements [54–57,79]. An extension introduced in this article is consideration of arbitrary anisotropic material. All symbolic calculations were carried out with *Mathematica*.

The x bending test is depicted in Figure 8. A Bernoulli-Euler plane beam of thin rectangular cross-section with height b and thickness h (normal to the plane of the figure) is bent under applied end moments M_x. The beam is fabricated of anisotropic material with the stress-strain law $\boldsymbol{\sigma} = \mathbf{E}\mathbf{e}$ of $(2)_2$. Except for possible end effects the exact solution of the beam problem (from both the theory-of-elasticity and beam-theory standpoints) is a constant bending moment $M(x) = M_x$ along the span. The associated stress field is $\sigma_{xx} = -M_x\, y/I_b$, $\sigma_{yy} = \sigma_{xy} = 0$, where $I_b = \frac{1}{12}hb^3$.

For the y bending test, depicted in Figure 9, the beam cross section has height a and thickness h, and is subjected to end moments M_y. The exact solution is $M(y) = M_y$. The associated stress field is

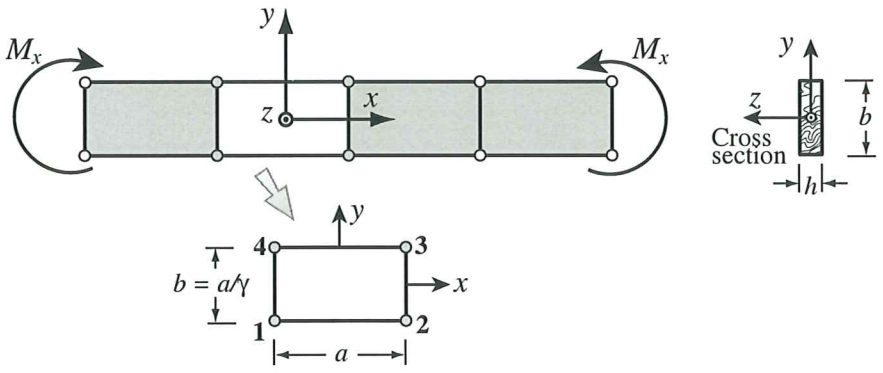

Figure 8. Constant-moment inplane-bending test along the x side dimension.

$\sigma_{yy} = M_y x/I_a$ and $\sigma_{xx} = \sigma_{xy} = 0$, where $I_a = \frac{1}{12}ha^3$. For comparing with the FEM discretizations below, the internal (complementary) energies taken up by beam segments of lengths a and b in the configurations of Figures 8 and 9, respectively, are

$$U_x^{\text{beam}} = \frac{6aC_{11}M_x^2}{b^3h}, \qquad U_y^{\text{beam}} = \frac{6bC_{22}M_y^2}{a^3h} \tag{36}$$

For the 2D element tests, each beam is modeled with one layer of identical 4-node rectangular panels dimensioned $a \times b$ as shown in Figures 8 and 9. The aspect ratio b/a is denoted by γ. By analogy with the exact solution, all rectangles in the finite element model will undergo the same deformations and stresses. We can therefore consider a typical element. For x bending the exact stress distribution is represented by (7) on taking $\mu_4 = -M_x b/I_b = -12M_x/(b^2h)$ and $\mu_1 = \mu_2 = \mu_3 = \mu_5 = 0$. The rigid body mode amplitudes are chosen to be zero for convenience: $\mu_6 = \mu_7 = \mu_8 = 0$. Inserting these μ_i into (14) we get the node displacement vector

$$\mathbf{u}_{bx} = \frac{12M_xC_{11}a}{b^2h}[-1 \quad 0 \quad 1 \quad 0 \quad -1 \quad 0 \quad 1 \quad 0]^T. \tag{37}$$

Likewise, for the y bending test the element stress field is obtained by taking $\mu_5 = M_y a/I_a = 12M_y/(a^2h)$ and $\mu_1 = \mu_2 = \mu_3 = \mu_4 = \mu_6 = \mu_7 = \mu_8 = 0$. The node displacement vector given by (14) is

$$\mathbf{u}_{by} = \frac{12M_yC_{22}b}{a^2h}[0 \quad 1 \quad 0 \quad -1 \quad 0 \quad 1 \quad 0 \quad -1]^T. \tag{38}$$

The strain energies absorbed by the panel element under these applied node displacements are $U_x^{\text{panel}} = \frac{1}{2}\mathbf{u}_{bx}^T\mathbf{K}\mathbf{u}_{bx}$ and $U_y^{\text{panel}} = \frac{1}{2}\mathbf{u}_{by}^T\mathbf{K}\mathbf{u}_{by}$, respectively. Define the bending energy ratios as

$$r_x = \frac{U_x^{\text{panel}}}{U_x^{\text{beam}}}, \qquad r_y = \frac{U_y^{\text{panel}}}{U_y^{\text{beam}}}. \tag{39}$$

These happen to be the ratios of the exact (beam) displacement solution to that of the of rectangular panel solution. Hence $r_x = 1$ means that we get the exact answer under M_x, that is, the panel is x-bending exact. If $r_x > 1$ or $r_x < 1$ the panel is overstiff or overflexible in x bending, respectively, and likewise for y bending.

If $r_x = 1$ and $r_y = 1$ for any aspect ratio $\gamma = b/a$ and arbitrary material properties the element is called *bending optimal*. If $r_x >> 1$ if $a >> b$ and/or $r_y >> 1$ if $a << b$ the element is said to experience *aspect ratio locking* along the x or y direction, respectively. This is known as *shear locking* in the FEM literature because it is traceable to spurious shear energy.

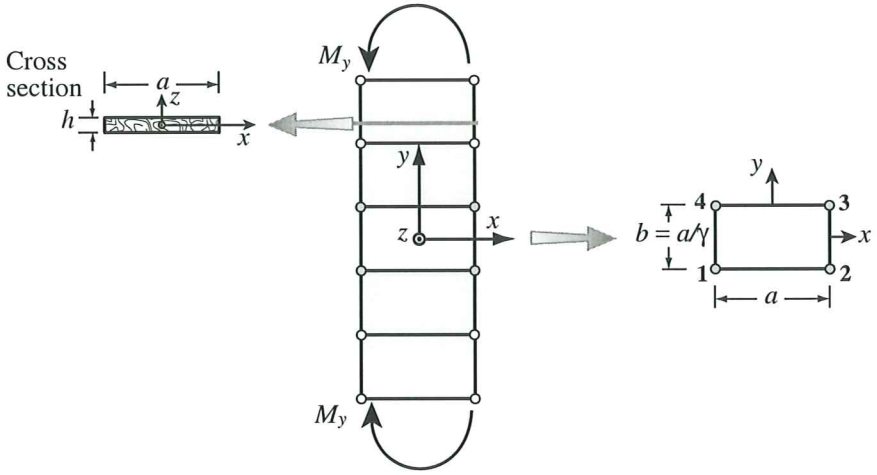

Figure 9. Constant-moment inplane-bending test along the y side dimension.

8.2. The Optimal Panel

Applying the tests to the template (31) yields

$$r_x = 3C_{11}R_{11}, \qquad r_y = 3C_{22}R_{22}. \tag{40}$$

Clearly to get $r_x = r_y = 1$ for any aspect ratio we must take

$$R_{11} = \tfrac{1}{3}C_{11}^{-1}, \quad R_{22} = \tfrac{1}{3}C_{22}^{-1} \tag{41}$$

Because R_{12} does not enter the optimality criterion one can set $R_{12} = 0$ for convenience. Comparing to the $\mathbf{R}_\sigma$ of (33) shows that the 5-parameter stress model of TCMT [1] (and its clones) is the bending-optimal rectangular panel. If the material is isotropic, $R_{11} = R_{22} = \frac{1}{3}E$. Accordingly the StressRP instance will be henceforth also identified by the acronym BORP, for Bending Optimal Rectangular Panel.

8.3. The Strain Element Does Not Lock

It is interesting to apply the result (40) to other elements. The StrainRP element generated by the $\mathbf{R}_e$ of (33) gives

$$r_x = C_{11}E_{11}, \qquad r_y = C_{22}E_{22}. \tag{42}$$

If the material is isotropic, $C_{11} = C_{22} = 1/E$ and $E_{11} = E_{22} = E/(1-\nu^2)$. This yields $r_x = r_y = 1/(1-\nu^2)$, which varies between 1 and 4/3. For an orthotropic body with principal material axes aligned with the rectangle sides, $E_{11} = E_1/(1-\nu_{12}\nu_{21})$, $E_{22} = E_2/(1-\nu_{12}\nu_{21})$, $C_{11} = 1/E_1$, $C_{22} = 1/E_2$, and $r_x = r_y = 1/(1-\nu_{12}\nu_{21})$. The ratios are independent of the aspect ratio γ. Consequently StrainRP and its clones *do not lock*, although the element is not generally optimal. Note that if $C_{11}E_{11}$ and/or $C_{22}E_{22}$ differ widely from 1, as may happen in highly anisotropic materials, the bending performance will be poor. See the Example problem in Section 12.2.

8.4. But the Displacement Element Does

DispRP is generated by the $\mathbf{R}_u$ of (33). Inserting its entries into (40) we get

$$\begin{aligned} r_x &= C_{11}(E_{11} + E_{33}\gamma^2) = \frac{(E_{22}E_{33} - E_{23}^2)(E_{11} + E_{33}\gamma^2)}{\det(\mathbf{E})}, \\ r_y &= C_{22}(E_{22} + E_{33}\gamma^{-2}) = \frac{(E_{11}E_{33} - E_{13}^2)(E_{22} + E_{33}\gamma^{-2})}{\det(\mathbf{E})}. \end{aligned} \tag{43}$$

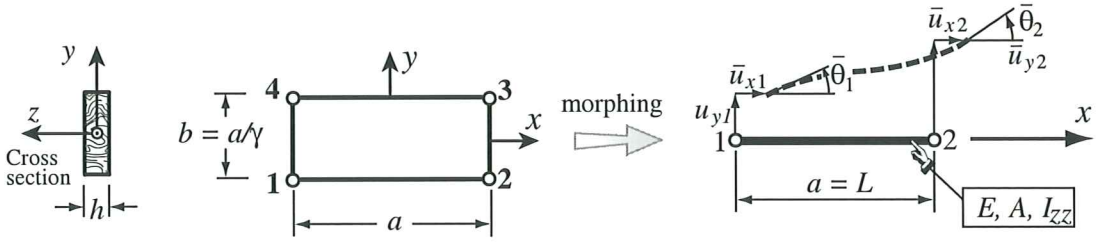

Figure 10. Morphing a 8-DOF rectangular panel unit to a 6-DOF beam-column element in the x direction.

in which $\det(\mathbf{E}) = E_{11}E_{22}E_{33} + 2E_{12}E_{13}E_{23} - E_{11}E_{23}^2 - E_{22}E_{13}^2 - E_{33}E_{12}^2$. For an isotropic material

$$r_x = \frac{2+\gamma^2(1-\nu)}{2(1-\nu^2)}, \qquad r_y = \frac{1+2\gamma^2-\nu}{2\gamma^2(1-\nu^2)}. \tag{44}$$

These relations clearly display aspect ratio locking for bending along the longest side dimension. For example, if $\nu = 0$ and $a = 10b$ whence $\gamma = a/b = 10$, $r_x = 51$ and DispRP is over 50 times stiffer in x bending than the Bernoulli-Euler beam element. The expression (43) makes clear that locking happens for any material law as long as $E_{33} \neq 0$. Since this is the shear modulus, the name *shear locking* used in the FEM literature is justified.

8.5. Multiple Element Layers

Results of the energy bending test can be readily extended to predict the behavior of $2n$ ($n = 1, 2, \ldots$) identical layers of elements symmetrically placed through the beam height. If $2n$ layers are placed along the y direction in the configuration of Figure 8 and γ stays the same, the energy ratio becomes

$$r_x^{(2n)} = \frac{2^{2n} - 1 + r_x}{2^{2n}}, \tag{45}$$

where r_x is the ratio (40) for one layer. If $r_x \equiv 1$, $r_x^{2n} \equiv 1$ so bending exactness is maintained, as can be expected. For example, if $n = 1$ (two element layers), $r_x^{(2)} = (3 + r_x)/4$. The same result holds for r_y if $2n$ layers are placed along the x direction in the configuration of Figure 9.

9. MORPHING INTO BEAM-COLUMN

Morphing means transforming an individual element or macroelement into a simpler model using kinematic constraints. Often the simpler element has lower dimensionality. For example a plate bending macroelement may be morphed to a Bernoulli-Euler beam or to a torqued shaft [75]. To illustrate the idea consider morphing the rectangular panel of Figure 10 into the two-node beam-column element shown on the right of that Figure. The length, cross sectional area and moment of inertia of the beam-column element, respectively, are denoted by $L = a$, $A = bh$ and $I_{zz} = b^3h/12 = a^3h/(12\gamma^3)$, respectively.

The transformation between the freedoms of the panel and those of the beam-column is

$$\mathbf{u}_R = \begin{bmatrix} u_{x1} \\ u_{y1} \\ u_{x2} \\ u_{y2} \\ u_{x3} \\ u_{y3} \\ u_{x4} \\ u_{y4} \end{bmatrix} = \begin{bmatrix} 1 & 0 & \frac{1}{2}b & 0 & 0 & 0 \\ 0 & 1 & 0 & 0 & 0 & 0 \\ 0 & 0 & 0 & 1 & 0 & \frac{1}{2}b \\ 0 & 0 & 0 & 0 & 1 & 0 \\ 0 & 0 & 0 & 1 & 0 & -\frac{1}{2}b \\ 0 & 0 & 0 & 0 & 1 & 0 \\ 1 & 0 & -\frac{1}{2}b & 0 & 0 & 0 \\ 0 & 1 & 0 & 0 & 0 & 0 \end{bmatrix} \begin{bmatrix} \bar{u}_{x1} \\ \bar{u}_{y1} \\ \bar{\theta}_1 \\ \bar{u}_{x2} \\ \bar{u}_{y2} \\ \bar{\theta}_2 \end{bmatrix} = \mathbf{T}_m \bar{\mathbf{u}}_m. \tag{46}$$

where a superposed bar distinguishes the beam-column freedoms grouped in array $\bar{\mathbf{u}}_m$. As source select StressRP fabricated of isotropic material. The morphed beam-column element stiffness is

$$\mathbf{K}_m = \mathbf{T}_m^T \mathbf{K}_\sigma \mathbf{T}_m = \frac{E}{L}\begin{bmatrix} A & 0 & 0 & -A & 0 & 0 \\ 0 & 12c_{22}I_{zz}/L^2 & 6c_{23}I_{zz}/L & 0 & -12c_{22}I_{zz}/L^2 & 6c_{23}I_{zz}/L \\ 0 & 6c_{23}I_{zz}/L & 4c_{33}I_{zz} & 0 & -6c_{23}I_{zz}/L & 4c_{33}I_{zz} \\ -A & 0 & 0 & A & 0 & 0 \\ 0 & 12c_{22}I_{zz}/L^2 & 6c_{23}I_{zz}/L & 0 & -12c_{22}I_{zz}/L^2 & 6c_{23}I_{zz}/L \\ 0 & 6c_{23}I_{zz}/L & 4c_{33}I_{zz} & 0 & -6c_{23}I_{zz}/L & 4c_{33}I_{zz} \end{bmatrix} \tag{47}$$

in which $c_{22} = c_{23} = \frac{1}{2}\gamma^2/(1+\nu)$, and $c_{33} = \frac{1}{4}(1+3c_{22})$. The entries in rows/columns 1 and 4 form the well known two-node bar stiffness. Those in rows and columns 2, 3, 5 and 6 are dimensionally homogeneous to those of a plane beam, and may be grouped into the following matrix configuration:

$$\mathbf{K}_m^{beam} = \frac{EI_{zz}}{L}\left(\begin{bmatrix} 0 & 0 & 0 & 0 \\ 0 & 1 & 0 & -1 \\ 0 & 0 & 0 & 0 \\ 0 & -1 & 0 & 1 \end{bmatrix} + \beta_m \begin{bmatrix} 12/L^2 & 6/L & -12/L^2 & 6/L \\ 6/L & 3 & -6/L & 3 \\ -12/L^2 & -6/L & 12/L^2 & -6/L \\ 6/L & 3 & -6/L & 3 \end{bmatrix}\right) \tag{48}$$

in which $\beta_m = c_{22} = c_{23} = \frac{1}{2}\gamma^2/(1+\nu)$. But (48), with β_m replaced by a free parameter β, happens to be the universal template of a prismatic plane beam, first presented in [69] and further studied, for the C^1 case, in [80,81] using Fourier methods.

The basic stiffness on the left characterizes the pure-bending symmetric response to a uniform moment, whereas the higher-order stiffness on the right characterizes the antisymmetric response to a linearly-varying, bending moment of zero mean. For the Bernoulli-Euler beam constructed with cubic shape functions, $\beta = 1$. For the Timoshenko beam, the exact equilibrium model [5, p. 80] is matched by $\beta = \beta_{C0} = 1/(1+\phi), \phi = 12EI_z/(GA_sL^2)$, in which $A_s = 5bh/6$ is the shear area and $G = \frac{1}{2}E/(1+\nu)$ the shear modulus.

It is readily verified that the morphed β_m is always higher than β_{C0} for all $0 \le \nu \le \frac{1}{2}$ and aspect ratios $\gamma > 0$. This indicates that in beam-like problems involving transverse shear the rectangular panel will be stiffer than the exact C^0 beam model. For example if $\nu = 1/4$,

$$\frac{\beta_{C0}}{\beta_m} = \frac{5}{2(3+\gamma^2)}, \tag{49}$$

which never exceeds 5/6 and goes to zero as $\gamma \to \infty$. This behavior can be expected, since the panel can only respond to such antisymmetric node motions by deforming in pure shear. However, the symmetric response is exact for any aspect ratio γ, which confirms the optimality of StressRP. Observe also that what was a higher order patch test on the two-triangle mesh unit becomes a basic (constant-moment) patch test on the morphed element. This is typical of morphing transformations that reduce spatial dimensionality.

For nonoptimal elements, one finds that the basic stiffness of the morphed beam is wrong except under special circumstances; for example isotropic StrainRP with zero ν, or one of the SRI elements studied next.

10. A G3 DEVICE: SELECTIVE REDUCED INTEGRATION

The three canonical models of Sections 4-6 were known by the end of Generation 2. Next a third generation tool will be studied in the context of templates.

Full Reduced Integration (FRI) and Selective Reduced Integration (SRI) emerged during 1969–72 [82–85] as tools to "unlock" isoparametric displacement models. Initially labeled as "variational crimes"

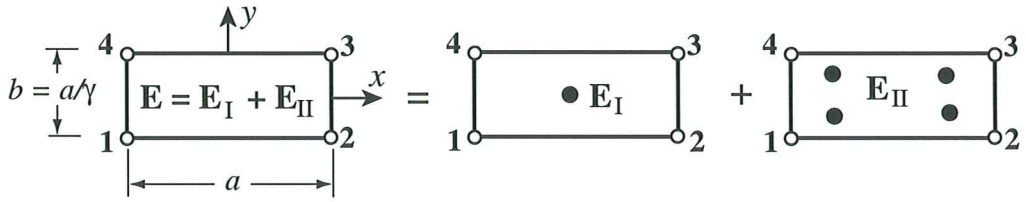

Figure 11. The two-way SRI matrix split.

[31], they were eventually justified through lawful association with mixed variational methods [86–88]. Both FRI and SRI turned out to be particularly useful for legacy and nonlinear codes since they allow shape function and numerical integration modules to be reused.

For the 4-node rectangular panel only SRI is considered because FRI leads to rank deficiency: $R_{11} = R_{12} = R_{22} = 0$. Two questions will be studied as it relates to templates:

(i) Can the template (31)–(32) be reproduced for any material law by a SRI scheme?

(ii) Can BORP be cloned for any material law by a SRI scheme that is independent of the aspect ratio?

As shown below, the answers are (i): yes if $R_{12} = 0$; (ii): yes.

10.1. Concept and Notation

In the FEM literature, SRI identifies a scheme for forming $\mathbf{K}$ as the sum of two or more matrices computed with different integration rules and different constitutive properties, within the framework of the isoparametric displacement model.

We consider primarely the case of a two-way constitutive decomposition. Split the plane stress constitutive matrix $\mathbf{E}$ into

$$\mathbf{E} = \mathbf{E}_{\rm I} + \mathbf{E}_{\rm II} \tag{50}$$

The isoparametric displacement formulation leads to the expression $\mathbf{K} = \int_{A^e} h\, \mathbf{B}_u^T \mathbf{E}\, \mathbf{B}_u\, d\Omega$ where A^e is the element area and $\mathbf{B}_u$ the isoparametric strain-displacement matrix. To apply SRI insert the splitting (50) to get two integrals:

$$\mathbf{K} = \int_{A^e} h\, \mathbf{B}_u^T \mathbf{E}_{\rm I}\, \mathbf{B}_u\, d\Omega + \int_{A^e} h\, \mathbf{B}_u^T \mathbf{E}_{\rm II}\, \mathbf{B}_u\, d\Omega = \mathbf{K}_{\rm I} + \mathbf{K}_{\rm II}. \tag{51}$$

The two matrices in (51) are done through different numerical quadrature schemes: rule (I) for the first integral and rule (II) for the second.

For the rectangular panel the isoparametric model is the 4-node bilinear element. Rules (I) and (II) will be the 1×1 (one point) and 2×2 (4-point) Gauss product rules, respectively. A general split of the elasticity matrix is

$$\mathbf{E} = \mathbf{E}_{\rm I} + \mathbf{E}_{\rm II} = \begin{bmatrix} E_{11}\,\rho_1 & E_{12}\rho_3 & E_{13}\tau_2 \\ E_{12}\,\rho_3 & E_{22}\,\rho_2 & E_{23}\tau_2 \\ E_{13}\,\tau_2 & E_{23}\,\tau_2 & E_{33}\tau_1 \end{bmatrix} + \begin{bmatrix} E_{11}(1-\rho_1) & E_{12}(1-\rho_3) & E_{13}(1-\tau_2) \\ E_{12}(1-\rho_3) & E_{22}(1-\rho_2) & E_{23}(1-\tau_3) \\ E_{13}(1-\tau_2) & E_{23}(1-\tau_3) & E_{33}(1-\tau_1) \end{bmatrix}, \tag{52}$$

in which ρ_1, ρ_2, ρ_3, τ_1, τ_2 and τ_3 are dimensionless coefficients to be chosen.

10.2. The Case $R_{12} = 0$

A template with $R_{12} = 0$ and arbitrary $\{R_{11}, R_{22}\}$ is matched by taking

$$\rho_1 = \frac{1 - 3R_{11}}{E_{11}}, \quad \rho_2 = \frac{1 - 3R_{22}}{E_{22}}, \quad \tau_1 = \tau_2 = \tau_3 = 1. \tag{53}$$

Since ρ_3 does not appear, it is convenient to set it to one to get a diagonal $\mathbf{E}_{\rm II}$. The resulting split is

$$\mathbf{E}_{\rm I} + \mathbf{E}_{\rm II} = \begin{bmatrix} E_{11} - 3R_{11} & E_{12} & E_{13} \\ E_{12} & E_{22} - 3R_{22} & E_{23} \\ E_{13} & E_{23} & E_{33} \end{bmatrix} + \begin{bmatrix} 3R_{11} & 0 & 0 \\ 0 & 3R_{22} & 0 \\ 0 & 0 & 0 \end{bmatrix}, \tag{54}$$

To get the optimal element (BORP) set $R_{11} = \frac{1}{3}C_{11}^{-1}$ and $R_{22} = \frac{1}{3}C_{22}^{-1}$:

$$\mathbf{E}_{\rm I} + \mathbf{E}_{\rm II} = \begin{bmatrix} E_{11} - C_{11}^{-1} & E_{12} & E_{13} \\ E_{12} & E_{22} - C_{22}^{-1} & E_{23} \\ E_{13} & E_{23} & E_{33} \end{bmatrix} + \begin{bmatrix} C_{11}^{-1} & 0 & 0 \\ 0 & C_{22}^{-1} & 0 \\ 0 & 0 & 0 \end{bmatrix}, \tag{55}$$

For isotropic material this becomes

$$\mathbf{E}_{\rm I} + \mathbf{E}_{\rm II} = \frac{E}{1-\nu^2} \begin{bmatrix} \nu^2 & \nu & 0 \\ \nu & \nu^2 & 0 \\ 0 & 0 & \frac{1}{2}(1-\nu) \end{bmatrix} + E \begin{bmatrix} 1 & 0 & 0 \\ 0 & 1 & 0 \\ 0 & 0 & 0 \end{bmatrix}. \tag{56}$$

To match the (suboptimal) StrainRP, in which $R_{11} = \frac{1}{3}E_{11}$ and $R_{22} = \frac{1}{3}E_{22}$ the apropriate split is

$$\mathbf{E}_{\rm I} + \mathbf{E}_{\rm II} = \begin{bmatrix} 0 & E_{12} & E_{13} \\ E_{12} & 0 & E_{23} \\ E_{13} & E_{23} & E_{33} \end{bmatrix} + \begin{bmatrix} E_{11} & 0 & 0 \\ 0 & E_{22} & 0 \\ 0 & 0 & 0 \end{bmatrix}. \tag{57}$$

For isotropic material this becomes

$$\mathbf{E}_{\rm I} + \mathbf{E}_{\rm II} = E \begin{bmatrix} 0 & \nu & 0 \\ \nu & 0 & 0 \\ 0 & 0 & \frac{1}{2}(1-\nu) \end{bmatrix} + E \begin{bmatrix} 1 & 0 & 0 \\ 0 & 1 & 0 \\ 0 & 0 & 0 \end{bmatrix}. \tag{58}$$

Some FEM books suggest using the dilatational elasticity law for $\mathbf{E}_I$. As can be seen, the recommendation is incorrect for this element.

10.3. The Case $R_{12} \neq 0$

The case $R_{12} \neq 0$, arises in anisotropic displacement models for which $E_{13} \neq 0$ and/or $E_{23} \neq 0$. Now τ_2 and τ_3 must verify $E_{13}\gamma^{-1}\tau_2 + E_{23}\gamma\tau_3 = E_{13}\gamma^{-1} + E_{23}\gamma - 3R_{12}$. Solve for that τ_i $(i = 2, 3)$ that has an associated nonzero modulus. Note that the aspect ratio γ will generally appear in the SRI rule.

This case lacks practical interest because optimality can be achieved with $R_{12} = 0$. But for DispRP an obvious solution that eliminates all aspect ratio dependent is $\rho_1 = \rho_2 = \rho_3 = \tau_1 = \tau_2 = \tau_3 = 0$, whence $\mathbf{E}_{\rm I} = \mathbf{0}$, $\mathbf{E}_{\rm II} = \mathbf{E}$ and the fully integrated isoP element, which locks, is recovered.

10.4. Selective Directional Integration

The template can also be generated by non-Gaussian rules. For example, the following three-way directional split

$$\mathbf{E}_{\rm I} + \mathbf{E}_{\rm II} + \mathbf{E}_{\rm III} = \begin{bmatrix} E_{11} - C_{11}^{-1} & E_{12} & E_{13} \\ E_{12} & E_{22} - C_{22}^{-1} & E_{23} \\ E_{13} & E_{23} & E_{33} \end{bmatrix} + \begin{bmatrix} C_{11}^{-1} & 0 & 0 \\ 0 & 0 & 0 \\ 0 & 0 & 0 \end{bmatrix} + \begin{bmatrix} 0 & 0 & 0 \\ 0 & C_{22}^{-1} & 0 \\ 0 & 0 & 0 \end{bmatrix}, \tag{59}$$

generates the optimal panel in conjunction with three rules. Rule (I) is one-point Gauss with $\{\xi, \eta\} = \{0, 0\}$ and weight 4; Rule (II) has two points on the $y = 0$ median: $\{\xi, \eta\} = \{0, \pm 1/\sqrt{3}\}$ with weight 2; rule (III) has two points on the $x = 0$ median: $\{\xi, \eta\} = \{\pm 1/\sqrt{3}, 0\}$ with weight 2. This selective directional integration is difficult to extend to arbitrary quadrilaterals while preserving observer invariance.

Table 2. Signatures and Bending Ratios for Stress Hybrid Family

n_σ	5	7	13	21	31
R_{11}/E	0.33333	2.21173	2.21762	2.22125	2.22235
R_{22}/E	0.33333	0.35650	0.35967	0.35979	0.35981
R_{12}	0	0	0	0	0
r_x	1.00000	6.63518	6.65386	6.66375	6.66705
r_y	1.00000	1.06949	1.07900	1.07938	1.07944

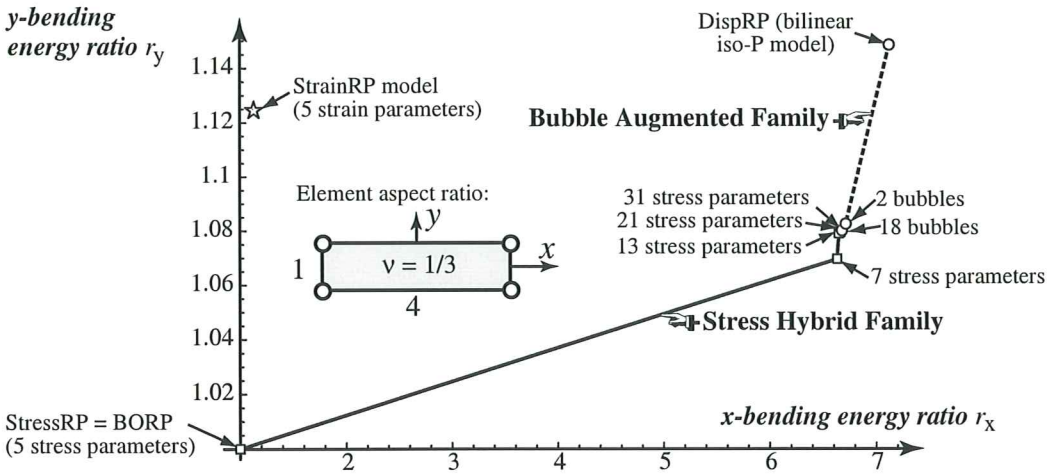

Figure 12. Representation of template families on the $\{r_x, r_y\}$ plane.

11. FUTILE FAMILIES

Families are template subsets that arise naturally from specific methods as function of discrete or continuous decision parameters. To render the concept more concrete, two historically important families for the rectangular panel are considered next.

11.1. Equilibrium Stress Hybrids

This family was studied in the late 1960s. It is obtained by generalizing the 5-parameter stress form of Section 4 with a polynomial series in $\{x, y\}$. An obvious choice is to make σ_{xx}, σ_{yy} and σ_{xy} complete polynomials in $\{x, y\}$:

$$\sigma_{xx} = \sum_{i,j} a_{ij}\, x^i y^j, \quad \sigma_{yy} = \sum_{i,j} b_{ij}\, x^i y^j, \quad \sigma_{xy} = \sum_{i,j} c_{ij}\, x^i y^j, \quad i \geq 0,\ j \geq 0,\ i + j \leq n. \tag{60}$$

For a complete expansion of order $n \geq 0$ one gets $3(n + 1)(n + 2)/2$ coefficients. Imposing strongly the two internal equilibrium equations $(1)_3$ for zero body forces reduces the set to $n_\sigma = 3 + 3n + n^2$ independent coefficients. For $n = 0, 1, 3, 5$ and 7 this gives $n_\sigma = 3, 7, 13, 21$ and 31 coefficients, respectively. (Only odd n is of interest beyond $n = 0$, since terms with $i + j = 2, 4, \ldots$ etc., cancel out on integrating strains over the rectangle and have no effect on the element stiffness.)

The stiffness equations of this family can be obtained by the hybrid stress method of Pian and Tong [26,46]. To display the effect of n_σ, the signature of the template (31)–(32) and the associated bending energy ratios were calculated for aspect ratio $\gamma = a/b = 4$, isotropic material with modulus E and Poisson's ratio $\nu = 1/3$.

Table 3. Signatures and Bending Ratios for Bubble-Augmented Family

n_b	0	2	18
R_{11}/E	2.37501	2.23894	2.22546
R_{22}/E	0.38281	0.36088	0.35998
R_{12}	0.	0.	0
r_x	7.12505	6.71683	6.67637
r_y	1.14844	1.08265	1.07994

The results are collected in Table 2. The bending energy ratios are displayed in Figure 12. Increasing the number of stress terms rapidly stiffens the element in x-bending. This is an instance of what may be called *equilibrium stress futility*: adding more stress terms makes things worse. (The phenomenon is well known but a representation such as that in Figure 12 is new.) As $n_\sigma \to \infty$ the template signature approaches the limit $R_{11}/E \approx 0.2224$ and $R_{22}/E \approx 0.3599$ to 4 places.

11.2. Bubble-Augmented Isoparametrics

A second family can be generated by starting from the conforming iso-P element DispRP of Section 6, and injecting n_b displacement bubble functions. (Bubble are shape functions that vanish over the element boundaries.) The idea is also a G2 curiosity but has resurfaced recently. Results for 2 and 18 bubbles (1 and 9 internal nodes, respectively) are collected in Table 3 and displayed also in Figure 12.

As can be expected injecting bubbles makes the element more flexible but the improvement is marginal. If $n_b \to \infty$ the signature approaches that of the $n_\sigma \to \infty$ hybrid-stress model of the previous subsection. For all this extra work (these models become expensive on account of high order Gauss integration rules and DOF condensation), r_x decreases from 7.12 to 6.67. This is a convincing illustration of *bubble futility*.

Figure 12 also marks the energy ratios of the StrainRP element. For this instance $R_{11}/E = R_{22}/E = 3/8 = 0.375$ and $r_x = r_y = 1.125$. Consequently the element is only slightly overstiff. Increasing the number of strain terms, however, would lead to another "futile family."

12. NUMERICAL EXAMPLES

Only three benchmark examples, all involving cantilever beams, are presented below.

12.1. Example 1: Slender Isotropic Cantilever

The slender 16:1 cantilever beam of Figure 13(a) is fabricated of isotropic material, with $E = 7680$, $\nu = 1/4$ and $G = (2/5)E = 3072$. The dimensions are shown in the Figure. Two end load cases are considered: an end moment $M = 1000$ and a transverse end shear $P = 48000/1027 = 46.7381$. The tip deflections $\delta_C = u_{yC}$ from beam theory: $ML^2/(2EI_z)$ and $PL^3/(3EI_z) + PL/(GA_s)$, in which $I_z = b^3h/12$ and $A_s = 5A/6 = 5bh/6$, are both exactly 100. For the second load case the shear deflection is only 0.293% of u_{yC}; thus the particular expression used for A_s is not very important.

Regular meshes with only one element ($N_y = 1$) through the beam height are considered. The number N_x of elements along the span is varied from 1 to 64, giving elements with aspect ratios that go from $\gamma = 16$ through $\gamma = \frac{1}{4}$. The root clamping condition is imposed by setting the u_x node displacement to zero at both root nodes, but u_y is only fixed at the lower one thus allowing for Poisson's contraction at the root.

Tables 4 and 5 report computed tip deflections u_{yC} for several element types. The first three rows list results for the 3 rectangular panel models of Sections 4–6. The last three rows give results for selected triangular elements. BODT is the Bending Optimal Drilling Triangle: a 3-node membrane element

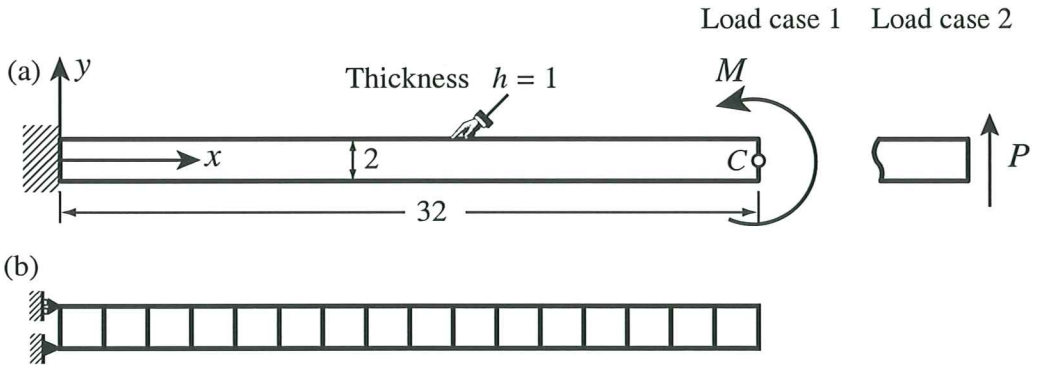

Figure 13. Slender cantilever beam for Examples 1 and 2.
A 16 × 1 FEM mesh with $\gamma = 1$ is shown in (b).

Table 4 Tip Deflections (exact=100) for Slender Isotropic Cantilever under End Moment

Element	Mesh: x-subdivisions × y-subdivisions ($N_x \times N_y$)						
	1 × 1 ($\gamma = 16$)	2 × 1 ($\gamma = 8$)	4 × 1 ($\gamma = 4$)	8 × 1 ($\gamma = 2$)	16 × 1 ($\gamma = 1$)	32 × 1 ($\gamma = \frac{1}{2}$)	64 × 1 ($\gamma = \frac{1}{4}$)
StressRP (BORP)	100.00	100.00	100.00	100.00	100.00	100.00	100.00
StrainRP	93.75	93.75	93.75	93.75	93.75	93.75	93.75
DispRP	0.97	3.75	13.39	37.49	68.18	85.71	91.60
ALL-EX	0.04	0.63	7.40	35.83	58.44	64.89	66.45
CST	0.32	1.25	4.46	12.50	22.73	28.57	30.53
BODT	100.00	100.00	100.00	100.00	100.00	100.00	100.00

Table 5 Tip Deflections (exact=100) for Slender Isotropic Cantilever under End Shear

Element	Mesh: x-subdivisions × y-subdivisions ($N_x \times N_y$)						
	1 × 1 ($\gamma = 16$)	2 × 1 ($\gamma = 8$)	4 × 1 ($\gamma = 4$)	8 × 1 ($\gamma = 2$)	16 × 1 ($\gamma = 1$)	32 × 1 ($\gamma = \frac{1}{2}$)	64 × 1 ($\gamma = \frac{1}{4}$)
StressRP (BORP)	75.02	93.72	98.39	99.56	99.86	99.94	99.97
StrainRP	70.35	87.88	92.26	93.35	93.63	93.71	93.73
DispRP	0.97	3.75	13.39	37.49	68.16	85.69	91.58
ALL-EX	0.24	0.69	6.36	35.18	59.59	65.70	67.03
CST	0.48	1.41	4.62	12.66	22.88	28.73	30.69
BODT	75.20	93.37	98.20	99.55	99.93	100.12	100.15

with drilling freedoms studied in [49,79,89,90]. ALL-EX is the exactly integrated 1988 Allman triangle with drilling freedoms [91]. CST is the Constant Strain Triangle, also called linear triangle and Turner triangle [1]. Both ALL-EX and BODT have three freedoms per node whereas all others have two. To get exactly 100.00% from BODT under an end-moment requires particular attention to the end load consistent lumping [90].

BORP is exact for all γ under end-moment and converges rapidly under end-shear. The performance of BODT is similar, inasmuch as this triangle is constructed to be bending exact in rectangular-mesh units. (In the end-shear load case BORP and BODT, which morph to different beam templates, converge to slightly different limits as $\gamma \to 0$.) StrainRP is about 6% stiffer than BORP, which can be expected since $1/(1-\nu^2) = 16/15$. DispRP, as well as the triangles ALL-EX and CST, lock as γ increases.

Table 6 Tip Deflections (exact=100) for Slender Anisotropic Cantilever under End Moment

Element	Mesh: x-subdivisions × y-subdivisions ($N_x \times N_y$)						
	1×1 ($\gamma = 16$)	2×1 ($\gamma = 8$)	4×1 ($\gamma = 4$)	8×1 ($\gamma = 2$)	16×1 ($\gamma = 1$)	32×1 ($\gamma = \frac{1}{2}$)	64×1 ($\gamma = \frac{1}{4}$)
StressRP (BORP)	100.00	100.00	100.00	100.00	100.00	100.00	100.00
StrainRP	2.26	2.26	2.26	2.26	2.26	2.26	2.26
DispRP	0.02	0.07	0.25	0.76	1.53	2.08	2.25

Table 7 Tip Deflections (exact=100) for Slender Anisotropic Cantilever under End Shear

Element	Mesh: x-subdivisions × y-subdivisions ($N_x \times N_y$)						
	1×1 ($\gamma = 16$)	2×1 ($\gamma = 8$)	4×1 ($\gamma = 4$)	8×1 ($\gamma = 2$)	16×1 ($\gamma = 1$)	32×1 ($\gamma = \frac{1}{2}$)	64×1 ($\gamma = \frac{1}{4}$)
StressRP (BORP)	74.95	93.68	98.37	99.54	99.84	99.92	99.96
StrainRP	1.70	2.12	2.22	2.26	2.26	2.26	2.26
DispRP	0.02	0.07	0.25	0.75	1.52	2.06	2.23

The response for more element layers through the height can be readily estimated from (45). Consequently those results are omitted to save space. For example, to predict the DispRP answer on a 8×4 mesh under end-moment, proceed as follows. The aspect ratio is $\gamma = 8$. From the $\gamma = 8$ column of Table 4 read off $r_x = 100/3.75 = 26.667$. Set $n = 2$ in (45) to get $r_x^{(4)} = (15 + r_x)/16 = 2.60417$. The estimated tip deflection is $100/2.60417 = 38.40$. Running the program gives $\delta_C = 38.3913$ as average of the y displacement of the two end nodes. Predictions for the end-shear-load case will not be as accurate.

12.2. Example 2: Slender Anisotropic Cantilever

Next assume that the beam of Figure 13(a) is fabricated of anisotropic material with the elasticity properties

$$\mathbf{E} = \begin{bmatrix} 880 & 600 & 250 \\ 600 & 420 & 150 \\ 250 & 150 & 480 \end{bmatrix}, \qquad \mathbf{C} = \mathbf{E}^{-1} = \frac{1}{35580}\begin{bmatrix} 1791 & -2505 & -150 \\ -2505 & 3599 & 180 \\ -150 & 180 & 96 \end{bmatrix}. \tag{61}$$

That these are physically realizable can be checked by getting the eigenvalues of $\mathbf{E}$: {1386.1, 387.3, 6.63}, whence both $\mathbf{E}$ and $\mathbf{C}$ are positive definite. The load magnitudes are adjusted to get beam-theory tip deflections of 100: $M = 2.58672$ and $P = 0.121153$. Since

$$E_{11}C_{11} = 44.297 \tag{62}$$

the energy ratio analysis of Sections 8.3–8.4, through equations (42) and (43), predict that the strain and displacement model will be big losers, because $r_x \geq 44.297$. This is verified in Tables 6 and 7, which report computed tip deflections u_{yC} for the three rectangular panel models. While BORP shines, the strain and displacement models are way off, regardless of how many elements one puts along x.

Putting more elements through the height will help StrainRP and DispRP but too slowly to be practical. To give an example, a 128×8 mesh of StrainRP (or clones) under end moment will have $r_x^{(8)} = (63 + 44.297)/64 = 1.68$ and estimated deflection of $100/1.67 = 59.67$. Running that mesh gives $u_{yC} = 59.65$. So using over 2000 freedoms in this trivial problem the results are still off by about 40%.

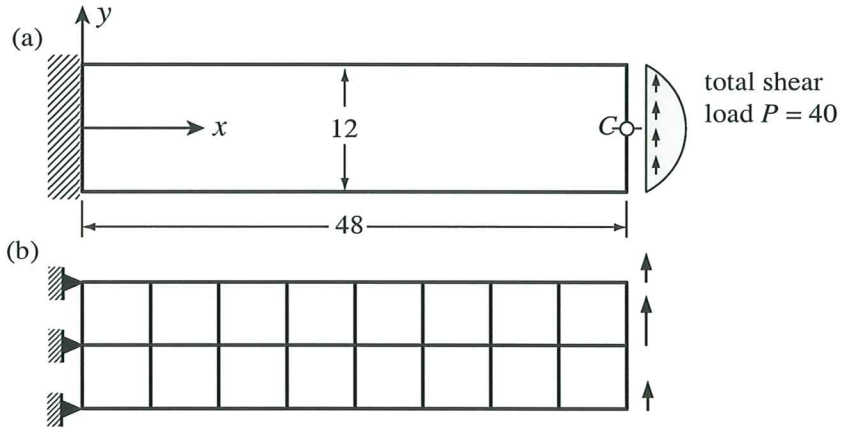

Figure 14. Short (Berkeley) cantilever under end shear: $E = 30000$, $\nu = 1/4$, $h = 1$; root contraction not allowed, a 8×2 mesh is shown in (b).

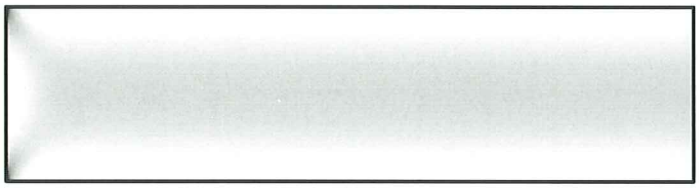

Figure 15. Intensity contour plot of σ_{xy} given by the 64×16 BORP mesh. Produced by *Mathematica* and Gaussian filtered by Adobe Photoshop. Stress node values averaged between adjacent elements. The root singularity pattern is clearly visible.

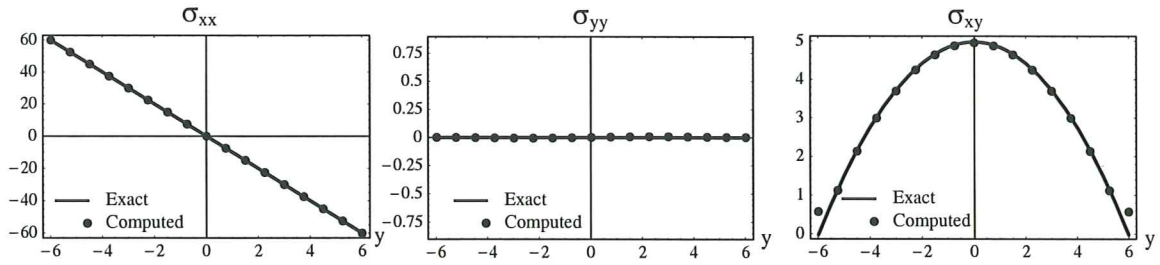

Figure 16. Distributions of σ_{xx}, σ_{yy} and σ_{xy} at $x = 12$ given by the 64×16 BORP mesh. Stress node values averaged between adjacent elements. Note different stress scales. Deviations at $y = \pm 6$ (free edges) due to "upwinded" y averaging.

12.3. Example 3: Short Cantilever Under End Shear

The shear-loaded cantilever beam defined in Figure 14 has been selected as a test problem for plane stress elements by many investigators since originally proposed in [92]. A full root-clamping condition is implemented by constraining both displacement components to zero at nodes located on at the root section $x = 0$. The applied shear load varies parabolically over the end section and is consistently lumped at the nodes. The main comparison value is the tip deflection $\delta_C = u_{yC}$ at the center of the end cross section. Reference [79] recommends $\delta_C = 0.35601$, which is also adopted here. The converged value of digits 4-5 is clouded by the mild singularity developing at the root section. This singularity is

Table 8 Tip Deflections (exact = 100) for Short Cantilever under End Shear

Element	Mesh: x-subdivisions × y-subdivisions ($N_x \times N_y$)				
	8 × 2	16 × 4	32 × 8	64 × 16	128 × 32
StressRP (BORP)	98.80	99.59	99.88	99.97	100.00
StrainRP	97.24	99.19	99.77	99.94	99.99
DispRP	88.83	96.83	99.16	99.78	99.95
ALL-EX	89.43	96.88	99.16	99.79	99.96
CST	55.09	82.59	94.90	98.65	99.66
BODT	101.68	100.30	100.03	100.00	100.00
	4 × 2	8 × 4	16 × 8	32 × 16	64 × 32
StressRP (BORP)	97.22	99.08	99.71	99.92	99.99
StrainRP	95.67	98.67	99.61	99.89	99.98
DispRP	69.88	90.05	97.24	99.28	99.82
ALL-EX	70.71	89.63	96.93	99.15	99.77
CST	37.85	69.86	90.04	97.25	99.28
BODT	96.68	98.44	99.37	99.78	99.93
	2 × 2	4 × 4	8 × 8	16 × 16	32 × 32
StressRP (BORP)	91.94	97.41	99.19	99.75	99.93
StrainRP	90.47	97.03	99.07	99.72	99.92
DispRP	37.84	70.57	90.39	97.35	99.31
ALL-EX	26.16	56.93	83.54	95.14	98.69
CST	17.83	43.84	75.01	92.13	97.86
BODT	92.24	96.99	98.70	99.48	99.81

displayed for σ_{xy} in the form of an intensity contour plot in Figure 15.

Table 8 gives computed deflections for rectangular mesh units with aspect ratios of 1, 2 and 4, using the three canonical rectangular panel models and the three triangles identified in Example 1. For end deflection reporting the load was scaled by (100/0.35601) so that the "theoretical solution" becomes 100.00. (In comparing stress values the unscaled load of $P = 40$ was used.)

There are no drastically small deflections because element aspect ratios only go up to 4:1. Elements StressRP (BORP), StrainRP and BODT outperformed the others. There is little to choose between these 3 models, which is typical of isotropic materials. The BODT triangle is geometrically more versatile but carries one more freedom per node.

Figure 16 plots averaged node stress values at section $x = 12$ computed from the 64 × 16 BODT mesh. The agreement with the standard beam stress distribution (that section being sufficiently away from the root) is very good except for σ_{xy} near the free edges $y = \pm 6$.

13. DISCUSSION AND CONCLUSIONS

What can templates contribute to FEM technology? Advantages in two areas are clear:

Synthesis. Only one procedure (module, function, subroutine) is written to do many elements. This simplifies comparison and verification benchmarking, as well as streamlining maintenance. A unified implementation automatically weeds out clones.

Customability. Templates can produce optimal and custom elements not obtainable (or hard to obtain) through conventional methods.

A striking example of the latter is the UBOTP macroelement presented in Section A.3 of the Appendix. This concludes a three decade search for a four noded trapezoid insensitive to distortion and that passes the patch test [67]. To the writer's knowledge, this model cannot be obtained with conventional formulations.

Will the synthesis power translate into teaching changes in finite element courses? This is not presently likely. Two reasons can be cited.

First, advantages may show up only in advanced or seminar-level courses. Beginning calculus students are not taught Lebesgue integration and distribution theory despite their wider scope. Likewise, introductory FEM courses are best organized around a few specific methods. Students must be exposed to a range of formulations and hands-on work before they can appreciate the advantages of unified implementation.

Second, the theory has not progressed to the point where the configuration of a template can be written down from first principles in front of an audience. Only two general rules are presently known: the fundamental decomposition into basic and higher order components, and the method to get the matrix structure of the basic part. No general rules to construct the higher order component can be stated aside from orthogonality and definiteness constraints.

How far can templates go? As of this writing templates are only known for a few elements in one and two dimensions, such as beams and flat plates of simple geometry. What is the major technical obstacle to go beyond those? Symbolic power. One must rely on computer-aided symbolic manipulation because geometric, constitutive and fabrication properties must be carried along as variables. This can lead, and does, to a combinatorial tarpit as elements become more complicated.

The good news is that computer algebra programs are gradually becoming more powerful, and are now routinely available on laptops and personal computers. Over the next ten years PCs are expected to migrate to 64-bit multiple-CPUs capable of addressing hundreds of GBs of memory at over 10GHz speeds. As that happens the development of templates for 3D solid and shell elements in reasonable time will become possible.

Acknowledgements

Preparation of this paper has been partly supported by the Finite Elements for Salinas contract with Sandia National Laboratories, and partly by the Spanish Ministerio of Educación y Cultura through a faculty fellowship while visiting the Centro Internacional de Métodos Numéricos en Ingeniería (CIMNE), in Barcelona, Spain, from April through June 2002.

References

[1] Turner, M. J., Clough, R. W., Martin, H. C., Topp, L. J., Stiffness and deflection analysis of complex structures, *J. Aero. Sci.*, **23**, 805–824, 1956.

[2] Argyris, J. H., Kelsey, S., *Energy Theorems and Structural Analysis*, London, Butterworth, 1960; Part I reprinted from *Aircr. Engrg.*, **26**, Oct-Nov 1954 and **27**, April-May 1955.

[3] Felippa, C. A., A historical outline of matrix structural analysis: a play in three acts, *Computers & Structures*, **79**, 1313–1324, 2001.

[4] Pestel, E. C., Leckie, F. A., *Matrix Methods in Elastomechanics*, McGraw-Hill, New York, 1963.

[5] Przemieniecki, J. S., *Theory of Matrix Structural Analysis*, McGraw-Hill, New York, 1968; Dover edition 1986.

[6] Gallaguer, R. H., *A Correlation Study of Methods of Matrix Structural Analysis*, Pergamon, Oxford, 1964.

[7] Melosh, R. J., Bases for the derivation of matrices for the direct stiffness method, *AIAA J.*, **1**, 1631–1637, 1963.

[8] Turner, M. J., The direct stiffness method of structural analysis, Structural and Materials Panel Paper, AGARD Meeting, Aachen, Germany, 1959.

[9] Turner, M. J., Dill, E. H., Martin, H. C., Melosh, R.J., Large deflection analysis of complex structures subjected to heating and external loads, *J. Aero. Sci.*, **27**, pp. 97-107, 1960.

[10] Turner, M. J., Martin, H. C., Weikel, R. C., Further development and applications of the stiffness method, in *AGARDograph 72: Matrix Methods of Structural Analysis*, ed. by B. M. Fraeijs de Veubeke, Pergamon Press, New York, 203–266, 1964.

[11] Melosh, R. J., Development of the stiffness method to define bounds on the elastic behavior of structures, *Ph.D. Dissertation*, University of Washington, Seattle, 1962.

[12] Fraeijs de Veubeke, B. M., Upper and lower bounds in matrix structural analysis, in *AGARDograph 72: Matrix Methods of Structural Analysis*, ed. by B. M. Fraeijs de Veubeke, Pergamon Press, New York, 174–265, 1964.

[13] Clough, R. W., The finite element method – a personal view of its original formulation, in *From Finite Elements to the Troll Platform – the Ivar Holand 70th Anniversary Volume*, ed. by K. Bell, Tapir, Norway, 89–100, 1994.

[14] Clough, R. W., The finite element method in plane stress analysis, *Proc. 2nd ASCE Conf. on Electronic Computation*, Pittsburgh, Pa, 1960.

[15] Clough, R. W., The finite element method in structural mechanics, in *stress Analysis*, ed. by O. C. Zienkiewicz and G. S. Holister, Wiley, London, 85–119, 1965.

[16] Fraeijs de Veubeke, B. M., Displacement and equilibrium models, in *Stress Analysis*, ed. by O. C. Zienkiewicz and G. Hollister, Wiley, London, 145–197, 1965; reprinted in *Int. J. Numer. Meth. Engrg.*, **52**, 287–342, 2001.

[17] Zienkiewicz, O. C., Cheung, Y. K., *The Finite Element Method in Engineering Science*, McGraw-Hill, London, 1967.

[18] Zienkiewicz, O. C., Cheung, Y. K., Finite elements in the solution of field problems, *The Engineer*, 507–510, 1965.

[19] Irons, B. M., Engineering application of numerical integration in stiffness methods, *AIAA J.*, **4**, pp. 2035–2037, 1966.

[20] Irons, B. M., Barlow, J., Comments on 'matrices for the direct stiffness method' by R. J. Melosh, *AIAA J.*, **2**, 403, 1964.

[21] Bazeley, G. P., Cheung, Y. K., Irons, B. M., Zienkiewicz, O. C., Triangular elements in plate bending – conforming and nonconforming solutions, in *Proc. 1st Conf. Matrix Meth. Struc. Mech.*, ed. by J. Przemieniecki et. al., AFFDL-TR-66-80, Air Force Institute of Technology, Dayton, Ohio, 1966, 547–576.

[22] Ergatoudis, J., Irons, B. M., Zienkiewicz, O. C., Curved, isoparametric, "quadrilateral" elements for finite element analysis, *Int. J. Solids Struc.*, **4**, 31–42, 1968.

[23] Irons, B. M., Ahmad, S., *Techniques of Finite Elements*, Ellis Horwood Ltd, Chichester, UK, 1980.

[24] Pian, T. H. H., Derivation of element stiffness matrices by assumed stress distributions, *AIAA J.*, **2**, 1333–1336, 1964.

[25] Pian, T. H. H., Element stiffness matrices for boundary compatibility and for prescribed boundary stresses, in *Proc. 1st Conf. on Matrix Methods in Structural Mechanics,* AFFDL-TR-66-80, Air Force Institute of Technology, Dayton, Ohio, 457–478, 1966.

[26] Pian, T. H. H., Tong, P., Basis of finite element methods for solid continua, *Int. J. Numer. Meth. Engrg.*, **1**, 3–29, 1969.

[27] Pian, T. H. H., Some notes on the early history of hybrid stress finite element method, *Int. J. Numer. Meth. Engrg.*, **47**, 2000, 419–425.

[28] Herrmann, L. R., Elasticity equations for nearly incompressible materials by a variational theorem, *AIAA Journal*, **3**, 1896–1900, 1965.

[29] Taylor, R. L., Pister, K. S., Herrmann, L. R., A variational principle for incompressible and nearly incompressible orthotropic elasticity, *Int. J. Solids Struc.*, **4**, 875-883, 1968.

[30] Strang, G., Fix, G., *An Analysis of the Finite Element Method.* Prentice-Hall, 1973.

[31] Strang, G., (1972). Variational crimes in the finite element method, in *The Mathematical Foundations of the Finite Element Method with Applications to Partial Differential Equations*, ed. by A. K. Aziz, Academic Press, New York, 689–710, 1972.

[32] Hughes, T. J. R., *The Finite Element Method: Linear Static and Dynamic Finite Element Analysis*, Prentice Hall, Englewood Cliffs, N. J., 1987.

[33] Atluri, S. N., Gallagher, R. N., Zienkiewicz, O. C. (eds.), *Hybrid and Mixed Finite Element Methods*, Wiley, New York, 1983.

[34] MacNeal, R. H., Derivation of element stiffness matrices by assumed strain distribution, *Nuclear Engrg. Design*, **70**, 3–12 (1978)

[35] Szabo, B., Babuska, I. , *Finite Element Analysis* Wiley, New York, 1991.

[36] MacNeal, R. H., The evolution of lower order plate and shell elements in MSC/NASTRAN, in T. J. R. Hughes and E. Hinton (eds.), *Finite Element Methods for Plate and Shell Structures, Vol. I: Element Technology*, Pineridge Press, Swansea, U.K., 1986, 85–127.

[37] MacNeal, R. H., *Finite Elements: Their Design and Performance*, Marcel Dekker, New York, 1994.

[38] Bergan, P. G., Finite elements based on energy orthogonal functions, *Int. J. Numer. Meth. Engrg.*, **15**, 1141–1555, 1980.

[39] Bergan, P. G., Nygård, M. K., Finite elements with increased freedom in choosing shape functions, *Int. J. Numer. Meth. Engrg.*, **20**, 643–664, 1984.

[40] Flanagan, D. P., Belytschko, T., A uniform strain hexahedron and quadrilateral with orthogonal hourglass control, *Int. J. Numer. Meth. Engrg.*, **17**, 679–706, 1981.

[41] Bathe, K. J., Dvorkin, E. N., A four-node plate bending element based on Mindlin-Reissner plate theory and a mixed interpolation, *Int. J. Numer. Meth. Engrg.*, **21**, 367–383, 1985.

[42] Huang, H. C., Hinton, E., A new nine node degenerated shell element with enhanced membrane and shear interpolation, *Int. J. Numer. Meth. Engrg.*, **22**, 73–92, 1986.

[43] Park, K. C., Stanley, G. M., A curved C^0 shell element based on assumed natural-coordinate strains, *J. Appl. Mech.*, **53**, 278–290, 1986.

[44] Stanley, G. M., Park, K. C., Hughes, T. J. R., Continuum based resultant shell elements, in T. J. R. Hughes and E. Hinton (eds.), *Finite Element Methods for Plate and Shell Structures, Vol. I: Element Technology*, Pineridge Press, Swansea, U.K., 1986, 1–45.

[45] Pian, T. H. H., Sumihara, K., Rational approach for assumed stress finite elements, *Int. J. Numer. Meth. Engrg.*, **20**, 1685–1695, 1984.

[46] Pian, T. H. H., Tong, P., Relations between incompatible displacement model and hybrid stress model, *Int. J. Numer. Meth. Engrg.*, **22**, 173-181, 1986.

[47] Punch, E. F., Atluri, S. N., Development and testing of stable, invariant, isoparametric curvilinear 2- and 3D hybrid stress elements, *Comp. Meths. Appl. Mech. Engrg.*, **47**, 331–356, 1984.

[48] Militello, C., Felippa, C. A., The First ANDES Elements: 9-DOF Plate Bending Triangles, *Comp. Meths. Appl. Mech. Engrg.*, **93**, 217–246, 1991.

[49] Felippa, C. A., Militello, C., Membrane triangles with corner drilling freedoms: II. The ANDES element, *Finite Elements Anal. Des.*, **12**, 189–201, 1992.

[50] Simo, J. C., Hughes, T. J. R., On the variational foundations of assumed strain methods, *J. Appl. Mech.*, **53**, 51–54, 1986.

[51] Simo, J. C., Rifai, M. S., A class of mixed assumed strain methods and the method of incompatible modes, *Int. J. Numer. Meth. Engrg.*, **29**, 1595–1638, 1990.

[52] Felippa, C. A., Militello, C., Developments in variational methods for high performance plate and shell elements, in *Analytical and Computational Models for Shells*, CED Vol. 3, Eds. A. K. Noor, T. Belytschko and J. C. Simo, The American Society of Mechanical Engineers, ASME, New York, 1989, 191–216.

[53] Fraeijs de Veubeke, B. M., Diffusive equilibrium models, in M. Geradin (ed.), *B. M. Fraeijs de Veubeke Memorial Volume of Selected Papers*, Sitthoff & Noordhoff, Alphen aan den Rijn, The Netherlands, 569–628, 1980.

[54] Bergan, P. G., Felippa, C. A., A triangular membrane element with rotational degrees of freedom, *Comp. Meths. Appl. Mech. Engrg.*, **50**, 25–69, 1985.

[55] Bergan, P. G., Felippa, C. A., Efficient implementation of a triangular membrane element with drilling freedoms, in T. J. R. Hughes and E. Hinton (eds.), *Finite Element Methods for Plate and Shell Structures, Vol. I: Element Technology*, Pineridge Press, Swansea, U.K., 1986, 128–152.

[56] Nygård, M. K., The Free Formulation for nonlinear finite elements with applications to shells, *Ph. D. Dissertation*, Division of Structural Mechanics, NTH, Trondheim, Norway, 1986.

[57] Felippa, C. A., Bergan, P. G., A triangular plate bending element based on an energy-orthogonal free formulation, *Comp. Meths. Appl. Mech. Engrg.*, **61**, 129–160, 1987.

[58] Felippa, C. A., Parametrized multifield variational principles in elasticity: II. Hybrid functionals and the free formulation, *Comm. Appl. Numer. Meth.*, **5**, 79–88, 1989.

[59] Felippa, C. A., The extended free formulation of finite elements in linear elasticity, *J. Appl. Mech.*, **56**, 609–616, 1989.

[60] Skeie, G., The Free Formulation: linear theory and extensions with applications to tetrahedral elements with rotational freedoms, *Ph. D. Dissertation*, Division of Structural Mechanics, NTH, Trondheim, Norway, 1991.

[61] Felippa, C. A., Clough, R. W., The finite element method in solid mechanics, in *Numerical Solution of Field Problems in Continuum Physics*, ed. by G. Birkhoff and R. S. Varga, SIAM–AMS Proceedings II, American Mathematical Society, Providence, R.I., 210–252, 1969.

[62] Taig, I. C., Kerr, R. I., Some problems in the discrete element representation of aircraft structures, in *Matrix Methods of Structural Analysis*, ed. by B. M. Fraeijs de Veubeke, Pergamon Press, London, 1964.

[63] Wilson, E. L., Taylor, R. L., Doherty, W. P., Ghaboussi, J., Incompatible displacement models, in *Numerical and Computer Models in Structural Mechanics*, ed. by S. J. Fenves, N. Perrone, A. R. Robinson and W. C. Schnobrich, Academic Press, New York, 43–57, 1973.

[64] Taylor, R. L., Wilson, E. L., Beresford, P. J., A nonconforming element for stress analysis, *Int. J. Numer. Meth. Engrg.*, **10**, 1211–1219, 1976.

[65] Belytschko, T., Liu, W. K., Engelmann, B. E., The gamma elements and related developments, in T. J. R. Hughes and E. Hinton (eds.), *Finite Element Methods for Plate and Shell Structures, Vol. I: Element Technology*, Pineridge Press, Swansea, U.K., 316–347, 1986.

[66] MacNeal, R. H., A simple quadrilateral shell element, *Computers & Structures*, **8**, 175–183, 1978.

[67] Lautersztajn-S, N., Samuelsson, A., Further discussion on four-node isoparametric elements in plane bending, *Int. J. Numer. Meth. Engrg.*, **47**, 129–140, 2000.

[68] Pian, T. H. H., Some notes on the early history of hybrid stress finite element method, *Int. J. Numer. Meth. Engrg.*, 419–425, 2000.

[69] Felippa, C. A., A survey of parametrized variational principles and applications to computational mechanics, *Comp. Meths. Appl. Mech. Engrg.*, **113**, 109–139, 1994.

[70] Felippa, C. A., Haugen, B., Militello, C., From the individual element test to finite element templates: evolution of the patch test, *Int. J. Numer. Meth. Engrg.*, **38**, 199–222, 1995.

[71] Felippa, C. A., Parametrized unification of matrix structural analysis: classical formulation and d-connected mixed elements, *Finite Elements Anal. Des.*, **21**, 45–74, 1995.

[72] Felippa, C. A., Recent developments in parametrized variational principles for mechanics, *Comput. Mech.*, **18**, 159–174, 1996.

[73] Felippa, C. A., Militello, C., Construction of optimal 3-node plate bending elements by templates, *Comput. Mech.*, **24**, 1–13 (1999).

[74] Felippa, C. A. Recent developments in basic finite element technologies, in *Computational Mechanics in Structural Engineering-Recent Developments*, ed. by F.Y. Cheng and Y. Gu, Elsevier, Amsterdam, 141–156, 1999.

[75] Felippa, C. A. Recent advances in finite element templates, in *Computational Mechanics for the Twenty-First Century*, ed. by B.J.V. Topping, Saxe-Coburn Publications, Edinburgh, U.K., 71–98, 2000.

[76] Bergan, P. G., Hanssen, L., A New Approach for Deriving 'Good' Finite Elements, in *The Mathematics of Finite Elements and Applications – Volume II*, ed. by J. R. Whiteman, Academic Press, London, 483–497, 1975.

[77] Hanssen, L., Bergan, P. G., Syversten, T. J., Stiffness derivation based on element convergence requirements, in *The Mathematics of Finite Elements and Applications – Volume III*, ed. by J. R. Whiteman, Academic Press, London, 83–96, 1979.

[78] Militello, C. and Felippa, C. A., The individual element patch revisited, in *The Finite Element Method in the 1990's — a book dedicated to O. C. Zienkiewicz*, ed. by E. Oñate, J. Periaux and A. Samuelsson, CIMNE, Barcelona and Springer-Verlag, Berlin, 554–564, 1991.

[79] Felippa, C. A., A study of optimal membrane triangles with drilling freedoms, submitted to *Comp. Meths. Appl. Mech. Engrg.*, 2002.

[80] Felippa, C. A., Customizing the mass and geometric stiffness of plane thin beam elements by Fourier methods, *Engrg. Comput.*, **18**, 286–303, 2001.

[81] Felippa, C. A., Customizing high performance elements by Fourier methods, *Trends in Computational Mechanics*, ed. by W. A. Wall, K.-U. Bleitzinger and K. Schweizerhof, CIMNE, Barcelona, Spain, 283-296, 2001.

[82] Doherty, W. P., Wilson, E. L., Taylor, R. L., Stress analysis of axisymmetric solids utilizing higher order quadrilateral finite elements, SESM Report 69-3, Department of Civil Engineering, University of California, Berkeley, 1969.

[83] Zienkiewicz, O. C., Taylor, R. L., Too, J. M., Reduced integration technique in general analysis of plates and shells, *Int. J. Numer. Meth. Engrg.*, **3**, 275–290, 1971.

[84] Pawsey, S. F., Clough, R. W., Improved numerical integration of thick shell finite elements, *Int. J. Numer. Meth. Engrg.*, **3**, 545–586, 1971.

[85] Kavanagh, K., Key, S. W., A note on selective and reduced integration techniques in the finite element method, *Int. J. Numer. Meth. Engrg.*, **4**, 148–150, 1972.

[86] Hughes, T. J. R., Generalization of selective integration procedures to anisotropic and nonlinear media, *Int. J. Numer. Meth. Engrg.*, **15**, 1413–148, 1980.

[87] Hughes, T. J. R., Malkus, D. S., Mixed finite element methods – reduced and selective integration techniques: a unification of concepts, *Comp. Meths. Appl. Mech. Engrg.*, bf 15, 63–81, 1978.

[88] Hughes, T. J. R., Malkus, D. S., A general penalty mixed equivalence theorem for anisotropic, incompressible finite elements, in *Hybrids and Mixed Finite Element Methods*, ed. by S. N. Atluri, R. H. Gallagher and O. C. Zienkiewicz, Wiley, London, 1983.

[89] Alvin, K., de la Fuente, H. M., Haugen, B., Felippa, C. A., Membrane triangles with corner drilling freedoms: I. The EFF element, *Finite Elements Anal. Des.*, **12**, 163–187, 1992.

[90] Felippa, C. A., Alexander, S., Membrane triangles with corner drilling freedoms: III. Implementation and performance evaluation, *Finite Elements Anal. Des.*, **12**, 203–239, 1992.

[91] Allman, D. J., Evaluation of the constant strain triangle with drilling rotations, *Int. J. Numer. Meth. Engrg.*, **26**, 2645–2655, 1988.

[92] Felippa, C. A., Refined finite element analysis of linear and nonlinear two-dimensional structures, *Ph.D. Dissertation*, Department of Civil Engineering, University of California at Berkeley, Berkeley, CA, 1966.

[93] Felippa, C. A., Optimal four noded membrane quadrilaterals, Report in preparation.

[94] Felippa, C. A., Fitting strains and displacements by minimizing dislocation energy, Report in preparation.

[95] Felippa, C. A., Park, K. C., The construction of free-free flexibility matrices for multilevel structural analysis, *Comp. Meths. Appl. Mech. Engrg.*, **191**, 2111-2140, 2002.

[96] MacNeal, R. H., Harder, R. L., A proposed standard set of problems to test finite element accuracy, *Finite Elements Anal. Des.*, **1**, 3–20, 1985.

[97] MacNeal, R. H., A theorem regarding the locking of tapered four noded membrane elements, *Int. J. Numer. Meth. Engrg.*, **24**, 1793–1799, 1987.

Appendix A. OTHER PANEL GEOMETRIES

The template framework of four noded membrane elements can be extended to more general geometries, at the cost of increased complexity in symbolic computations. This Appendix presents templates for parallelogram and trapezoidal geometries. The template for a general quadrilateral is the topic of a separate article [93].

The G1 direct elasticity methods of Sections 4–5 do not work beyond the parallelogram. The resulting "node collocation" elements fail the patch test and cannot be fitted in the template framework. Variational methods are required to get stress-assumed and strain-assumed elements that work. For stress elements the Hellinger-Reissner (HR) principle is used. For strain elements, a strain-fit method [94] in conjunction with de Veubeke's strain-displacement mixed functional is used.

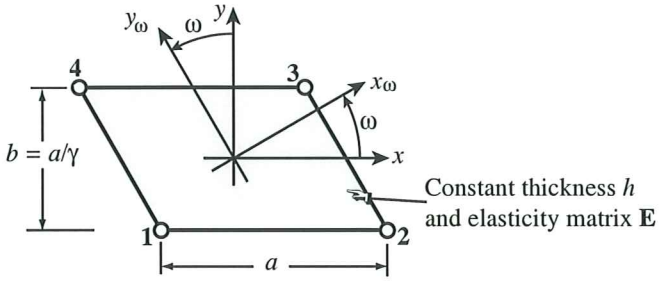

Figure 17. The 4-node parallelogram (swept) panel.

A.1 Parallelogram (Swept) Panel

The geometry of the parallelogram panel shown in Figure 17 is defined by the dimensions a, b and the skewangle ω, positive counterclockwise. The template again has the configuration (31) displayed in Figure 6. With $s = \tan\omega$ the matrices to be adjusted are

$$\mathbf{H}_c = \frac{1}{2ab}\begin{bmatrix} -b & 0 & b & 0 & b & 0 & -b & 0 \\ 0 & -a-bs & 0 & -a+bs & 0 & a+bs & 0 & a-bs \\ -a-bs & -b & -a+bs & b & a+bs & b & a-bs & -b \end{bmatrix}, \quad \mathbf{W} = \begin{bmatrix} \frac{1}{a} & 0 \\ -\frac{s}{b} & \frac{1}{b} \end{bmatrix}. \tag{63}$$

The higher order projector $\mathbf{H}_h$ is exactly as in (32), whereas $\mathbf{R}$ depends on the formulation, as explained below. For future use the compliance and elasticity in the median direction y_ω (see Figure 17) are denoted by

$$\begin{aligned} C^\omega_{22} &= C_{22}\cos^4\omega - 2C_{23}\cos^3\omega\sin\omega + (2C_{12}+C_{33})\cos^2\omega\sin^2\omega - 2C_{13}\cos\omega\sin^3\omega + C_{11}\sin^4\omega \\ &= \frac{C_{22} - 2C_{23}s + (2C_{12}+C_{33})s^2 - 2C_{13}s^3 + C_{11}s^4}{(1+s^2)^2}, \\ E^\omega_{22} &= E_{22}\cos^4\omega - 4E_{23}\cos^3\omega\sin\omega + (2E_{12}+4E_{33})\cos^2\omega\sin^2\omega - 4E_{13}\cos\omega\sin^3\omega + E_{11}\sin^4\omega \\ &= \frac{E_{22} - 4E_{23}s + (2E_{12}+4E_{33})s^2 - 4E_{13}s^3 + E_{11}s^4}{(1+s^2)^2}. \end{aligned} \tag{64}$$

Stress element. A 5-parameter stress element StressPP can be constructed either directly, as done by Gallagher [6, Ch. 3A], or by the HR principle, starting from the energy-orthogonal stress field

$$\begin{bmatrix} \sigma_{xx} \\ \sigma_{yy} \\ \sigma_{xy} \end{bmatrix} = \begin{bmatrix} 1 & 0 & 0 & y/b & \sin^2\omega\, x_\omega \\ 0 & 1 & 0 & 0 & \cos^2\omega\, x_\omega \\ 0 & 0 & 1 & 0 & -\sin\omega\cos\omega\, x_\omega \end{bmatrix} \begin{bmatrix} \mu_1 \\ \mu_2 \\ \mu_3 \\ \mu_4 \\ \mu_5 \end{bmatrix}, \tag{65}$$

in which $\sin\omega = s/\sqrt{1+s^2}$, $\cos\omega = 1/\sqrt{1+s^2}$, and $x_\omega = (x\cos\omega + y\sin\omega)/(a\cos\omega) = (x+ys)/a$. Both methods give the same stiffness. [Because (65) is an equilibrium field, an equilibrium stress hybrid formulation gives the same answer.] The stiffness is matched by the template with

$$R_{11} = \frac{1}{3C_{11}}, \quad R_{12} = 0, \quad R_{22} = \frac{1}{3C^\omega_{22}(1+s^2)^2}. \tag{66}$$

If the material is isotropic the diagonal entries are $R_{11} = \frac{1}{3}E$ and $R_{22} = \frac{1}{3}E/(1+s^2)^2$. The Q6 and QM6 elements continue to be clones of StressPP.

Strain element. A 5-parameter strain element StrainPP can be constructed by the direct elasticity method of Section 5, or by a variational strain-fitting method [94], starting from the companion of (65):

$$\begin{bmatrix} e_{xx} \\ e_{yy} \\ 2e_{xy} \end{bmatrix} = \begin{bmatrix} 1 & 0 & 0 & y/b & \sin^2\omega\, x_\omega \\ 0 & 1 & 0 & 0 & \cos^2\omega\, x_\omega \\ 0 & 0 & 1 & 0 & -2\sin\omega\cos\omega\, x_\omega \end{bmatrix} \begin{bmatrix} \chi_1 \\ \chi_2 \\ \chi_3 \\ \chi_4 \\ \chi_5 \end{bmatrix}. \tag{67}$$

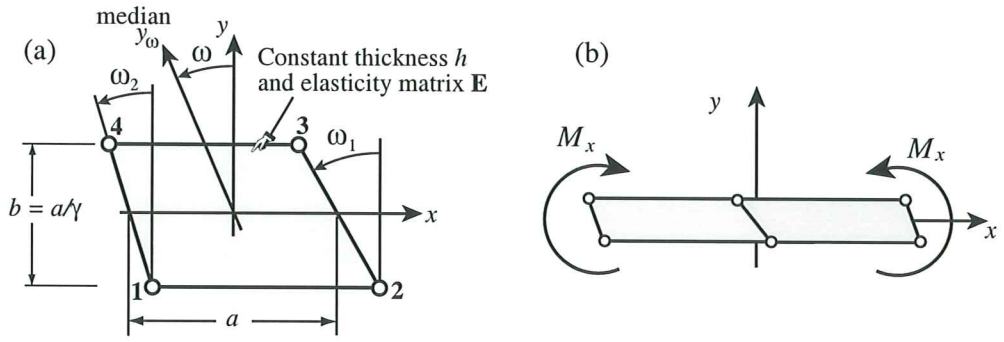

Figure 18. The four noded trapezoidal panel and a two-trapezoid repeatable macroelement.

Both methods give the same result. The stiffness is matched by setting

$$R_{11} = \tfrac{1}{3}E_{11}, \quad R_{12} = 0, \quad R_{22} = \frac{E^{\omega}_{22}}{3(1+s^2)^2}. \tag{68}$$

Displacement element. The conforming, exactly integrated isoparametric element DispPP is matched by setting

$$R_{11} = \frac{1}{3}\left(E_{11} + 4E_{13}s + (2E_{12}+4E_{33})s^2 + 4E_{23}s^3 + E_{22}s^4 + (E_{33} + 2E_{23}s + E_{22}s^2)\gamma^2\right),$$
$$R_{12} = \frac{1}{3\gamma}\left(E_{13} + (E_{12}+2E_{33})s + 3E_{23}s^2 + E_{22}s^3 + (E_{23}+E_{22}s)\gamma^2\right), \quad R_{22} = \frac{1}{3\gamma^2}(E_{33} + 2E_{23}s + E_{22}(s^2+\gamma^2)). \tag{69}$$

The StressPP element (as well as its clones Q6 and QM6) is again bending optimal along both x and y_ω (median) directions. The symbolic verification is far more involved than for the rectangular element because it requires the use of free-free flexibility methods [95], and is omitted.

A.2 Trapezoidal Panel

The geometry of the trapezoidal panel shown in Figure 18 is defined by the dimensions a, $b = a/\gamma$ and the two angles ω_1 and ω_2, both positive counterclockwise. Define

$$s_1 = \tan\omega_1, \quad s_2 = \tan\omega_2, \quad s = \tfrac{1}{2}(s_1 + s_2), \quad d = \tfrac{1}{2}(s_1 - s_2), \quad \phi = bd/a = d/\gamma. \tag{70}$$

The template is again given by the matrix form (34). Matrices $\mathbf{H}_c$ and $\mathbf{W}$ are as in (63), except that s has the new definition (70). The higher order projector matrix is

$$\mathbf{H}_h = \tfrac{1}{2}\begin{bmatrix} 1-\phi & 0 & -1+\phi & 0 & 1+\phi & 0 & -1-\phi & 0 \\ 0 & 1-\phi & 0 & -1+\phi & 0 & 1+\phi & 0 & -1-\phi \end{bmatrix}, \tag{71}$$

whereas $\mathbf{R}$ depends on the formulation, as detailed next.

Stress element. Element StressTP is generated by the 5-parameter stress assumption (65), with one change: the (1,4) entry y/b is replaced by $(y - y_C)/b$. If $y_C = -b^2(s_2 - s_1)/(12a) = -\frac{1}{6}ad/\gamma^2$ the bending stresses are energy orthogonal to constant stress fields. The stiffness matrix derived with the HR principle is matched by

$$R_{11} = \frac{1}{C_{11}(3 - d^2/\gamma^2)}, \quad R_{12} = 0, \quad R_{22} = \frac{1}{3C^{\omega}_{22}(1 + d^2/\gamma^2)(1+s^2)^2}, \tag{72}$$

in which C^{ω}_{22} is the compliance along the median y_ω (cf. Figure 18), given by (64).

QM6 element. The incompatible-mode element QM6 of [64] is no longer a clone of the stress element unless $d = 0$. Its stiffness is matched by

$$R_{11} = \frac{1}{C_{11}(3 - d^2/\gamma^2)}, \quad R_{12} = 0, \quad R_{22} = \frac{1}{C^{\omega}_{22}(3 - d^2/\gamma^2)(1+s^2)^2}. \tag{73}$$

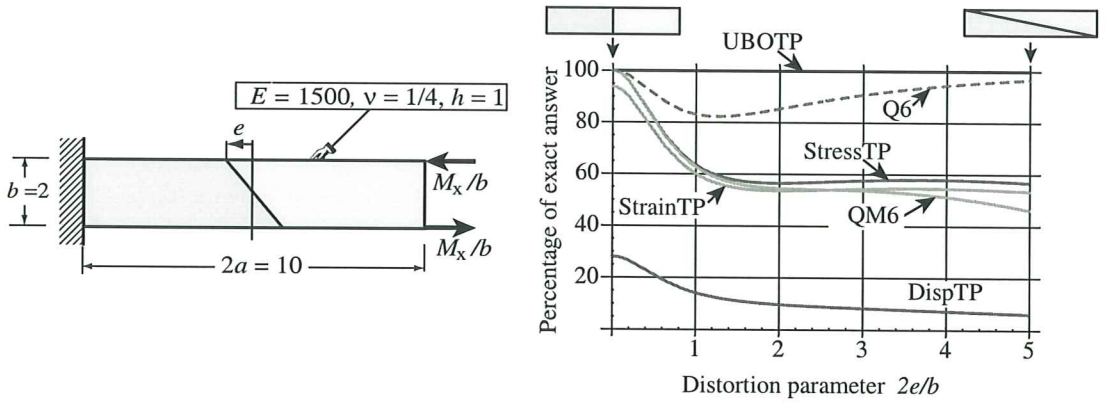

Figure 19. A well known distortion benchmark test. Dashed lines mark elements that fail the patch test (only Q6 in this plot). For additional results on other elements such as Pian-Sumihara and Enhanced Assumed Strain, see [67].

The only change is in R_{22}. The original incompatible-mode element Q6 of [63] fails the patch test if $d \neq 0$ and consequently cannot be matched by the template (31).

Strain element. Element StrainTP is generated by the 5-parameter strain assumption (67), with one change: the (1,4) entry y/b is replaced by $(y-y_C)/b$. Energy orthogonality is again obtained if $y_C = -b^2(s_2-s_1)/(12a) = -\frac{1}{6}ad/\gamma^2$. A strain-fitting variational formulation [94] yields a stiffness matched by

$$R_{11} = \frac{E_{11}}{3-d^2/\gamma^2}, \quad R_{12} = 0, \quad R_{22} = \frac{E^{\omega}_{22}}{3(1+d^2/\gamma^2)(1+s^2)^2}, \tag{74}$$

in which E^{ω}_{22} is the direct elasticity along the median y_ω direction, as given by (64).

Displacement element. The conforming isoparametric displacement element DispTP with 2×2 Gauss integration is matched by

$$\begin{aligned} R_{11} &= \frac{E_{11}+4E_{13}s+s^2(2E_{12}+4E_{33}+4E_{23}s+E_{22}s^2)+(E_{33}+2E_{23}s+E_{22}s^2)\gamma^2}{3-d^2/\gamma^2}, \\ R_{12} &= \frac{E_{13}+s(E_{12}+2E_{33}+3E_{23}s+E_{22}s^2)+(E_{23}+E_{22}s)\gamma^2}{\gamma(3-d^2/\gamma^2)}, \quad R_{22} = \frac{E_{33}+2E_{23}s+E_{22}(s^2+\gamma^2)}{\gamma^2(3-d^2/\gamma^2)} \end{aligned} \tag{75}$$

A.3 A Unidirectional-Bending-Optimal Trapezoidal Panel

Element StressTP is x-bending optimal (XBO) as an individual element, but far from it as a repeating macroelement. Consider the configuration of Figure 18(b): two mirror-image trapezoidal elements are put toghether to form a parallelogram macroelement. The macroelement shape is that of a swept panel, and is obviously repeatable along x.

If $a >> b$ and $s_1 \neq s_2$ the StressTP-fabricated macroelement rapidly becomes overstiff and overflexible in x- and y-bending, respectively. For example if $a/b = \gamma = 8$, $s_1 = 0$, $s_2 = 1/2$ and isotropic material with $\nu = 1/4$ the bending ratios are $r_x = 11.97$ and $r_y = 0.1414$. For the anisotropic elasticity matrix (61), $r_x = 6.93$ and $r_y = 0.0792$. If an elongated macroelement is supposed to model unidirectional x-bending correctly, the overstiffness caused by $s_1 \neq s_2$ is called *distortion locking*. This phenomenon has been widely studied since the MacNeal-Harder test suite gained popularity [96].

It is possible to construct a trapezoidal panel that is exact in unidirectional x bending when configured to form a repeatable macroelement as in Figure 18(b), for any aspect ratio γ as well as arbitrary side slopes s_1 and s_2. This template instance will be called UBOTP. A compact expression is obtained by taking the **R** matrix of StressTP,

generated by (72) and modifying the (2,1) entry of **W**:

$$\mathbf{W} = \begin{bmatrix} 1/a & 0 \\ -\dfrac{\left(C_{11}(3\gamma^2 - ds) + C_{13}\right)(s-d) - C_{12}d}{C_{11}(3\gamma^2 - d^2)b} & 1/b \end{bmatrix} \tag{76}$$

It would be equally possible to keep **W** of (63) and adjust the entries of **R**. However, the correction (76) points the way as to how to extend this result to arbitrary quadrilaterals [93].

It is not difficult to show that $\mathbf{W}^T\mathbf{R}\mathbf{W}$ for UBOTP is positive definite as long as the trapezoid is convex. Consequently the element stiffness is definite and has the proper rank.

Figure 19 presents results for a widely used mesh distortion test, which involves one macroelement of the type discussed. Results for six element types: UBOTP, StressTP, StrainTP, DispTP, Q6 and QM6 are shown. The percentage of the correct answer is of course $100/r_x$. Of these six models only Q6 fails the patch test, but otherwise works better than all others but UBOTP. StressTP, StrainTP and QM6 give similar results, as can be expected, whereas DispTP is way overstiff even for zero distortion. UBOTP gives the correct result for all distortion parameters from 0 through 5, since $r_x \equiv 1$. If the aspect ratio of the cantilever is changed to, say $2a/b = 10$, the differences between elements become more dramatic.

At first sight the existence of UBOTP contradicts a theorem by MacNeal [97], which says that four noded quadrilaterals cannot both pass the patch test and be insensitive to distortion. The escape hatch is that y-bending optimality (along the skew angular direction ω_1 of the macroelement) is not attempted. If one tries imposing $r_x = r_y = 1$, the solutions for $\{R_{11}, R_{12}, R_{22}\}$ become complex if $\gamma >> 1$ as soon as d deviates slightly from 0.

A Template Tutorial: Panels, Families, Clones, Winners and Losers

C. A. Felippa

Publication CIMNE Nº-219, September 2002

A Template Tutorial: Panels, Families, Clones, Winners and Losers

C.A. Felippa

Publication CIMNE Nº-219, September 2002

International Center for Numerical Methods in Engineering
Gran Capitán s/n, 08034 Barcelona, Spain

TABLE OF CONTENTS

A Template Tutorial: Panels, Families, Clones, Winners and Losers

CARLOS A. FELIPPA

Department of Aerospace Engineering Sciences
and Center for Aerospace Structures
University of Colorado
Boulder, Colorado 80309-0429, USA

Abstract

The article has a dual historical and educational theme. It is a tutorial on finite element templates for two-dimensional structural problems. The exposition focuses on the four-node plane stress element of flat rectangular geometry, called here the "rectangular panel" for brevity. This is one of the two oldest two-dimensional structural elements, soon to reach its gold anniversary. On the other hand the concept of finite element templates is a recent development. Interweaving the old and the new throws historical perspective into the "golden age" of discovery of finite elements. Templates provide a framework in which diverse element development methods can be fitted, compared and traced back to the sources. On the technical side templates have the virtue of facilitating the unified implementation of element families as well as the construction of custom elements. As an illustration of customization power, the Appendix presents the construction of a four noded bending optimal trapezoid that has eluded FEM investigators for several decades.

El agua es como un espejo en que desfilan las imágenes del pasado.
Ricardo Güiraldes, Don Segundo Sombra (1926)

Keywords: finite elements; history; templates; instances; clones; inplane bending; optimality; quadrilateral; membrane; plane stress; patch test; distortion sensitivity

1. INTRODUCTION

This article has a dual theme: historical and educational. To serve the latter, the exposition is written as a tutorial article on two-dimensional finite element templates. Part of this material is extracted from an advanced FEM course. Templates are parametrized algebraic forms that provide a continuum of consistent and stable finite element models of a given type and node/freedom configuration. Template instances produced by setting values to parameters furnish specific elements. If the template embodies all possible consistent and stable elements of a given type, it is called universal.

Befitting the tutorial aim, the exposition centers on the simplest 2D element that possesses a nontrivial template: the four-node plane stress element of flat rectangular geometry. [The three-node linear triangle is simpler but its template is trivial.] This is called the *rectangular panel* for brevity.

The rectangular panel is interesting from both historical and instructional viewpoints because:

1. It is one of the two oldest continuum mechanical elements, the other being the linear triangle [1].
2. Along with its plane strain and axisymmetric cousins, it is the configuration treated by most new methods since the birth of finite elements. Thus it provides an *in-vivo* specimen of FEM evolution over the past 50 years.
3. It is amenable to complete analytical development, even for anisotropic material law. This makes the element particularly suitable for homework and project assignments.
4. Analytical forms make the concept of template signatures and clones highly visible to students.

The paper is organized as follows. Section 2 outlines element formulations from 1950 to date. Section 3 introduces the focus problem. Sections 4–6 follow up on the historical theme by developing stress, strain and displacement-based models for the rectangular panel.

The concept of template is introduced in Section 7 by calling attention to a common structure lurking behind the stiffness expressions of stress, strain and displacement elements. Template terminology follows as consequence of this idea: families, signatures, instances and clones. The role of higher order patch tests in optimality is illustrated in Chapters 8–9. The SRI scheme is worked out in Section 10 to show that templates naturally lead to correct splittings of the elasticity law. The concept of element families is illustrated in Section 11 using stress hybrid and displacement bubbles as examples. Section 11 provides numerical examples and Section 12 discussion and conclusions. The Appendix collects templates for more general geometries to give a glimpse into the unifying power of this concept for constructing custom elements.

2. HISTORICAL SKETCH

This section summarizes the history of structural finite elements since 1950 to date. It functions as a hub for dispersed historical references. Readers uninterested in historical aspects should skip directly to Section 3.

For exposition convenience, structural "finitelementology" may be divided into fourth generations that span 10 to 15 years each. There are no sharp intergenerational breaks but noticeable change of emphasis. The following summary does not cover the conjoint evolution of Matrix Structural Analysis into the Direct Stiffness Method from 1934 through 1970. This was the subject of a separate essay [3].

2.1. G1: The Pioneers

The 1956 paper by Turner, Clough, Martin and Topp [1], henceforth abbreviated to TCMT, is recognized as the start of the current FEM, as used in the overwhelming majority of commercial codes. Along with Argyris' serial [2] they prototype the first generation, which spans 1950 through 1962. A panoramic picture of this period is available in two textbooks [4,5]. Przemieniecki's text is still reprinted by Dover. The survey by Gallagher [6] was influential but is now difficult to access outside libraries.

The pioneers were structural engineers, schooled in classical mechanics. They followed a century of tradition in regarding structural elements as a device to transmit forces. This "element as force transducer" was the standard view in pre-computer structural analysis. It explains the use of flux assumptions to derive stiffness equations. Element developers worked in, or interacted closely with, the aircraft industry. (One reason is that only large aerospace companies were then able to afford mainframe computers.) Accordingly they focused on thin structures built up with bars, ribs, spars, stiffeners and panels. Although the Classical Force method dominated stress analysis during the 1950s, stiffness methods were kept alive by use in dynamics.

2.2. G2: The Golden Age

The next period spans the golden age of FEM: 1962–1972. This is the "variational generation." Melosh [7] showed that conforming displacement models are a form of Rayleigh-Ritz based on the minimum potential energy principle. This influential paper marks the confluence of three lines of research: Argyris' dual formulation of energy methods [2], the Direct Stiffness Method (DSM) of Turner [8–10], and early ideas of interelement compatibility as basis for error bounding and convergence [11,12]. G1 workers thought of finite elements as idealizations of structural components. From 1962 onward a two-step interpretation emerges: discrete elements approximate continuum models, which in turn approximate real structures.

By the early 1960s FEM begins to expand into Civil Engineering through Clough's Boeing-Berkeley connection [13] and had been named [14,15]. Reading de Veubeke's famous article [16] side by side with

TCMT [1] one can sense the ongoing change in perspective opened up by the variational framework. The first book devoted to FEM appears in 1967 [17]. Applications to nonstructural problems start by 1965 [18].

From 1962 onwards the displacement formulation dominates. This was given a big boost by the invention of the isoparametric formulation and related tools (numerical integration, fitted coordinates, shape functions, patch test) by Irons and coworkers [19–23]. Low order displacement models often exhibit disappointing performance. Thus there was a frenzy to develop higher order elements. Other variational formulations, notably hybrids [24–27], mixed [28,29] and equilibrium models [16] emerged. G2 can be viewed as closed by the monograph of Strang and Fix [30], the first book to focus on the mathematical foundations.

2.3. G3: Consolidation

The post-Vietnam economic doldrums are mirrored during this post-1972 period. Gone is the youthful exuberance of the golden age. This is consolidation time. Substantial effort is put into improving the stock of G2 displacement elements by tools initially labeled "variational crimes" [31], but later justified. A comprehensive exposition may be found in Hughes' textbook [32]. Hybrid and mixed formulations record steady progress [33]. Assumed strain formulations appear [34]. A booming activity in error estimation and mesh adaptivity is fostered by better understanding of the mathematical foundations [35].

Commercial FEM codes gradually gain importance. They provide a reality check on what works in the real world and what doesn't. By the mid-1980s there was gathering evidence that complex and high order elements were commercial flops. Exotic gadgetry interweaved amidst millions of lines of code easily breaks down in new releases. Complexity is particularly dangerous in nonlinear and dynamic analyses conducted by novice users. A trend back toward simplicity starts [36,37].

2.4. G4: Back to Basics

The fourth generation begins by the early 1980s. More approaches come on the scene, notably the Free Formulation [38,39], orthogonal hourglass control [40], Assumed Natural Strain methods [41–44], stress hybrid models in natural coordinates [45–47], as well as derivatives: ANDES [48,49], EAS [50,51] and others. Although technically diverse the G4 approaches share two common objectives:

(i) Elements must fit into DSM-based programs since that includes the vast majority of production codes, commercial or otherwise.

(ii) Elements are kept simple but should provide answers of engineering accuracy with relatively coarse meshes. These were collectively labeled "high performance elements" in 1989 [52].

"Things are always at their best in the beginning," said Pascal. Indeed. By now FEM looks like an aggregate of largely disconnected methods and recipes. Sections 4-6 look at three disparate components of this edifice to set up the subsequent exhibition of common features by templates.

3. PROBLEM DESCRIPTION

3.1. Governing Equations

Consider the thin homogeneous plate in plane stress sketched in Figure 1. The inplane displacements are $\{u_x, u_y\}$, the associated strains are $\{e_{xx}, e_{yy}, e_{xy}\}$ and the inplane (membrane) stresses are $\{\sigma_{xx}, \sigma_{yy}, \sigma_{xy}\}$. Prescribed inplane body forces are $\{b_x, b_y\}$, but they will be set to zero in derivations of equilibrium elements. Prescribed displacements and surface tractions are denoted by $\{\hat{u}_x, \hat{u}_y\}$ and $\{\hat{t}_x, \hat{t}_y\}$ respectively. All fields are considered uniform through the thickness h. The governing plane-stress elasticity equations

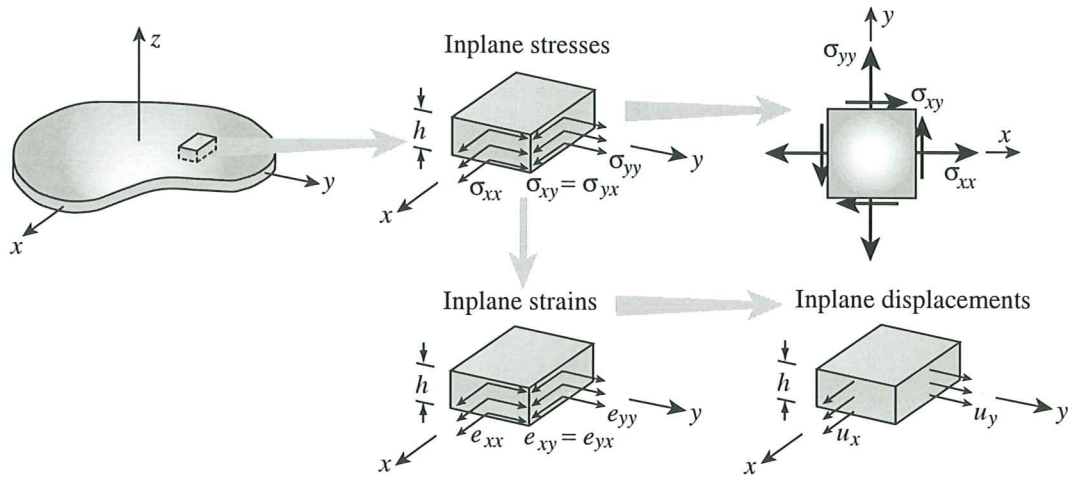

Figure 1. A thin plate in plane stress, illustrating notation.

are

$$\begin{bmatrix} e_{xx} \\ e_{yy} \\ 2e_{xy} \end{bmatrix} = \begin{bmatrix} \partial/\partial x & 0 \\ 0 & \partial/\partial y \\ \partial/\partial y & \partial/\partial x \end{bmatrix} \begin{bmatrix} u_x \\ u_y \end{bmatrix}, \qquad \begin{bmatrix} \sigma_{xx} \\ \sigma_{yy} \\ \sigma_{xy} \end{bmatrix} = \begin{bmatrix} E_{11} & E_{12} & E_{13} \\ E_{12} & E_{22} & E_{23} \\ E_{13} & E_{23} & E_{33} \end{bmatrix} \begin{bmatrix} e_{xx} \\ e_{yy} \\ 2e_{xy} \end{bmatrix},$$
$$\begin{bmatrix} \partial/\partial x & 0 & \partial/\partial y \\ 0 & \partial/\partial y & \partial/\partial x \end{bmatrix} \begin{bmatrix} \sigma_{xx} \\ \sigma_{yy} \\ \sigma_{xy} \end{bmatrix} + \begin{bmatrix} b_x \\ b_y \end{bmatrix} = \begin{bmatrix} 0 \\ 0 \end{bmatrix}. \tag{1}$$

The compact matrix version of (1) is

$$\mathbf{e} = \mathbf{D}\mathbf{u}, \qquad \boldsymbol{\sigma} = \mathbf{E}\mathbf{e}, \qquad \mathbf{D}^T\boldsymbol{\sigma} + \mathbf{b} = \mathbf{0}, \tag{2}$$

in which $\mathbf{E}$ is the plane stress elasticity matrix. The inverse of $\boldsymbol{\sigma} = \mathbf{E}\mathbf{e}$ is

$$\begin{bmatrix} e_{xx} \\ e_{yy} \\ 2e_{xy} \end{bmatrix} = \begin{bmatrix} C_{11} & C_{12} & C_{13} \\ C_{12} & C_{22} & C_{23} \\ C_{13} & C_{23} & C_{33} \end{bmatrix} \begin{bmatrix} \sigma_{xx} \\ \sigma_{yy} \\ \sigma_{xy} \end{bmatrix}, \quad \text{or} \quad \mathbf{e} = \mathbf{C}\boldsymbol{\sigma}, \tag{3}$$

where $\mathbf{C} = \mathbf{E}^{-1}$ is the matrix of elastic compliances.

3.2. The Rectangular Panel

The focus of this article, called the "rectangular panel," is shown in Figure 2. For an individual element the side-aligned local axes are also denoted as $\{x, y\}$ for brevity. The inplane dimensions are a and $b = a/\gamma$, where $\gamma = a/b$ is the aspect ratio. The thickness and elastic properties are constant over the element. The element has 4 corner nodes and 8 external (connective) degrees of freedom. The node displacement and force vectors are configured as

$$\mathbf{u} = [\, u_{x1} \quad u_{y1} \quad u_{x2} \quad u_{y2} \quad u_{x3} \quad u_{y3} \quad u_{x4} \quad u_{y4} \,]^T, \tag{4}$$

$$\mathbf{f} = [\, f_{x1} \quad f_{y1} \quad f_{x2} \quad f_{y2} \quad f_{x3} \quad f_{y3} \quad f_{x4} \quad f_{y4} \,]^T. \tag{5}$$

As noted in the Introduction most of the FEM formulation methods chronicled in Section 2 have been tried on this configuration as well as its plane strain and axisymmetric cousins. The reason for this popularity is that the rectangular panel is the *simplest multidimensional element that can be improved.* (The three-node linear triangle is simpler but cannot be improved.)

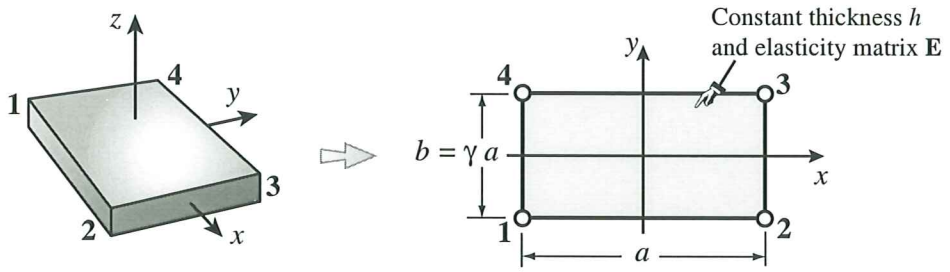

Figure 2. The rectangular panel.

In keeping with the expository theme, the next three sections derive the rectangular panel stiffness from stress, strain and displacement assumptions, respectively. Mirroring history, the derivation of stress and strain models follows the matrix-based direct elasticity approach used by the first generation, as summarized in Gallagher's review [6].

Ironically, the direct derivation will give optimal or near-optimal elements with no sweat whereas the variationally derived displacement model needs tweaking (e.g., by SRI) to become useful.

4. THE STRESS ELEMENT

TCMT [1] is the starting point. In a historical summary Clough [13] remarks that the paper belatedly reports work performed at Boeing's Commercial Airplane Division in 1952-53 (indeed [1, p. 805] states that the material was presented at the 22nd Annual Meeting of IAS, held on January 25–29, 1954.) In addition to bars, beams and spars, TCMT presents two plane stress elements for modeling wing cover plates: the three-node triangle and the four-node flat rectangular panel. Quadrilateral panels of arbitrary geometry, not necessarily flat, were constructed as assemblies of four triangles.

Readers perusing that article for the first time have a surprise in store. The stiffness properties of both panel elements are derived from stress assumptions, rather than displacements, as became popular in the second generation. More precisely, simple patterns of interelement boundary tractions (a.k.a. stress flux modes) that satisfy internal equilibrium are taken as starting point. Twenty years later and apparently unaware of TCMT, Fraeijs de Veubeke [53] systematically extended the same idea in a variational setting, to produce what he called diffusive equilibrium elements. These are designed to weakly enforce interelement flux conservation. The comedy continues: twenty year later mathematicians rediscovered flux elements, now renamed as "Discontinuous Galerkin Methods," blessfully unaware of previous work.

The derivation below largely follows Chapter 3 of Gallagher [6], who presents a step by step procedure for what he calls the "equivalent force" approach. The main extension provided here is allowing anisotropy.

4.1. The 5-Parameter Stress Field

Since TCMT the appropriate stress field for the rectangular panel is known to be [6, p. 19]

$$\sigma_{xx} = \mu_1 + \mu_4 \frac{y}{b}, \qquad \sigma_{yy} = \mu_2 + \mu_5 \frac{x}{a}, \qquad \sigma_{xy} = \mu_3. \tag{6}$$

The five μ_i are stress-amplitude parameters with dimension of stress. They are collected in the 5-vector

$$\boldsymbol{\mu} = [\,\mu_1 \quad \mu_2 \quad \mu_3 \quad \mu_4 \quad \mu_5\,]^T. \tag{7}$$

The field (6) satisfies the internal equilibrium equations $(1)_3$ under zero body forces. Evaluation over element sides produces the traction flux patterns of Figure 3, copied verbatim from TCMT. Why five? "These load states are seen to represent uniform and linearly varying stresses plus constant shear, along

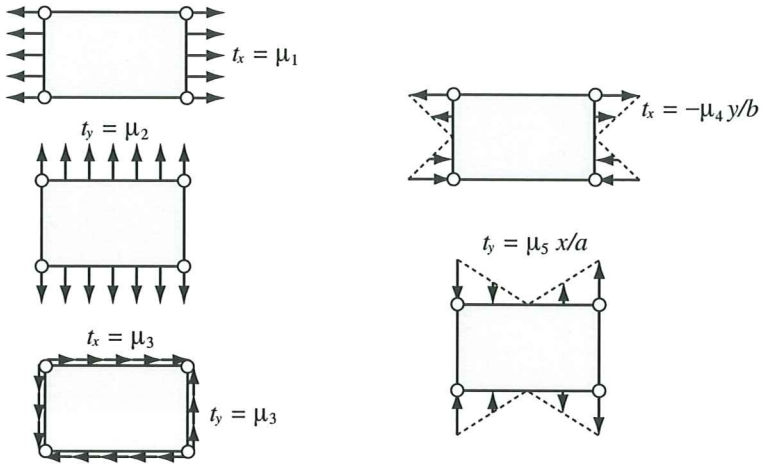

Figure 3. Nonzero interelement boundary tractions associated with the stress parameters μ_i in (7). After [1, p. 812], in which these five patterns are called "load states."

the plate edges. Later it will be seen that the number of load states must be $2n - 3$, where n = number of nodes." [1, p. 813].

To establish connection to node displacements, $\boldsymbol{\mu}$ is extended as

$$\boldsymbol{\mu}_+ = [\,\mu_1 \quad \mu_2 \quad \mu_3 \quad \mu_4 \quad \mu_5 \quad \mu_6 \quad \mu_7 \quad \mu_8\,]^T \tag{8}$$

This array contains three dimensionless coefficients: μ_6, μ_7 and μ_8, which define amplitudes of the three element rigid body modes (RBMs):

$$\text{RBM\#1: } u_x = \mu_6 a,\ u_y = 0, \quad \text{RBM\#2: } u_x = 0,\ u_y = \mu_7 b, \quad \text{RBM\#3: } u_x = -\mu_8 y,\ u_y = \mu_8 x, \tag{9}$$

These modes produce zero stress. The foregoing relations may be recast in matrix form:

$$\boldsymbol{\sigma} = \mathbf{N}\boldsymbol{\mu} = \mathbf{N}_+\boldsymbol{\mu}_+, \quad \mathbf{N} = \begin{bmatrix} 1 & 0 & 0 & \frac{y}{b} & 0 \\ 0 & 1 & 0 & 0 & \frac{x}{a} \\ 0 & 0 & 1 & 0 & 0 \end{bmatrix}, \quad \mathbf{N}_+ = \begin{bmatrix} 1 & 0 & 0 & \frac{y}{b} & 0 & 0 & 0 & 0 \\ 0 & 1 & 0 & 0 & \frac{x}{a} & 0 & 0 & 0 \\ 0 & 0 & 1 & 0 & 0 & 0 & 0 & 0 \end{bmatrix}. \tag{10}$$

The boundary traction patterns of Figure 3 are converted to node forces by statics. This yields

$$\mathbf{f} = \mathbf{A}\,\boldsymbol{\mu}, \qquad \mathbf{A}^T = \tfrac{1}{2}h \begin{bmatrix} -b & 0 & b & 0 & b & 0 & -b & 0 \\ 0 & -a & 0 & -a & 0 & a & 0 & a \\ -a & -b & -a & b & a & b & a & -b \\ \frac{1}{6}b & 0 & -\frac{1}{6}b & 0 & \frac{1}{6}b & 0 & -\frac{1}{6}b & 0 \\ 0 & \frac{1}{6}a & 0 & -\frac{1}{6}a & 0 & \frac{1}{6}a & 0 & -\frac{1}{6}a \end{bmatrix}. \tag{11}$$

Matrix $\mathbf{A}$ is the equilibrium matrix, also called the leverage matrix in the early FEM literature. When restricted to the constant stress states (the first three columns of $\mathbf{A}$), it is called a force-lumping matrix and denoted by $\mathbf{L}$ in the Free Formulation of Bergan [38,39,54–60].

4.2. The Generalized Stiffness

Integrating the complementary energy density $\mathcal{U}^* = \frac{1}{2}\boldsymbol{\sigma}^T\mathbf{C}\boldsymbol{\sigma}$ over the element volume V and identifying $U^* = \int_{V^e} \mathcal{U}^*\, dV$ with $\frac{1}{2}\boldsymbol{\mu}^T\mathbf{F}_\mu\boldsymbol{\mu}$ yields the 5×5 flexibility matrix $\mathbf{F}_\mu$ in terms of the stress parameters.

Its inverse is the generalized stiffness matrix $\mathbf{S}_\mu = \mathbf{F}_\mu^{-1}$:

$$\mathbf{F}_\mu = V\begin{bmatrix} C_{11} & C_{12} & C_{13} & 0 & 0 \\ C_{12} & C_{22} & C_{23} & 0 & 0 \\ C_{13} & C_{23} & C_{33} & 0 & 0 \\ 0 & 0 & 0 & \frac{1}{12}C_{11} & 0 \\ 0 & 0 & 0 & 0 & \frac{1}{12}C_{22} \end{bmatrix}, \quad \mathbf{S}_\mu = \frac{1}{V}\begin{bmatrix} E_{11} & E_{12} & E_{13} & 0 & 0 \\ E_{12} & E_{22} & E_{23} & 0 & 0 \\ E_{13} & E_{23} & E_{33} & 0 & 0 \\ 0 & 0 & 0 & 12C_{11}^{-1} & 0 \\ 0 & 0 & 0 & 0 & 12C_{22}^{-1} \end{bmatrix}, \quad (12)$$

in which $V = abh$ is the volume of the element.

4.3. The Physical Stiffness

Integration of the slave strain field $\mathbf{e} = \mathbf{E}^{-1}\boldsymbol{\sigma} = \mathbf{C}\mathbf{N}_+\boldsymbol{\mu}_+$ produces the displacement field

$$\begin{aligned} u_x(x,y) &= \mu_6 a + \tfrac{1}{8}\omega_6 + (\mu_1 C_{11} + \mu_2 C_{12} + \mu_3 C_{13})x + (\tfrac{1}{2}(\mu_1 C_{13} + \mu_2 C_{23} + \mu_3 C_{33}) - \mu_8)y \\ &\quad + \tfrac{1}{2}(\mu_5/a)C_{12}x^2 + (\mu_4/b)C_{11}xy + \tfrac{1}{2}\big((\mu_4/b)C_{13} - (\mu_5/a)C_{22}\big)y^2, \\ u_y(x,y) &= \mu_7 b + \tfrac{1}{8}\omega_7 + (\tfrac{1}{2}(\mu_1 C_{13} + \mu_2 C_{23} + \mu_3 C_{33}) + \mu_8)x + (\mu_1 C_{12} + \mu_2 C_{22} + \mu_3 C_{23})y \\ &\quad + \tfrac{1}{2}\big((\mu_5/a)C_{23} - (\mu_4/b)C_{11}\big)x^2 + (\mu_5/a)C_{22}xy + \tfrac{1}{2}(\mu_4/b)C_{12}y^2. \end{aligned} \quad (13)$$

with $\omega_6 = -b^2C_{13}\mu_4/b + (b^2C_{22} - a^2C_{12})(\mu_5/a)$ and $\omega_7 = (a^2C_{11} - b^2C_{12})(\mu_4/b) - a^2C_{23}\mu_5/a$. The constant terms in u_x and u_y, which do not affect strains and stresses, have been adjusted to get relatively simple terms in columns 4 through 8 of the matrix $\mathbf{T}_+$ below. Physically, (13) aligns the bending deformation patterns along the $\{x, y\}$ axes. Evaluating (13) at the nodes we obtain the matrix that connects node displacements to stress parameters: $\mathbf{u} = \mathbf{T}_+\boldsymbol{\mu}_+$, where

$$\mathbf{T}_+ = \tfrac{1}{4}\begin{bmatrix} -2aC_{11} - bC_{13} & -2aC_{12} - bC_{23} & -2aC_{13} - bC_{33} & aC_{11} & 0 & 4a & 0 & 2b \\ -2bC_{12} - aC_{13} & -2bC_{22} - aC_{23} & -2bC_{23} - aC_{33} & 0 & bC_{22} & 0 & 4b & -2a \\ 2aC_{11} - bC_{13} & 2aC_{12} - bC_{23} & 2aC_{13} - bC_{33} & -aC_{11} & 0 & 4a & 0 & 2b \\ -2bC_{12} + aC_{13} & -2bC_{22} + aC_{23} & -2bC_{23} + aC_{33} & 0 & -bC_{22} & 0 & 4b & 2a \\ 2aC_{11} + bC_{13} & 2aC_{12} + bC_{23} & 2aC_{13} + bC_{33} & aC_{11} & 0 & 4a & 0 & -2b \\ 2bC_{12} + aC_{13} & 2bC_{22} + aC_{23} & 2bC_{23} + aC_{33} & 0 & bC_{22} & 0 & 4b & 2a \\ -2aC_{11} + bC_{13} & -2aC_{12} + bC_{23} & -2aC_{13} + bC_{33} & -aC_{11} & 0 & 4a & 0 & -2b \\ 2bC_{12} - aC_{13} & 2bC_{22} - aC_{23} & 2bC_{23} - aC_{33} & 0 & -bC_{22} & 0 & 4b & -2a \end{bmatrix} \quad (14)$$

The determinant of $\mathbf{T}_+$ is $a^4b^4C_{11}C_{22}\det(\mathbf{C})$, so $\mathbf{T}_+$ is invertible if $a \neq 0$, $b \neq 0$, $C_{11} \neq 0$, $C_{22} \neq 0$ and $\mathbf{C}$ is nonsingular. Inversion yields $\boldsymbol{\mu}_+ = \mathbf{U}_+\mathbf{u}$, where

$$\mathbf{U}_+ = \mathbf{T}_+^{-1} = \frac{1}{ab}\begin{bmatrix} U_{11} & U_{12} & U_{13} & U_{14} & U_{15} & U_{16} & U_{17} & U_{18} \\ U_{21} & U_{22} & U_{23} & U_{24} & U_{25} & U_{26} & U_{27} & U_{28} \\ U_{31} & U_{32} & U_{33} & U_{34} & U_{35} & U_{36} & U_{37} & U_{38} \\ bC_{11}^{-1} & 0 & -bC_{11}^{-1} & 0 & bC_{11}^{-1} & 0 & -bC_{11}^{-1} & 0 \\ 0 & aC_{22}^{-1} & 0 & -aC_{22}^{-1} & 0 & aC_{22}^{-1} & 0 & -aC_{22}^{-1} \\ \frac{1}{4}b & 0 & \frac{1}{4}b & 0 & \frac{1}{4}b & 0 & \frac{1}{4}b & 0 \\ 0 & \frac{1}{4}a & 0 & \frac{1}{4}a & 0 & \frac{1}{4}a & 0 & \frac{1}{4}a \\ \frac{1}{4}a & -\frac{1}{4}b & \frac{1}{4}a & \frac{1}{4}b & -\frac{1}{4}a & \frac{1}{4}b & -\frac{1}{4}a & -\frac{1}{4}b \end{bmatrix}, \quad (15)$$

in which $U_{11} = -\frac{1}{2}(bE_{11} + aE_{13})$, $U_{12} = -\frac{1}{2}(aE_{12} + bE_{13})$, $U_{13} = \frac{1}{2}(bE_{11} - aE_{13})$, $U_{14} = -\frac{1}{2}(aE_{12} - bE_{13})$, $U_{15} = \frac{1}{2}(bE_{11} + aE_{13})$, $U_{16} = \frac{1}{2}(aE_{12} + bE_{13})$, $U_{17} = -\frac{1}{2}(bE_{11} - aE_{13})$, $U_{18} = \frac{1}{2}(aE_{12} - bE_{13})$, $U_{21} = -\frac{1}{2}(bE_{12} + aE_{23})$, $U_{22} = -\frac{1}{2}(aE_{22} + bE_{23})$, $U_{23} = \frac{1}{2}(bE_{12} - aE_{23})$, $U_{24} = -\frac{1}{2}(aE_{22} - bE_{23})$, $U_{25} = \frac{1}{2}(bE_{12} + aE_{23})$, $U_{26} = \frac{1}{2}(aE_{22} + bE_{23})$, $U_{27} = -\frac{1}{2}(bE_{12} - aE_{23})$, $U_{28} =$

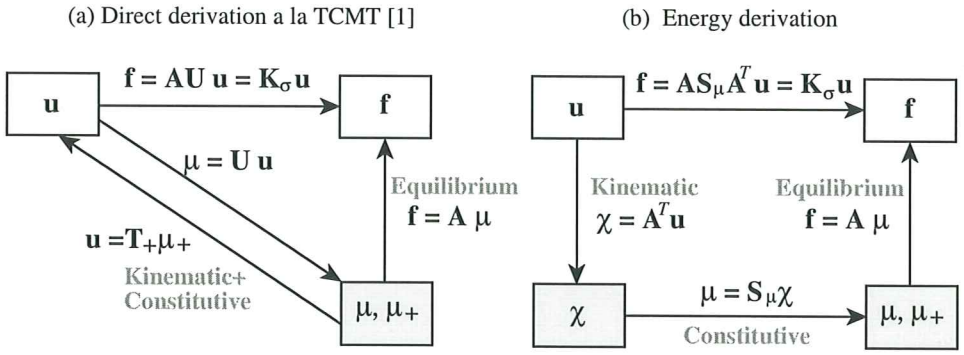

Figure 4. Derivation of the stress-assumed rectangular panel stiffness. Left side shows derivation bypassing energy methods.

$\frac{1}{2}(aE_{22}-bE_{23})$, $U_{31} = -\frac{1}{2}(bE_{13}+aE_{33})$, $U_{32} = -\frac{1}{2}(aE_{23}+bE_{33})$, $U_{33} = \frac{1}{2}(bE_{13}-aE_{33})$, $U_{34} = -\frac{1}{2}(aE_{23}-bE_{33})$, $U_{35} = \frac{1}{2}(bE_{13}+aE_{33})$, $U_{36} = \frac{1}{2}(aE_{23}+bE_{33})$, $U_{37} = -\frac{1}{2}(bE_{13}-aE_{33})$ and $U_{38} = \frac{1}{2}(aE_{23}-bE_{33})$. The stress-displacement matrix $\mathbf{U}$ that relates stress parameters to displacements: $\boldsymbol{\mu} = \mathbf{U}\,\mathbf{u}$, is obtained by extracting the first five rows of $\mathbf{U}_+$:

$$\mathbf{U} = \frac{1}{ab}\begin{bmatrix} U_{11} & U_{12} & U_{13} & U_{14} & U_{15} & U_{16} & U_{17} & U_{18} \\ U_{21} & U_{22} & U_{23} & U_{24} & U_{25} & U_{26} & U_{27} & U_{28} \\ U_{31} & U_{32} & U_{33} & U_{34} & U_{35} & U_{36} & U_{37} & U_{38} \\ bC_{11}^{-1} & 0 & -bC_{11}^{-1} & 0 & bC_{11}^{-1} & 0 & -bC_{11}^{-1} & 0 \\ 0 & aC_{22}^{-1} & 0 & -aC_{22}^{-1} & 0 & aC_{22}^{-1} & 0 & -aC_{22}^{-1} \end{bmatrix} = \mathbf{S}_\mu\,\mathbf{A}^T. \quad (16)$$

The relation $\mathbf{U} = \mathbf{S}_\mu\mathbf{A}^T$ can be checked directly. For this element it can be proven to hold by energy methods, but that was not obvious in 1952. It must have been a relief when the element stiffness came out symmetric. As Gallagher remarks [6, p. 22] symmetry is the exception rather than the rule for more complicated configurations. That difficulty proved a big boost for the energy and variational methods of the second generation.

The physical stiffness $\mathbf{K}_\sigma$ relates $\mathbf{f} = \mathbf{K}_\sigma\,\mathbf{u}$, where the σ subscript flags the stress element. Combining $\mathbf{f} = \mathbf{A}\,\boldsymbol{\mu}$ and $\boldsymbol{\mu} = \mathbf{U}\,\mathbf{u} = \mathbf{S}_\mu\,\mathbf{A}^T\,\mathbf{u}$ yields

$$\mathbf{K}_\sigma = \mathbf{A}\,\mathbf{U} = \mathbf{A}\,\mathbf{S}_\mu\,\mathbf{A}^T. \quad (17)$$

Figure 4 summarizes the foregoing derivation steps. Note that one can bypass the calculation of the generalized stiffness $\mathbf{S}_\mu$ if so desired, as diagrammed on the left of that figure. This is convenient for presentation to students without a background on energy methods.

Note that the displacement field (13) contains quadratic terms if μ_4 or μ_5 are nonzero. Hence the element is nonconforming. This is acknowledged but dismissed as innocuous in TCMT [1, p. 814].

5. THE STRAIN ELEMENT

A strain-assumed element can be developed through an entirely analogous procedure. The counterpart of (6) is

$$e_{xx} = \chi_1 + \chi_4\,\frac{y}{b}, \qquad e_{yy} = \chi_2 + \chi_5\,\frac{x}{a}, \qquad 2e_{xy} = \chi_3. \quad (18)$$

where the χ_i are dimensionless strain-amplitude parameters. They are collected in the 5-vector

$$\boldsymbol{\chi} = [\,\chi_1 \quad \chi_2 \quad \chi_3 \quad \chi_4 \quad \chi_5\,]^T. \quad (19)$$

An extended vector is constructed by appending the RBM amplitudes

$$\chi_+ = [\,\chi_1 \quad \chi_2 \quad \chi_3 \quad \chi_4 \quad \chi_5 \quad \chi_6 \quad \chi_7 \quad \chi_8\,]^T . \tag{20}$$

in which χ_6, χ_7 and χ_8 are defined a a manner similar to (9). Note that $\mathbf{e} = \mathbf{N}\chi = \mathbf{N}_+\chi_+$ where $\mathbf{N}$ and $\mathbf{N}_+$ are defined in (10). Integrating the strains yields the displacement field

$$\begin{aligned} u_x(x, y) &= \chi_6 + \chi_8 y + (\chi_1 + \chi_4/b)xy - \tfrac{1}{2}(\chi_5/a)y^2, \\ u_y(x, y) &= \chi_7 + (\chi_3 - \chi_8)x + \chi_2 y - \tfrac{1}{2}(\chi_4/b)x^2 + (\chi_5/a)xy. \end{aligned} \tag{21}$$

Evaluating at the nodes and inverting yields $\chi_+ = \mathbf{B}_+\mathbf{u}$ where

$$\mathbf{B}_+ = \frac{1}{8ab}\begin{bmatrix} -4b & 0 & 4b & 0 & 4b & 0 & -4b & 0 \\ 0 & -4a & 0 & -4a & 0 & 4a & 0 & 4a \\ -4a & -4b & -4a & 4b & 4a & 4b & 4a & -4b \\ 8b & 0 & -8b & 0 & 8b & 0 & -8b & 0 \\ 0 & 8a & 0 & -8a & 0 & 8a & 0 & -8a \\ 2ab & b^2 & 2ab & -b^2 & 2ab & b^2 & 2ab & -b^2 \\ a^2 & 2ab & -a^2 & 2ab & a^2 & 2ab & -a^2 & 2ab \\ -4a & 0 & -4a & 0 & 4a & 0 & 4a & 0 \end{bmatrix} \tag{22}$$

from which we extract the first five rows to get the strain-displacement matrix relating $\chi = \mathbf{B}_\chi\mathbf{u}$:

$$\mathbf{B}_\chi = \frac{h}{2V}\begin{bmatrix} -b & 0 & b & 0 & b & 0 & -b & 0 \\ 0 & -a & 0 & -a & 0 & a & 0 & a \\ -a & -b & -a & b & a & b & a & -b \\ 2b & 0 & -2b & 0 & 2b & 0 & -2b & 0 \\ 0 & 2a & 0 & -2a & 0 & 2a & 0 & -2a \end{bmatrix} \tag{23}$$

For use below we note the following relation between the transformation matrices of the stress and strain elements

$$\mathbf{A}^T = V\,\mathbf{D}_A\,\mathbf{B}_\chi, \quad \mathbf{B}_\chi = \frac{1}{V}\mathbf{D}_A^{-1}\mathbf{A}^T, \quad \mathbf{D}_A = \begin{bmatrix} 1 & 0 & 0 & 0 & 0 \\ 0 & 1 & 0 & 0 & 0 \\ 0 & 0 & 1 & 0 & 0 \\ 0 & 0 & 0 & \frac{1}{12} & 0 \\ 0 & 0 & 0 & 0 & \frac{1}{12} \end{bmatrix} = \begin{bmatrix} \mathbf{I}_3 & \mathbf{0} \\ \mathbf{0} & \frac{1}{12}\mathbf{I}_2 \end{bmatrix} = \mathbf{D}_A^T. \tag{24}$$

From (11) the lumping of the slave stress field $\mathbf{E}\mathbf{e} = \mathbf{E}\mathbf{N}\chi$ to node forces can be worked out to be

$$\mathbf{f} = \mathbf{A}\mathbf{E}_+\chi = V\,\mathbf{B}_\chi^T\mathbf{D}_A\mathbf{E}_+\chi, \quad \text{with} \quad \mathbf{E}_+ = \begin{bmatrix} E_{11} & E_{12} & E_{13} & 0 & 0 \\ E_{12} & E_{22} & E_{23} & 0 & 0 \\ E_{13} & E_{23} & E_{33} & 0 & 0 \\ 0 & 0 & 0 & E_{11} & 0 \\ 0 & 0 & 0 & 0 & E_{22} \end{bmatrix} \tag{25}$$

Combining previous equations, the physical element stiffness is

$$\mathbf{K}_e = V\,\mathbf{B}_\chi^T\mathbf{D}_A\mathbf{E}_+\mathbf{B}_\chi = \mathbf{B}_\chi^T\mathbf{K}_\chi\mathbf{B}_\chi, \quad \text{with} \quad \mathbf{K}_\chi = V\,\mathbf{D}_A\mathbf{E}_+. \tag{26}$$

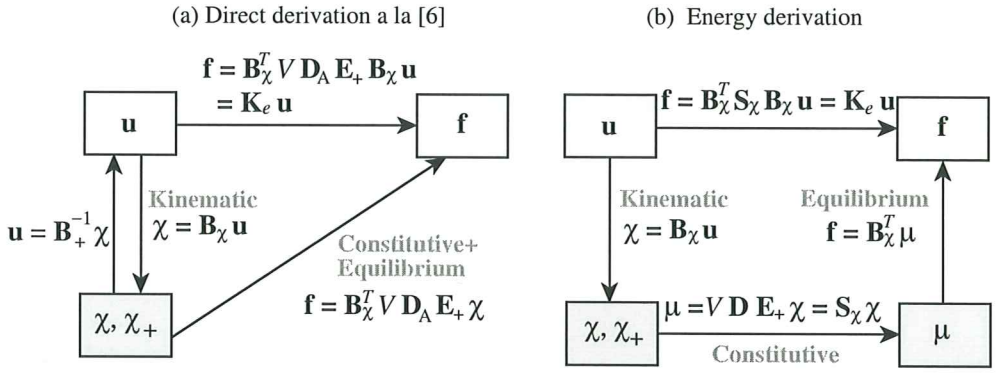

Figure 5. Derivation of the strain-assumed rectangular panel stiffness. Left diagram shows derivation bypassing energy methods.

Here $\mathbf{K}_\chi$ denotes the generalized stiffness in terms of $\boldsymbol{\chi}$. This matrix may be obtained also from standard energy arguments: the strain energy density is $\mathcal{U} = \frac{1}{2}\boldsymbol{\chi}^T\mathbf{E}\boldsymbol{\chi}$. Integrating over the element volume: $U = \int_{V^e} \mathcal{U}\, dV$ and identifying with $\frac{1}{2}\boldsymbol{\chi}^T\mathbf{K}_\chi\boldsymbol{\chi}$ gives

$$\mathbf{K}_\chi = V\,\mathbf{D}_A\mathbf{E}_+ = V\begin{bmatrix} E_{11} & E_{12} & E_{13} & 0 & 0 \\ E_{12} & E_{22} & E_{23} & 0 & 0 \\ E_{13} & E_{23} & E_{33} & 0 & 0 \\ 0 & 0 & 0 & \frac{1}{12}E_{11} & 0 \\ 0 & 0 & 0 & 0 & \frac{1}{12}E_{22} \end{bmatrix} \tag{27}$$

Figure 5 summarizes the foregoing derivation steps. The direct step from $\boldsymbol{\chi}$ to $\mathbf{f}$ on the left is more difficult to explain to students than the step from $\mathbf{u}$ to $\boldsymbol{\mu}$ in Figure 4. The energy based formulation shown on the right of Figure 5 tends to be more palatable.

6. THE CONFORMING DISPLACEMENT ELEMENT

This derivation of the assumed-displacement element starts from a conforming displacement field that enforces linear edge displacements. Using the matrix notation of [61, p. 227] for Irons' isoparametric formulation [23] specialized to the rectangle, the displacement field is bilinearly interpolated as

$$\begin{bmatrix} u_x(x,y) \\ u_y(x,y) \end{bmatrix} = \tfrac{1}{2}\begin{bmatrix} -a & 0 & a & 0 & a & 0 & -a & 0 \\ 0 & -b & 0 & -b & 0 & b & 0 & b \end{bmatrix}\begin{bmatrix} \frac{1}{4}(1-\xi)(1-\eta) \\ \frac{1}{4}(1+\xi)(1-\eta) \\ \frac{1}{4}(1+\xi)(1+\eta) \\ \frac{1}{4}(1-\xi)(1+\eta) \end{bmatrix}, \tag{28}$$

where $\xi = 2x/a$ and $\eta = 2y/b$ are the dimensionless quadrilateral coordinates. The derivation based on the minimum potential energy principle is standard textbook material and only the final result is presented here:

$$\mathbf{K}_u = \mathbf{B}_u^T\mathbf{K}_q\mathbf{B}_u, \quad \text{with} \quad \mathbf{K}_q = \frac{1}{V}\begin{bmatrix} E_{11} & E_{12} & E_{13} & 0 & 0 \\ E_{12} & E_{22} & E_{23} & 0 & 0 \\ E_{13} & E_{23} & E_{33} & 0 & 0 \\ 0 & 0 & 0 & Q_{11} & Q_{12} \\ 0 & 0 & 0 & Q_{12} & Q_{22} \end{bmatrix}, \tag{29}$$

in which $\mathbf{B}_u = \mathbf{A}^T$ as given by (11) and

$$Q_{11} = 12\frac{b^2E_{11} + a^2E_{33}}{ab^3h}, \quad Q_{12} = 12\left(\frac{E_{13}}{a^2h} + \frac{E_{23}}{b^2h}\right), \quad Q_{22} = 12\frac{a^2E_{22} + b^2E_{33}}{a^3bh} \tag{30}$$

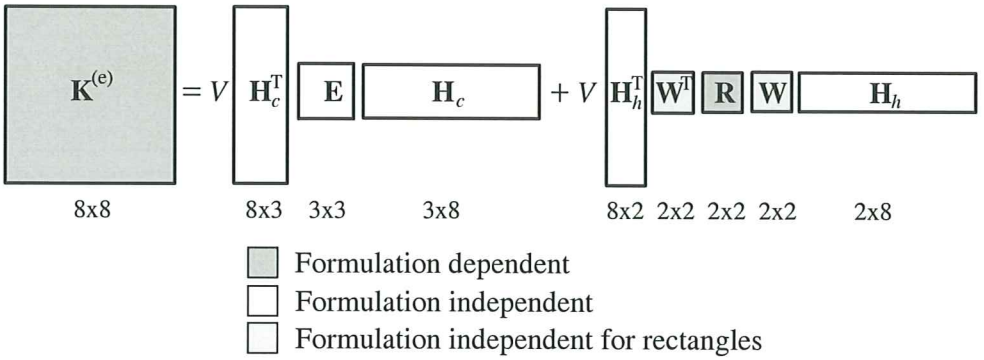

Figure 6. The template for the rectangular panel, illustrating formulation dependent and independent parts.

This model has a checkered history. It was first derived as a rectangular panel with edge reinforcements (omitted here) by Argyris in his 1954 *Aircraft Engineering* series [2, p. 49 in reprint]. He used bilinear displacement interpolation in Cartesian coordinates. After much flailing, a conforming generalization to arbitrary geometry was published in 1964 by Taig and Kerr [62] using quadrilateral-fitted coordinates called $\{\xi, \eta\}$ but running from 0 to 1. (Reference [62] cites an 1961 English Electric Aircraft internal report as original source but [23, p. 520] remarks that the work goes back to 1957.) Bruce Irons, who was aware of Taig's work while at Rolls Royce, created the seminal isoparametric family as a far-reaching extension upon moving to Swansea [19–22].

7. TEMPLATES

7.1. Stiffness Decomposition

The stiffnesses $\mathbf{K}_\sigma$, $\mathbf{K}_\sigma$ and $\mathbf{K}_u$ derived in the foregoing three Sections do not appear to have much in common. Indeed if one looks at just the matrix entries no pattern is readily seen. Closer examination reveals, however, that they are instances of the algebraic form

$$\mathbf{K} = \mathbf{K}_b + \mathbf{K}_h = V\,\mathbf{H}_c^T\mathbf{E}\mathbf{H}_c + V\,\mathbf{H}_h^T\mathbf{W}^T\mathbf{R}\mathbf{W}\mathbf{H}_h, \tag{31}$$

where $V = abh$ is the element volume and

$$\begin{aligned}
\mathbf{H}_c &= \frac{1}{2ab}\begin{bmatrix} -b & 0 & b & 0 & b & 0 & -b & 0 \\ 0 & -a & 0 & -a & 0 & a & 0 & a \\ -a & -b & -a & b & a & b & a & -b \end{bmatrix}, \\
\mathbf{H}_h &= \tfrac{1}{2}\begin{bmatrix} 1 & 0 & -1 & 0 & 1 & 0 & -1 & 0 \\ 0 & 1 & 0 & -1 & 0 & 1 & 0 & -1 \end{bmatrix}, \\
\mathbf{W} &= \begin{bmatrix} 1/a & 0 \\ 0 & 1/b \end{bmatrix}, \quad \mathbf{R} = \begin{bmatrix} R_{11} & R_{12} \\ R_{12} & R_{22} \end{bmatrix}.
\end{aligned} \tag{32}$$

Matrices $\mathbf{H}_c$ and $\mathbf{H}_h$ are the same for the three elements. Matrix $\mathbf{R}$ (a generalized bending rigidity) depends on the formulation. The transition matrix $\mathbf{W}$ is formulation independent for rectangular panels. For more complex geometries discussed in the Appendix, $\mathbf{W}$ may be formulation-adjusted to make $\mathbf{R}$ simpler.

For the stress, strain and displacement elements $\mathbf{R}$ is $\mathbf{R}_\sigma$, $\mathbf{R}_e$ and $\mathbf{R}_u$, respectively, where

$$\mathbf{R}_\sigma = \tfrac{1}{3}\begin{bmatrix} C_{11}^{-1} & 0 \\ 0 & C_{22}^{-1} \end{bmatrix}, \quad \mathbf{R}_e = \tfrac{1}{3}\begin{bmatrix} E_{11} & 0 \\ 0 & E_{22} \end{bmatrix}, \quad \mathbf{R}_u = \tfrac{1}{3}\begin{bmatrix} E_{11} + \dfrac{a^2E_{33}}{b^2} & \dfrac{bE_{13}}{a} + \dfrac{aE_{23}}{b} \\ \dfrac{bE_{13}}{a} + \dfrac{aE_{23}}{b} & E_{22} + \dfrac{b^2E_{33}}{a^2} \end{bmatrix}. \tag{33}$$

```
RectPanel4TemplateStiffness[{a_,b_},Emat_,Cmat_,h_,name_,Rlist_]:=
  Module[{V,found,Hc,Hh,W,Ke}, V=a*b*h;
  {WRW,found}=RectPanel4TemplateWRW[{a,b},Emat,Cmat,name,Rlist];
  If [Not[found], Print["Illegal elem name: ",name]; Abort[]];
  Hc={{-b,0,b,0,b,0,-b,0}, {0,-a,0,-a,0,a,0,a},
      {-a,-b,-a,b,a,b,a,-b}}/(2*a*b);
  Hh={{1,0,-1,0,1,0,-1,0},{0,1,0,-1,0,1,0,-1}}/2;
  Ke=V*Transpose[Hc].Emat.Hc+V*Transpose[Hh].WRW.Hh;
  Return[Simplify[Ke]]];

RectPanel4TemplateWRW[{a_,b_},Emat_,Cmat_,name_,Rlist_]:=
 Module[{R11,R12,R22,Rmat,E11,E12,E13,E22,E23,E33,
 found=False,C11,C22,C33,C12,C13,C23,Edet,Cdet,W,WRW},
  {{E11,E12,E13},{E12,E22,E23},{E13,E23,E33}}=Emat;
  If [Length[Cmat]<=0,
     Edet=E11*E22*E33+2*E12*E13*E23-E11*E23^2-E22*E13^2-E33*E12^2;
     C11=(E22*E33-E23^2)/Edet; C22=(E11*E33-E13^2)/Edet;
     C33=(E11*E22-E12^2)/Edet; C12=(E13*E23-E12*E33)/Edet;
     C13=(E12*E23-E13*E22)/Edet; C23=(E12*E13-E11*E23)/Edet,
     {{C11,C12,C13},{C12,C22,C23},{C13,C23,C33}}=Cmat,
     {{C11,C12,C13},{C12,C22,C23},{C13,C23,C33}}=Cmat];
  If [name=="Stress"||name=="QM6"||name=="Q6",
     R11=1/(3*C11); R22=1/(3*C22); R12=0; found=True];
  If [name=="Strain", R11=E11/3; R22=E22/3; R12=0; found=True];
  If [name=="Disp",  R11=(E11+E33*a^2/b^2)/3;
     R22=(E22+E33*b^2/a^2)/3; R12=(E13*b/a+E23*a/b)/3; found=True];
  If [name=="Arbitrary", {R11,R12,R22}=Rlist; found=True];
  W={{1/a,0},{0,1/b}}; Rmat={{R11,R12},{R12,R22}};
  WRW=Transpose[W].Rmat.W; Return[{WRW,found}]];
```

Figure 7. A *Mathematica* implementation of the rectangular panel template (31).

But actually we are not restricted to these. Other expressions for $\mathbf{R}$ would yield other $\mathbf{K}$. These are possible, although not necessarily useful, stiffnesses for the rectangular panel if $\mathbf{R}$ is symmetric and positive definite, and if its entries have physical dimensions of elastic moduli. Further if $E_{13} = E_{23} = 0$ we set $R_{12} = 0$. The key discovery is that the element formulation affects only part of the stiffness expression. See Figure 6.

7.2. Template Terminology

The algebraic form (31)-(32) is called a finite element stiffness template, or *template* for short.

Matrices $\mathbf{K}_b$ and $\mathbf{K}_h$ are called the basic and higher-order stiffness matrix, respectively, in accordance with the fundamental decomposition of the Free Formulation [38,39,54–60]. These matrices play different and complementary roles.

The basic stiffness $\mathbf{K}_b$ takes care of consistency and mixability. In the Free Formulation a restatement of (31) is preferred:

$$\mathbf{K}_b = V^{-1}\,\mathbf{L}\,\mathbf{E}\,\mathbf{L}^T, \tag{34}$$

where $\mathbf{L} = \mathbf{H}_c/V$ is called the force lumping matrix, or simply lumping matrix.

The higher order stiffness $\mathbf{K}_h$ is a *stabilization* term that provides the correct rank and may be adjusted for accuracy. This matrix is orthogonal to rigid body motions and constant strain states. To verify the claim for this template introduce the following 8×6 matrix, called the basic-mode matrix in the Free

Formulation:

$$\mathbf{G}_{rc} = \begin{bmatrix} 1 & 0 & y_1 & x_1 & 0 & y_1 \\ 0 & 1 & -x_1 & 0 & y_1 & x_1 \\ 1 & 0 & y_2 & x_2 & 0 & y_2 \\ 0 & 1 & -x_2 & 0 & y_2 & x_2 \\ 1 & 0 & y_3 & x_3 & 0 & y_3 \\ 0 & 1 & -x_3 & 0 & y_3 & x_3 \\ 1 & 0 & y_4 & x_4 & 0 & y_4 \\ 0 & 1 & -x_4 & 0 & y_4 & x_4 \end{bmatrix} = \tfrac{1}{2} \begin{bmatrix} 2 & 0 & -b & -a & 0 & -b \\ 0 & 2 & a & 0 & -b & -a \\ 2 & 0 & -b & a & 0 & -b \\ 0 & 2 & -a & 0 & -b & a \\ 2 & 0 & b & a & 0 & b \\ 0 & 2 & -a & 0 & b & a \\ 2 & 0 & b & -a & 0 & b \\ 0 & 2 & a & 0 & b & -a \end{bmatrix}. \tag{35}$$

The six columns of $\mathbf{G}_{rc}$ span the rigid body modes and constant strain states evaluated at the nodes (these bases are not orthonormalized as that property is not required here). It is readily checked that $\mathbf{H}_h\mathbf{G}_{rc} = \mathbf{0}$. Therefore those modes, and any linear combination thereof, are orthogonal to the higher order stiffness: $\mathbf{K}_h\mathbf{G}_{rc} = \mathbf{0}$. So the role of $\mathbf{H}_h$ is essentially that of a geometric *projector*.

A *Mathematica* implementation of (31) is shown in Figure 7, as module `RectPanel4TemplateStiffness`. The module arguments are the rectangle dimensions as list `{a,b}`, the 3 × 3 elasticity matrix as list `Emat={{E11,E12,E13},{E12,E22,E23},{E13,E23,E33}}`, the 3 × 3 compliance matrix as list `Cmat={{C11,C12,C13},{C12,C22,C23},{C13,C23,C33}}`, the thickness `h`, the name as one of `"Stress"` ,`"Strain"`, `"Disp"`, `"Q6"`, `"QM6"` or `"Arbitrary"`, and finally the list `Rlist={R11,R12,R22}`. The latter is used if the name is `"Arbitrary"`. This comes handy for finding the signature of known elements leaving the entries of `Rlist` symbolic and using the `Solve` command. If `Cmat` is supplied as the empty list `{ }`, the compliance matrix is calculated internally as inverse of `Emat`.

The module returns the 8 × 8 stiffness matrix `Ke` as function value. To get the basic stiffness $\mathbf{K}_b$ only, call with `name = "Arbitrary"` and `Rlist={0,0,0}`.

7.3. Requirements

An acceptable template fulfills four conditions: (C) consistency, (S) stability (correct rank), (I) observer invariance and (P) parametrization. These are discussed at length in other papers [69–75]. Conditions (C) and (S) are imposed to ensure convergence as the mesh size is reduced by enforcing *a priori* satisfaction of the Individual Element Test (IET) of Bergan and Hanssen [76,77]

Condition (P) means that the template contains free parameters or free matrix entries. In the case of (31), the simplest choice of parameters are the entries R_{11}, R_{12}, R_{22} themselves. To fulfill stability, $R_{11} > 0$, $R_{22} > 0$ and $R_{11}R_{22} - R_{12}^2 > 0$. Parametrization facilitates performance optimization as well as tuning elements, or combinations of elements, to fulfill specific needs.

Using the IET as departure point it is not difficult to show [78] that (31), under the stated restrictions on $\mathbf{R}$, includes all stiffnesses that satisfy the IET and stability. Observer invariance is a moot point for this element since $\{x, y\}$ are side aligned. As per the definition in the Introduction, (31) is an universal template.

7.4. Instances, Signatures, Clones

Setting the free parameters to specific values yields element instances. The set of free parameters is called the template *signature*, a term introduced in [73,74]. Borrowing terminology from biogenetics, the signature may be viewed as an "element DNA" that uniquely characterizes it as an individual entity. Elements derived by different techniques that share the same signature are called *clones*.

One of the "template services" is automatic identification of clones. If two elements fitting the template (31) share R_{11}, R_{12} and R_{22}, they are clones. Inasmuch as most FEM formulation schemes have been

Table 1. A Clone Gallery

Name	Description	Clones and sources
StressRP (a.k.a. BORP)	5-stress-mode element of Section 4	Direct derivation: TCMT [1], Gallagher [6] Pian 5-mode stress hybrid [25,27] Wilson-Taylor-Doherty-Ghaboussi Q6 [63] Taylor-Wilson-Beresford QM6 [64] Belytschko-Liu-Engelmann QBI [65] SRI of iso-P with **E** split as per (54)
StrainRP	5-strain-mode element of Section 5	MacNeal QUAD4 [36,66] SRI of iso-P with **E** split as per (56)
DispRP	Bilinear iso-P element of Section 6	Argyris [2] as edge stiffened rectangular panel Taig-Kerr [62] as specialized quadrilateral

Note 1: Many plane stress models listed above were derived for quadrilateral geometries, and a few as membrane component of shells. The right-hand-column classification only pertains to the rectangular panel specialization. For example, Q6 and QM6 differ for non-parallelogram shapes.
Note 2: Instances of the stress-hybrid and displacement-bubble-function "futile families" studied in Section 11 are omitted, as they lack practical value.
Note 3: Post-1990 clones (e.g. EAS [51]) omitted to save space. See [67] for a recent survey.

tried on the rectangular panel, it should come as no surprise that there are many clones, particularly of the stress element. Those presented before 1990 are collected in Table 1. For example, the incompatible mode element Q6 of Wilson et al. [63] is a clone of StressRP. The version QM6 of Taylor et al. [64], which passes the patch test for arbitrary geometries, reduces to Q6 for rectangular and parallelogram shapes. Even for this simple geometry recognition of some of the coalescences took a long time, as recently narrated in [68].

8. FINDING THE BEST

An universal template is nice to have. But an obvious question arises: among the infinity of elements that it can generate, is there a best one? By construction all instances verify exactly the IET for rigid body modes and uniform strain states. Hence the optimality criterion must rely on higher order patch tests.

8.1. The Bending Tests

The obvious tests involve response to in-plane bending along the side directions. This leads to comparisons in the form of energy ratios. These have been used since 1984 to tune up the higher order stiffness of triangular elements [54–57,79]. An extension introduced in this article is consideration of arbitrary anisotropic material. All symbolic calculations were carried out with *Mathematica*.

The x bending test is depicted in Figure 8. A Bernoulli-Euler plane beam of thin rectangular cross-section with height b and thickness h (normal to the plane of the figure) is bent under applied end moments M_x. The beam is fabricated of anisotropic material with the stress-strain law $\boldsymbol{\sigma} = \mathbf{E}\mathbf{e}$ of $(2)_2$. Except for possible end effects the exact solution of the beam problem (from both the theory-of-elasticity and beam-theory standpoints) is a constant bending moment $M(x) = M_x$ along the span. The associated stress field is $\sigma_{xx} = -M_x\, y/I_b$, $\sigma_{yy} = \sigma_{xy} = 0$, where $I_b = \frac{1}{12}hb^3$.

For the y bending test, depicted in Figure 9, the beam cross section has height a and thickness h, and is subjected to end moments M_y. The exact solution is $M(y) = M_y$. The associated stress field is

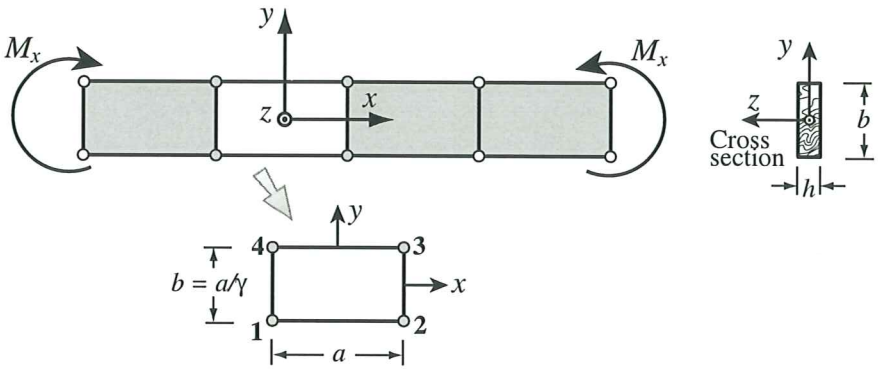

Figure 8. Constant-moment inplane-bending test along the x side dimension.

$\sigma_{yy} = M_y\, x/I_a$ and $\sigma_{xx} = \sigma_{xy} = 0$, where $I_a = \frac{1}{12}ha^3$. For comparing with the FEM discretizations below, the internal (complementary) energies taken up by beam segments of lengths a and b in the configurations of Figures 8 and 9, respectively, are

$$U_x^{\text{beam}} = \frac{6aC_{11}M_x^2}{b^3h}, \qquad U_y^{\text{beam}} = \frac{6bC_{22}M_y^2}{a^3h} \tag{36}$$

For the 2D element tests, each beam is modeled with one layer of identical 4-node rectangular panels dimensioned $a \times b$ as shown in Figures 8 and 9. The aspect ratio b/a is denoted by γ. By analogy with the exact solution, all rectangles in the finite element model will undergo the same deformations and stresses. We can therefore consider a typical element. For x bending the exact stress distribution is represented by (7) on taking $\mu_4 = -M_x b/I_b = -12M_x/(b^2h)$ and $\mu_1 = \mu_2 = \mu_3 = \mu_5 = 0$. The rigid body mode amplitudes are chosen to be zero for convenience: $\mu_6 = \mu_7 = \mu_8 = 0$. Inserting these μ_i into (14) we get the node displacement vector

$$\mathbf{u}_{bx} = \frac{12M_xC_{11}a}{b^2h}[-1 \quad 0 \quad 1 \quad 0 \quad -1 \quad 0 \quad 1 \quad 0]^T. \tag{37}$$

Likewise, for the y bending test the element stress field is obtained by taking $\mu_5 = M_y a/I_a = 12M_y/(a^2h)$ and $\mu_1 = \mu_2 = \mu_3 = \mu_4 = \mu_6 = \mu_7 = \mu_8 = 0$. The node displacement vector given by (14) is

$$\mathbf{u}_{by} = \frac{12M_yC_{22}b}{a^2h}[0 \quad 1 \quad 0 \quad -1 \quad 0 \quad 1 \quad 0 \quad -1]^T. \tag{38}$$

The strain energies absorbed by the panel element under these applied node displacements are $U_x^{\text{panel}} = \frac{1}{2}\mathbf{u}_{bx}^T\mathbf{K}\mathbf{u}_{bx}$ and $U_y^{\text{panel}} = \frac{1}{2}\mathbf{u}_{by}^T\mathbf{K}\mathbf{u}_{by}$, respectively. Define the bending energy ratios as

$$r_x = \frac{U_x^{\text{panel}}}{U_x^{\text{beam}}}, \qquad r_y = \frac{U_y^{\text{panel}}}{U_y^{\text{beam}}}. \tag{39}$$

These happen to be the ratios of the exact (beam) displacement solution to that of the of rectangular panel solution. Hence $r_x = 1$ means that we get the exact answer under M_x, that is, the panel is x-bending exact. If $r_x > 1$ or $r_x < 1$ the panel is overstiff or overflexible in x bending, respectively, and likewise for y bending.

If $r_x = 1$ and $r_y = 1$ for any aspect ratio $\gamma = b/a$ and arbitrary material properties the element is called *bending optimal*. If $r_x >> 1$ if $a >> b$ and/or $r_y >> 1$ if $a << b$ the element is said to experience *aspect ratio locking* along the x or y direction, respectively. This is known as *shear locking* in the FEM literature because it is traceable to spurious shear energy.

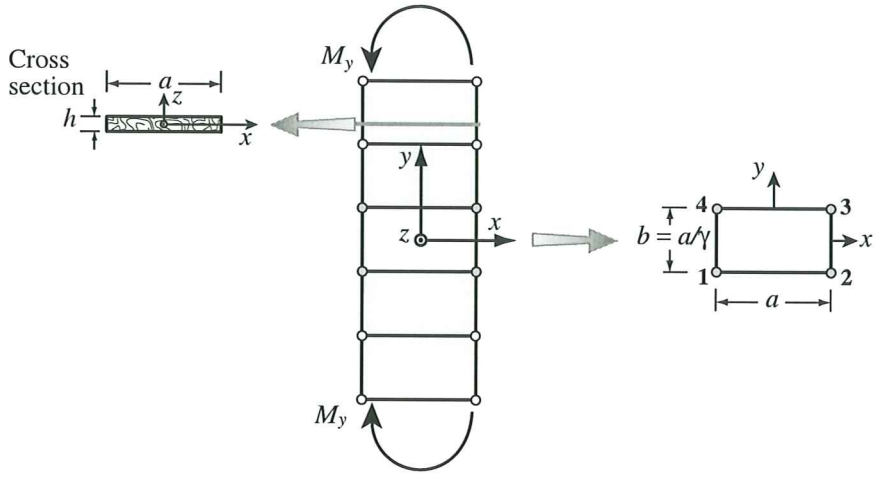

Figure 9. Constant-moment inplane-bending test along the y side dimension.

8.2. The Optimal Panel

Applying the tests to the template (31) yields

$$r_x = 3C_{11}R_{11}, \qquad r_y = 3C_{22}R_{22}. \tag{40}$$

Clearly to get $r_x = r_y = 1$ for any aspect ratio we must take

$$R_{11} = \tfrac{1}{3}C_{11}^{-1}, \quad R_{22} = \tfrac{1}{3}C_{22}^{-1} \tag{41}$$

Because R_{12} does not enter the optimality criterion one can set $R_{12} = 0$ for convenience. Comparing to the $\mathbf{R}_\sigma$ of (33) shows that the 5-parameter stress model of TCMT [1] (and its clones) is the bending-optimal rectangular panel. If the material is isotropic, $R_{11} = R_{22} = \frac{1}{3}E$. Accordingly the StressRP instance will be henceforth also identified by the acronym BORP, for Bending Optimal Rectangular Panel.

8.3. The Strain Element Does Not Lock

It is interesting to apply the result (40) to other elements. The StrainRP element generated by the $\mathbf{R}_e$ of (33) gives

$$r_x = C_{11}E_{11}, \qquad r_y = C_{22}E_{22}. \tag{42}$$

If the material is isotropic, $C_{11} = C_{22} = 1/E$ and $E_{11} = E_{22} = E/(1-\nu^2)$. This yields $r_x = r_y = 1/(1-\nu^2)$, which varies between 1 and 4/3. For an orthotropic body with principal material axes aligned with the rectangle sides, $E_{11} = E_1/(1-\nu_{12}\nu_{21})$, $E_{22} = E_2/(1-\nu_{12}\nu_{21})$, $C_{11} = 1/E_1$, $C_{22} = 1/E_2$, and $r_x = r_y = 1/(1-\nu_{12}\nu_{21})$. The ratios are independent of the aspect ratio γ. Consequently StrainRP and its clones *do not lock*, although the element is not generally optimal. Note that if $C_{11}E_{11}$ and/or $C_{22}E_{22}$ differ widely from 1, as may happen in highly anisotropic materials, the bending performance will be poor. See the Example problem in Section 12.2.

8.4. But the Displacement Element Does

DispRP is generated by the $\mathbf{R}_u$ of (33). Inserting its entries into (40) we get

$$\begin{aligned} r_x &= C_{11}(E_{11} + E_{33}\gamma^2) = \frac{(E_{22}E_{33} - E_{23}^2)(E_{11} + E_{33}\gamma^2)}{\det(\mathbf{E})}, \\ r_y &= C_{22}(E_{22} + E_{33}\gamma^{-2}) = \frac{(E_{11}E_{33} - E_{13}^2)(E_{22} + E_{33}\gamma^{-2})}{\det(\mathbf{E})}. \end{aligned} \tag{43}$$

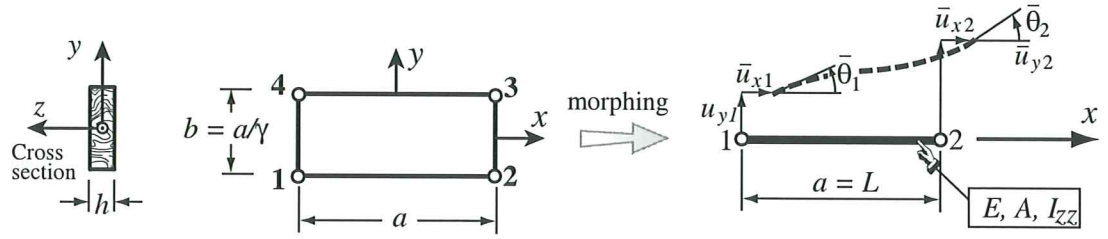

Figure 10. Morphing a 8-DOF rectangular panel unit to a 6-DOF beam-column element in the x direction.

in which $\det(\mathbf{E}) = E_{11}E_{22}E_{33} + 2E_{12}E_{13}E_{23} - E_{11}E_{23}^2 - E_{22}E_{13}^2 - E_{33}E_{12}^2$. For an isotropic material

$$r_x = \frac{2+\gamma^2(1-\nu)}{2(1-\nu^2)}, \qquad r_y = \frac{1+2\gamma^2-\nu}{2\gamma^2(1-\nu^2)}. \tag{44}$$

These relations clearly display aspect ratio locking for bending along the longest side dimension. For example, if $\nu = 0$ and $a = 10b$ whence $\gamma = a/b = 10$, $r_x = 51$ and DispRP is over 50 times stiffer in x bending than the Bernoulli-Euler beam element. The expression (43) makes clear that locking happens for any material law as long as $E_{33} \neq 0$. Since this is the shear modulus, the name *shear locking* used in the FEM literature is justified.

8.5. Multiple Element Layers

Results of the energy bending test can be readily extended to predict the behavior of $2n$ ($n = 1, 2, \ldots$) identical layers of elements symmetrically placed through the beam height. If $2n$ layers are placed along the y direction in the configuration of Figure 8 and γ stays the same, the energy ratio becomes

$$r_x^{(2n)} = \frac{2^{2n} - 1 + r_x}{2^{2n}}, \tag{45}$$

where r_x is the ratio (40) for one layer. If $r_x \equiv 1$, $r_x^{2n} \equiv 1$ so bending exactness is maintained, as can be expected. For example, if $n = 1$ (two element layers), $r_x^{(2)} = (3 + r_x)/4$. The same result holds for r_y if $2n$ layers are placed along the x direction in the configuration of Figure 9.

9. MORPHING INTO BEAM-COLUMN

Morphing means transforming an individual element or macroelement into a simpler model using kinematic constraints. Often the simpler element has lower dimensionality. For example a plate bending macroelement may be morphed to a Bernoulli-Euler beam or to a torqued shaft [75]. To illustrate the idea consider morphing the rectangular panel of Figure 10 into the two-node beam-column element shown on the right of that Figure. The length, cross sectional area and moment of inertia of the beam-column element, respectively, are denoted by $L = a$, $A = bh$ and $I_{zz} = b^3h/12 = a^3h/(12\gamma^3)$, respectively.

The transformation between the freedoms of the panel and those of the beam-column is

$$\mathbf{u}_R = \begin{bmatrix} u_{x1} \\ u_{y1} \\ u_{x2} \\ u_{y2} \\ u_{x3} \\ u_{y3} \\ u_{x4} \\ u_{y4} \end{bmatrix} = \begin{bmatrix} 1 & 0 & \frac{1}{2}b & 0 & 0 & 0 \\ 0 & 1 & 0 & 0 & 0 & 0 \\ 0 & 0 & 0 & 1 & 0 & \frac{1}{2}b \\ 0 & 0 & 0 & 0 & 1 & 0 \\ 0 & 0 & 0 & 1 & 0 & -\frac{1}{2}b \\ 0 & 0 & 0 & 0 & 1 & 0 \\ 1 & 0 & -\frac{1}{2}b & 0 & 0 & 0 \\ 0 & 1 & 0 & 0 & 0 & 0 \end{bmatrix} \begin{bmatrix} \bar{u}_{x1} \\ \bar{u}_{y1} \\ \bar{\theta}_1 \\ \bar{u}_{x2} \\ \bar{u}_{y2} \\ \bar{\theta}_2 \end{bmatrix} = \mathbf{T}_m \bar{\mathbf{u}}_m. \tag{46}$$

where a superposed bar distinguishes the beam-column freedoms grouped in array $\bar{\mathbf{u}}_m$. As source select StressRP fabricated of isotropic material. The morphed beam-column element stiffness is

$$\mathbf{K}_m = \mathbf{T}_m^T \mathbf{K}_\sigma \mathbf{T}_m = \frac{E}{L}\begin{bmatrix} A & 0 & 0 & -A & 0 & 0 \\ 0 & 12c_{22}I_{zz}/L^2 & 6c_{23}I_{zz}/L & 0 & -12c_{22}I_{zz}/L^2 & 6c_{23}I_{zz}/L \\ 0 & 6c_{23}I_{zz}/L & 4c_{33}I_{zz} & 0 & -6c_{23}I_{zz}/L & 4c_{33}I_{zz} \\ -A & 0 & 0 & A & 0 & 0 \\ 0 & 12c_{22}I_{zz}/L^2 & 6c_{23}I_{zz}/L & 0 & -12c_{22}I_{zz}/L^2 & 6c_{23}I_{zz}/L \\ 0 & 6c_{23}I_{zz}/L & 4c_{33}I_{zz} & 0 & -6c_{23}I_{zz}/L & 4c_{33}I_{zz} \end{bmatrix} \tag{47}$$

in which $c_{22} = c_{23} = \frac{1}{2}\gamma^2/(1+\nu)$, and $c_{33} = \frac{1}{4}(1+3c_{22})$. The entries in rows/columns 1 and 4 form the well known two-node bar stiffness. Those in rows and columns 2, 3, 5 and 6 are dimensionally homogeneous to those of a plane beam, and may be grouped into the following matrix configuration:

$$\mathbf{K}_m^{beam} = \frac{EI_{zz}}{L}\left(\begin{bmatrix} 0 & 0 & 0 & 0 \\ 0 & 1 & 0 & -1 \\ 0 & 0 & 0 & 0 \\ 0 & -1 & 0 & 1 \end{bmatrix} + \beta_m \begin{bmatrix} 12/L^2 & 6/L & -12/L^2 & 6/L \\ 6/L & 3 & -6/L & 3 \\ -12/L^2 & -6/L & 12/L^2 & -6/L \\ 6/L & 3 & -6/L & 3 \end{bmatrix}\right) \tag{48}$$

in which $\beta_m = c_{22} = c_{23} = \frac{1}{2}\gamma^2/(1+\nu)$. But (48), with β_m replaced by a free parameter β, happens to be the universal template of a prismatic plane beam, first presented in [69] and further studied, for the C^1 case, in [80,81] using Fourier methods.

The basic stiffness on the left characterizes the pure-bending symmetric response to a uniform moment, whereas the higher-order stiffness on the right characterizes the antisymmetric response to a linearly-varying, bending moment of zero mean. For the Bernoulli-Euler beam constructed with cubic shape functions, $\beta = 1$. For the Timoshenko beam, the exact equilibrium model [5, p. 80] is matched by $\beta = \beta_{C0} = 1/(1+\phi), \phi = 12EI_z/(GA_sL^2)$, in which $A_s = 5bh/6$ is the shear area and $G = \frac{1}{2}E/(1+\nu)$ the shear modulus.

It is readily verified that the morphed β_m is always higher than β_{C0} for all $0 \le \nu \le \frac{1}{2}$ and aspect ratios $\gamma > 0$. This indicates that in beam-like problems involving transverse shear the rectangular panel will be stiffer than the exact C^0 beam model. For example if $\nu = 1/4$,

$$\frac{\beta_{C0}}{\beta_m} = \frac{5}{2(3+\gamma^2)}, \tag{49}$$

which never exceeds 5/6 and goes to zero as $\gamma \to \infty$. This behavior can be expected, since the panel can only respond to such antisymmetric node motions by deforming in pure shear. However, the symmetric response is exact for any aspect ratio γ, which confirms the optimality of StressRP. Observe also that what was a higher order patch test on the two-triangle mesh unit becomes a basic (constant-moment) patch test on the morphed element. This is typical of morphing transformations that reduce spatial dimensionality.

For nonoptimal elements, one finds that the basic stiffness of the morphed beam is wrong except under special circumstances; for example isotropic StrainRP with zero ν, or one of the SRI elements studied next.

10. A G3 DEVICE: SELECTIVE REDUCED INTEGRATION

The three canonical models of Sections 4-6 were known by the end of Generation 2. Next a third generation tool will be studied in the context of templates.

Full Reduced Integration (FRI) and Selective Reduced Integration (SRI) emerged during 1969–72 [82–85] as tools to "unlock" isoparametric displacement models. Initially labeled as "variational crimes"

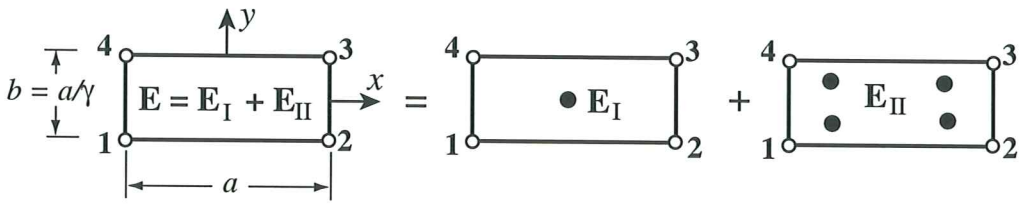

Figure 11. The two-way SRI matrix split.

[31], they were eventually justified through lawful association with mixed variational methods [86–88]. Both FRI and SRI turned out to be particularly useful for legacy and nonlinear codes since they allow shape function and numerical integration modules to be reused.

For the 4-node rectangular panel only SRI is considered because FRI leads to rank deficiency: $R_{11} = R_{12} = R_{22} = 0$. Two questions will be studied as it relates to templates:

(i) Can the template (31)–(32) be reproduced for any material law by a SRI scheme?

(ii) Can BORP be cloned for any material law by a SRI scheme that is independent of the aspect ratio?

As shown below, the answers are (i): yes if $R_{12} = 0$; (ii): yes.

10.1. Concept and Notation

In the FEM literature, SRI identifies a scheme for forming $\mathbf{K}$ as the sum of two or more matrices computed with different integration rules and different constitutive properties, within the framework of the isoparametric displacement model.

We consider primarely the case of a two-way constitutive decomposition. Split the plane stress constitutive matrix $\mathbf{E}$ into

$$\mathbf{E} = \mathbf{E}_{\rm I} + \mathbf{E}_{\rm II} \tag{50}$$

The isoparametric displacement formulation leads to the expression $\mathbf{K} = \int_{A^e} h\, \mathbf{B}_u^T \mathbf{E}\, \mathbf{B}_u\, d\Omega$ where A^e is the element area and $\mathbf{B}_u$ the isoparametric strain-displacement matrix. To apply SRI insert the splitting (50) to get two integrals:

$$\mathbf{K} = \int_{A^e} h\, \mathbf{B}_u^T \mathbf{E}_{\rm I}\, \mathbf{B}_u\, d\Omega + \int_{A^e} h\, \mathbf{B}_u^T \mathbf{E}_{\rm II}\, \mathbf{B}_u\, d\Omega = \mathbf{K}_{\rm I} + \mathbf{K}_{\rm II}. \tag{51}$$

The two matrices in (51) are done through different numerical quadrature schemes: rule (I) for the first integral and rule (II) for the second.

For the rectangular panel the isoparametric model is the 4-node bilinear element. Rules (I) and (II) will be the 1×1 (one point) and 2×2 (4-point) Gauss product rules, respectively. A general split of the elasticity matrix is

$$\mathbf{E} = \mathbf{E}_{\rm I} + \mathbf{E}_{\rm II} = \begin{bmatrix} E_{11}\,\rho_1 & E_{12}\rho_3 & E_{13}\tau_2 \\ E_{12}\,\rho_3 & E_{22}\,\rho_2 & E_{23}\tau_2 \\ E_{13}\,\tau_2 & E_{23}\,\tau_2 & E_{33}\tau_1 \end{bmatrix} + \begin{bmatrix} E_{11}(1-\rho_1) & E_{12}(1-\rho_3) & E_{13}(1-\tau_2) \\ E_{12}(1-\rho_3) & E_{22}(1-\rho_2) & E_{23}(1-\tau_3) \\ E_{13}(1-\tau_2) & E_{23}(1-\tau_3) & E_{33}(1-\tau_1) \end{bmatrix}, \tag{52}$$

in which ρ_1, ρ_2, ρ_3, τ_1, τ_2 and τ_3 are dimensionless coefficients to be chosen.

10.2. The Case $R_{12} = 0$

A template with $R_{12} = 0$ and arbitrary $\{R_{11}, R_{22}\}$ is matched by taking

$$\rho_1 = \frac{1 - 3R_{11}}{E_{11}}, \quad \rho_2 = \frac{1 - 3R_{22}}{E_{22}}, \quad \tau_1 = \tau_2 = \tau_3 = 1. \tag{53}$$

Since ρ_3 does not appear, it is convenient to set it to one to get a diagonal $\mathbf{E}_{\rm II}$. The resulting split is

$$\mathbf{E}_{\rm I} + \mathbf{E}_{\rm II} = \begin{bmatrix} E_{11} - 3R_{11} & E_{12} & E_{13} \\ E_{12} & E_{22} - 3R_{22} & E_{23} \\ E_{13} & E_{23} & E_{33} \end{bmatrix} + \begin{bmatrix} 3R_{11} & 0 & 0 \\ 0 & 3R_{22} & 0 \\ 0 & 0 & 0 \end{bmatrix}, \tag{54}$$

To get the optimal element (BORP) set $R_{11} = \frac{1}{3}C_{11}^{-1}$ and $R_{22} = \frac{1}{3}C_{22}^{-1}$:

$$\mathbf{E}_{\rm I} + \mathbf{E}_{\rm II} = \begin{bmatrix} E_{11} - C_{11}^{-1} & E_{12} & E_{13} \\ E_{12} & E_{22} - C_{22}^{-1} & E_{23} \\ E_{13} & E_{23} & E_{33} \end{bmatrix} + \begin{bmatrix} C_{11}^{-1} & 0 & 0 \\ 0 & C_{22}^{-1} & 0 \\ 0 & 0 & 0 \end{bmatrix}, \tag{55}$$

For isotropic material this becomes

$$\mathbf{E}_{\rm I} + \mathbf{E}_{\rm II} = \frac{E}{1-\nu^2} \begin{bmatrix} \nu^2 & \nu & 0 \\ \nu & \nu^2 & 0 \\ 0 & 0 & \frac{1}{2}(1-\nu) \end{bmatrix} + E \begin{bmatrix} 1 & 0 & 0 \\ 0 & 1 & 0 \\ 0 & 0 & 0 \end{bmatrix}. \tag{56}$$

To match the (suboptimal) StrainRP, in which $R_{11} = \frac{1}{3}E_{11}$ and $R_{22} = \frac{1}{3}E_{22}$ the apropriate split is

$$\mathbf{E}_{\rm I} + \mathbf{E}_{\rm II} = \begin{bmatrix} 0 & E_{12} & E_{13} \\ E_{12} & 0 & E_{23} \\ E_{13} & E_{23} & E_{33} \end{bmatrix} + \begin{bmatrix} E_{11} & 0 & 0 \\ 0 & E_{22} & 0 \\ 0 & 0 & 0 \end{bmatrix}. \tag{57}$$

For isotropic material this becomes

$$\mathbf{E}_{\rm I} + \mathbf{E}_{\rm II} = E \begin{bmatrix} 0 & \nu & 0 \\ \nu & 0 & 0 \\ 0 & 0 & \frac{1}{2}(1-\nu) \end{bmatrix} + E \begin{bmatrix} 1 & 0 & 0 \\ 0 & 1 & 0 \\ 0 & 0 & 0 \end{bmatrix}. \tag{58}$$

Some FEM books suggest using the dilatational elasticity law for $\mathbf{E}_I$. As can be seen, the recommendation is incorrect for this element.

10.3. The Case $R_{12} \neq 0$

The case $R_{12} \neq 0$, arises in anisotropic displacement models for which $E_{13} \neq 0$ and/or $E_{23} \neq 0$. Now τ_2 and τ_3 must verify $E_{13}\gamma^{-1}\tau_2 + E_{23}\gamma\tau_3 = E_{13}\gamma^{-1} + E_{23}\gamma - 3R_{12}$. Solve for that τ_i $(i = 2, 3)$ that has an associated nonzero modulus. Note that the aspect ratio γ will generally appear in the SRI rule.

This case lacks practical interest because optimality can be achieved with $R_{12} = 0$. But for DispRP an obvious solution that eliminates all aspect ratio dependent is $\rho_1 = \rho_2 = \rho_3 = \tau_1 = \tau_2 = \tau_3 = 0$, whence $\mathbf{E}_{\rm I} = \mathbf{0}$, $\mathbf{E}_{\rm II} = \mathbf{E}$ and the fully integrated isoP element, which locks, is recovered.

10.4. Selective Directional Integration

The template can also be generated by non-Gaussian rules. For example, the following three-way directional split

$$\mathbf{E}_{\rm I} + \mathbf{E}_{\rm II} + \mathbf{E}_{\rm III} = \begin{bmatrix} E_{11} - C_{11}^{-1} & E_{12} & E_{13} \\ E_{12} & E_{22} - C_{22}^{-1} & E_{23} \\ E_{13} & E_{23} & E_{33} \end{bmatrix} + \begin{bmatrix} C_{11}^{-1} & 0 & 0 \\ 0 & 0 & 0 \\ 0 & 0 & 0 \end{bmatrix} + \begin{bmatrix} 0 & 0 & 0 \\ 0 & C_{22}^{-1} & 0 \\ 0 & 0 & 0 \end{bmatrix}, \tag{59}$$

generates the optimal panel in conjunction with three rules. Rule (I) is one-point Gauss with $\{\xi, \eta\} = \{0, 0\}$ and weight 4; Rule (II) has two points on the $y = 0$ median: $\{\xi, \eta\} = \{0, \pm 1/\sqrt{3}\}$ with weight 2; rule (III) has two points on the $x = 0$ median: $\{\xi, \eta\} = \{\pm 1/\sqrt{3}, 0\}$ with weight 2. This selective directional integration is difficult to extend to arbitrary quadrilaterals while preserving observer invariance.

Table 2. Signatures and Bending Ratios for Stress Hybrid Family

n_σ	5	7	13	21	31
R_{11}/E	0.33333	2.21173	2.21762	2.22125	2.22235
R_{22}/E	0.33333	0.35650	0.35967	0.35979	0.35981
R_{12}	0	0	0	0	0
r_x	1.00000	6.63518	6.65386	6.66375	6.66705
r_y	1.00000	1.06949	1.07900	1.07938	1.07944

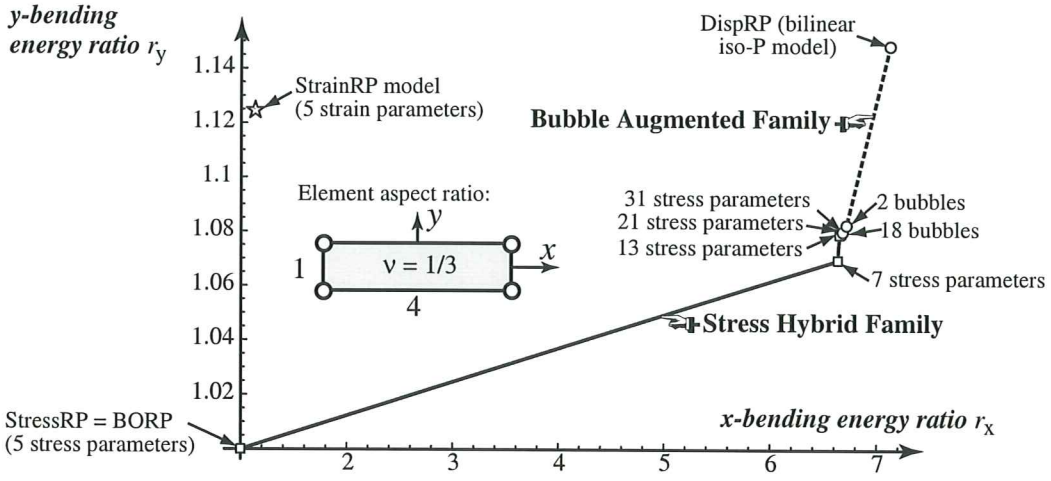

Figure 12. Representation of template families on the $\{r_x, r_y\}$ plane.

11. FUTILE FAMILIES

Families are template subsets that arise naturally from specific methods as function of discrete or continuous decision parameters. To render the concept more concrete, two historically important families for the rectangular panel are considered next.

11.1. Equilibrium Stress Hybrids

This family was studied in the late 1960s. It is obtained by generalizing the 5-parameter stress form of Section 4 with a polynomial series in $\{x, y\}$. An obvious choice is to make σ_{xx}, σ_{yy} and σ_{xy} complete polynomials in $\{x, y\}$:

$$\sigma_{xx} = \sum_{i,j} a_{ij}\, x^i y^j, \quad \sigma_{yy} = \sum_{i,j} b_{ij}\, x^i y^j, \quad \sigma_{xy} = \sum_{i,j} c_{ij}\, x^i y^j, \quad i \geq 0,\ j \geq 0,\ i + j \leq n. \tag{60}$$

For a complete expansion of order $n \geq 0$ one gets $3(n+1)(n+2)/2$ coefficients. Imposing strongly the two internal equilibrium equations $(1)_3$ for zero body forces reduces the set to $n_\sigma = 3 + 3n + n^2$ independent coefficients. For $n = 0, 1, 3, 5$ and 7 this gives $n_\sigma = 3, 7, 13, 21$ and 31 coefficients, respectively. (Only odd n is of interest beyond $n = 0$, since terms with $i + j = 2, 4, \ldots$ etc., cancel out on integrating strains over the rectangle and have no effect on the element stiffness.)

The stiffness equations of this family can be obtained by the hybrid stress method of Pian and Tong [26,46]. To display the effect of n_σ, the signature of the template (31)–(32) and the associated bending energy ratios were calculated for aspect ratio $\gamma = a/b = 4$, isotropic material with modulus E and Poisson's ratio $\nu = 1/3$.

Table 3. Signatures and Bending Ratios for Bubble-Augmented Family

n_b	0	2	18
R_{11}/E	2.37501	2.23894	2.22546
R_{22}/E	0.38281	0.36088	0.35998
R_{12}	0.	0.	0
r_x	7.12505	6.71683	6.67637
r_y	1.14844	1.08265	1.07994

The results are collected in Table 2. The bending energy ratios are displayed in Figure 12. Increasing the number of stress terms rapidly stiffens the element in x-bending. This is an instance of what may be called *equilibrium stress futility*: adding more stress terms makes things worse. (The phenomenon is well known but a representation such as that in Figure 12 is new.) As $n_\sigma \to \infty$ the template signature approaches the limit $R_{11}/E \approx 0.2224$ and $R_{22}/E \approx 0.3599$ to 4 places.

11.2. Bubble-Augmented Isoparametrics

A second family can be generated by starting from the conforming iso-P element DispRP of Section 6, and injecting n_b displacement bubble functions. (Bubble are shape functions that vanish over the element boundaries.) The idea is also a G2 curiosity but has resurfaced recently. Results for 2 and 18 bubbles (1 and 9 internal nodes, respectively) are collected in Table 3 and displayed also in Figure 12.

As can be expected injecting bubbles makes the element more flexible but the improvement is marginal. If $n_b \to \infty$ the signature approaches that of the $n_\sigma \to \infty$ hybrid-stress model of the previous subsection. For all this extra work (these models become expensive on account of high order Gauss integration rules and DOF condensation), r_x decreases from 7.12 to 6.67. This is a convincing illustration of *bubble futility*.

Figure 12 also marks the energy ratios of the StrainRP element. For this instance $R_{11}/E = R_{22}/E = 3/8 = 0.375$ and $r_x = r_y = 1.125$. Consequently the element is only slightly overstiff. Increasing the number of strain terms, however, would lead to another "futile family."

12. NUMERICAL EXAMPLES

Only three benchmark examples, all involving cantilever beams, are presented below.

12.1. Example 1: Slender Isotropic Cantilever

The slender 16:1 cantilever beam of Figure 13(a) is fabricated of isotropic material, with $E = 7680$, $\nu = 1/4$ and $G = (2/5)E = 3072$. The dimensions are shown in the Figure. Two end load cases are considered: an end moment $M = 1000$ and a transverse end shear $P = 48000/1027 = 46.7381$. The tip deflections $\delta_C = u_{yC}$ from beam theory: $ML^2/(2EI_z)$ and $PL^3/(3EI_z) + PL/(GA_s)$, in which $I_z = b^3h/12$ and $A_s = 5A/6 = 5bh/6$, are both exactly 100. For the second load case the shear deflection is only 0.293% of u_{yC}; thus the particular expression used for A_s is not very important.

Regular meshes with only one element ($N_y = 1$) through the beam height are considered. The number N_x of elements along the span is varied from 1 to 64, giving elements with aspect ratios that go from $\gamma = 16$ through $\gamma = \frac{1}{4}$. The root clamping condition is imposed by setting the u_x node displacement to zero at both root nodes, but u_y is only fixed at the lower one thus allowing for Poisson's contraction at the root.

Tables 4 and 5 report computed tip deflections u_{yC} for several element types. The first three rows list results for the 3 rectangular panel models of Sections 4–6. The last three rows give results for selected triangular elements. BODT is the Bending Optimal Drilling Triangle: a 3-node membrane element

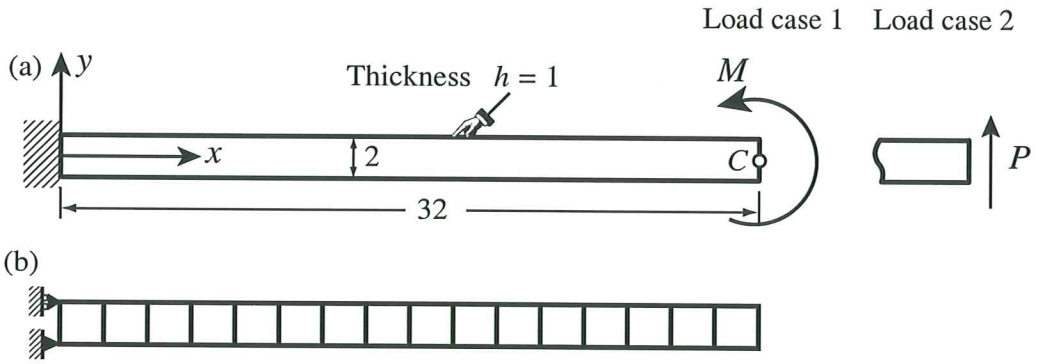

Figure 13. Slender cantilever beam for Examples 1 and 2.
A 16 × 1 FEM mesh with $\gamma = 1$ is shown in (b).

Table 4 Tip Deflections (exact=100) for Slender Isotropic Cantilever under End Moment

Element	Mesh: x-subdivisions × y-subdivisions ($N_x \times N_y$)						
	1 × 1 ($\gamma = 16$)	2 × 1 ($\gamma = 8$)	4 × 1 ($\gamma = 4$)	8 × 1 ($\gamma = 2$)	16 × 1 ($\gamma = 1$)	32 × 1 ($\gamma = \frac{1}{2}$)	64 × 1 ($\gamma = \frac{1}{4}$)
StressRP (BORP)	100.00	100.00	100.00	100.00	100.00	100.00	100.00
StrainRP	93.75	93.75	93.75	93.75	93.75	93.75	93.75
DispRP	0.97	3.75	13.39	37.49	68.18	85.71	91.60
ALL-EX	0.04	0.63	7.40	35.83	58.44	64.89	66.45
CST	0.32	1.25	4.46	12.50	22.73	28.57	30.53
BODT	100.00	100.00	100.00	100.00	100.00	100.00	100.00

Table 5 Tip Deflections (exact=100) for Slender Isotropic Cantilever under End Shear

Element	Mesh: x-subdivisions × y-subdivisions ($N_x \times N_y$)						
	1 × 1 ($\gamma = 16$)	2 × 1 ($\gamma = 8$)	4 × 1 ($\gamma = 4$)	8 × 1 ($\gamma = 2$)	16 × 1 ($\gamma = 1$)	32 × 1 ($\gamma = \frac{1}{2}$)	64 × 1 ($\gamma = \frac{1}{4}$)
StressRP (BORP)	75.02	93.72	98.39	99.56	99.86	99.94	99.97
StrainRP	70.35	87.88	92.26	93.35	93.63	93.71	93.73
DispRP	0.97	3.75	13.39	37.49	68.16	85.69	91.58
ALL-EX	0.24	0.69	6.36	35.18	59.59	65.70	67.03
CST	0.48	1.41	4.62	12.66	22.88	28.73	30.69
BODT	75.20	93.37	98.20	99.55	99.93	100.12	100.15

with drilling freedoms studied in [49,79,89,90]. ALL-EX is the exactly integrated 1988 Allman triangle with drilling freedoms [91]. CST is the Constant Strain Triangle, also called linear triangle and Turner triangle [1]. Both ALL-EX and BODT have three freedoms per node whereas all others have two. To get exactly 100.00% from BODT under an end-moment requires particular attention to the end load consistent lumping [90].

BORP is exact for all γ under end-moment and converges rapidly under end-shear. The performance of BODT is similar, inasmuch as this triangle is constructed to be bending exact in rectangular-mesh units. (In the end-shear load case BORP and BODT, which morph to different beam templates, converge to slightly different limits as $\gamma \to 0$.) StrainRP is about 6% stiffer than BORP, which can be expected since $1/(1-\nu^2) = 16/15$. DispRP, as well as the triangles ALL-EX and CST, lock as γ increases.

Table 6 Tip Deflections (exact=100) for Slender Anisotropic Cantilever under End Moment

Element	Mesh: x-subdivisions × y-subdivisions ($N_x \times N_y$)						
	1×1 ($\gamma = 16$)	2×1 ($\gamma = 8$)	4×1 ($\gamma = 4$)	8×1 ($\gamma = 2$)	16×1 ($\gamma = 1$)	32×1 ($\gamma = \frac{1}{2}$)	64×1 ($\gamma = \frac{1}{4}$)
StressRP (BORP)	100.00	100.00	100.00	100.00	100.00	100.00	100.00
StrainRP	2.26	2.26	2.26	2.26	2.26	2.26	2.26
DispRP	0.02	0.07	0.25	0.76	1.53	2.08	2.25

Table 7 Tip Deflections (exact=100) for Slender Anisotropic Cantilever under End Shear

Element	Mesh: x-subdivisions × y-subdivisions ($N_x \times N_y$)						
	1×1 ($\gamma = 16$)	2×1 ($\gamma = 8$)	4×1 ($\gamma = 4$)	8×1 ($\gamma = 2$)	16×1 ($\gamma = 1$)	32×1 ($\gamma = \frac{1}{2}$)	64×1 ($\gamma = \frac{1}{4}$)
StressRP (BORP)	74.95	93.68	98.37	99.54	99.84	99.92	99.96
StrainRP	1.70	2.12	2.22	2.26	2.26	2.26	2.26
DispRP	0.02	0.07	0.25	0.75	1.52	2.06	2.23

The response for more element layers through the height can be readily estimated from (45). Consequently those results are omitted to save space. For example, to predict the DispRP answer on a 8×4 mesh under end-moment, proceed as follows. The aspect ratio is $\gamma = 8$. From the $\gamma = 8$ column of Table 4 read off $r_x = 100/3.75 = 26.667$. Set $n = 2$ in (45) to get $r_x^{(4)} = (15 + r_x)/16 = 2.60417$. The estimated tip deflection is $100/2.60417 = 38.40$. Running the program gives $\delta_C = 38.3913$ as average of the y displacement of the two end nodes. Predictions for the end-shear-load case will not be as accurate.

12.2. Example 2: Slender Anisotropic Cantilever

Next assume that the beam of Figure 13(a) is fabricated of anisotropic material with the elasticity properties

$$\mathbf{E} = \begin{bmatrix} 880 & 600 & 250 \\ 600 & 420 & 150 \\ 250 & 150 & 480 \end{bmatrix}, \qquad \mathbf{C} = \mathbf{E}^{-1} = \frac{1}{35580}\begin{bmatrix} 1791 & -2505 & -150 \\ -2505 & 3599 & 180 \\ -150 & 180 & 96 \end{bmatrix}. \tag{61}$$

That these are physically realizable can be checked by getting the eigenvalues of $\mathbf{E}$: $\{1386.1, 387.3, 6.63\}$, whence both $\mathbf{E}$ and $\mathbf{C}$ are positive definite. The load magnitudes are adjusted to get beam-theory tip deflections of 100: $M = 2.58672$ and $P = 0.121153$. Since

$$E_{11}C_{11} = 44.297 \tag{62}$$

the energy ratio analysis of Sections 8.3–8.4, through equations (42) and (43), predict that the strain and displacement model will be big losers, because $r_x \geq 44.297$. This is verified in Tables 6 and 7, which report computed tip deflections u_{yC} for the three rectangular panel models. While BORP shines, the strain and displacement models are way off, regardless of how many elements one puts along x.

Putting more elements through the height will help StrainRP and DispRP but too slowly to be practical. To give an example, a 128×8 mesh of StrainRP (or clones) under end moment will have $r_x^{(8)} = (63 + 44.297)/64 = 1.68$ and estimated deflection of $100/1.67 = 59.67$. Running that mesh gives $u_{yC} = 59.65$. So using over 2000 freedoms in this trivial problem the results are still off by about 40%.

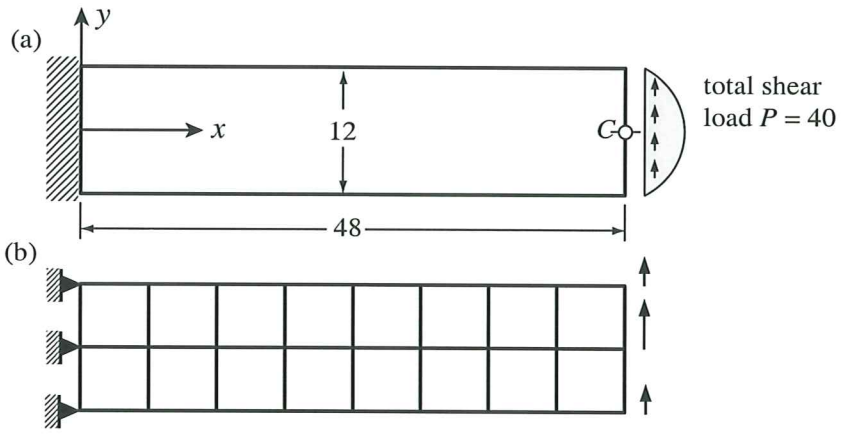

Figure 14. Short (Berkeley) cantilever under end shear: $E = 30000$, $\nu = 1/4$, $h = 1$; root contraction not allowed, a 8×2 mesh is shown in (b).

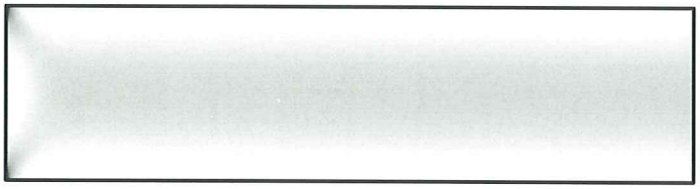

Figure 15. Intensity contour plot of σ_{xy} given by the 64×16 BORP mesh. Produced by *Mathematica* and Gaussian filtered by Adobe Photoshop. Stress node values averaged between adjacent elements. The root singularity pattern is clearly visible.

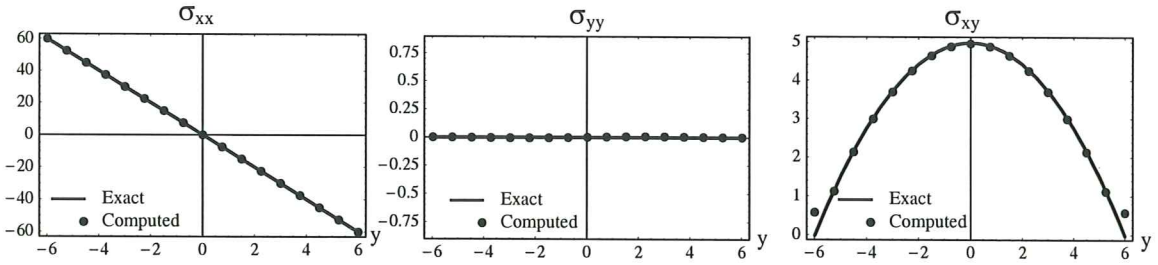

Figure 16. Distributions of σ_{xx}, σ_{yy} and σ_{xy} at $x = 12$ given by the 64×16 BORP mesh. Stress node values averaged between adjacent elements. Note different stress scales. Deviations at $y = \pm 6$ (free edges) due to "upwinded" y averaging.

12.3. Example 3: Short Cantilever Under End Shear

The shear-loaded cantilever beam defined in Figure 14 has been selected as a test problem for plane stress elements by many investigators since originally proposed in [92]. A full root-clamping condition is implemented by constraining both displacement components to zero at nodes located on at the root section $x = 0$. The applied shear load varies parabolically over the end section and is consistently lumped at the nodes. The main comparison value is the tip deflection $\delta_C = u_{yC}$ at the center of the end cross section. Reference [79] recommends $\delta_C = 0.35601$, which is also adopted here. The converged value of digits 4-5 is clouded by the mild singularity developing at the root section. This singularity is

Table 8 Tip Deflections (exact = 100) for Short Cantilever under End Shear

Element	Mesh: x-subdivisions × y-subdivisions ($N_x \times N_y$)				
	8 × 2	16 × 4	32 × 8	64 × 16	128 × 32
StressRP (BORP)	98.80	99.59	99.88	99.97	100.00
StrainRP	97.24	99.19	99.77	99.94	99.99
DispRP	88.83	96.83	99.16	99.78	99.95
ALL-EX	89.43	96.88	99.16	99.79	99.96
CST	55.09	82.59	94.90	98.65	99.66
BODT	101.68	100.30	100.03	100.00	100.00
	4 × 2	8 × 4	16 × 8	32 × 16	64 × 32
StressRP (BORP)	97.22	99.08	99.71	99.92	99.99
StrainRP	95.67	98.67	99.61	99.89	99.98
DispRP	69.88	90.05	97.24	99.28	99.82
ALL-EX	70.71	89.63	96.93	99.15	99.77
CST	37.85	69.86	90.04	97.25	99.28
BODT	96.68	98.44	99.37	99.78	99.93
	2 × 2	4 × 4	8 × 8	16 × 16	32 × 32
StressRP (BORP)	91.94	97.41	99.19	99.75	99.93
StrainRP	90.47	97.03	99.07	99.72	99.92
DispRP	37.84	70.57	90.39	97.35	99.31
ALL-EX	26.16	56.93	83.54	95.14	98.69
CST	17.83	43.84	75.01	92.13	97.86
BODT	92.24	96.99	98.70	99.48	99.81

displayed for σ_{xy} in the form of an intensity contour plot in Figure 15.

Table 8 gives computed deflections for rectangular mesh units with aspect ratios of 1, 2 and 4, using the three canonical rectangular panel models and the three triangles identified in Example 1. For end deflection reporting the load was scaled by (100/0.35601) so that the "theoretical solution" becomes 100.00. (In comparing stress values the unscaled load of $P = 40$ was used.)

There are no drastically small deflections because element aspect ratios only go up to 4:1. Elements StressRP (BORP), StrainRP and BODT outperformed the others. There is little to choose between these 3 models, which is typical of isotropic materials. The BODT triangle is geometrically more versatile but carries one more freedom per node.

Figure 16 plots averaged node stress values at section $x = 12$ computed from the 64 × 16 BODT mesh. The agreement with the standard beam stress distribution (that section being sufficiently away from the root) is very good except for σ_{xy} near the free edges $y = \pm 6$.

13. DISCUSSION AND CONCLUSIONS

What can templates contribute to FEM technology? Advantages in two areas are clear:

Synthesis. Only one procedure (module, function, subroutine) is written to do many elements. This simplifies comparison and verification benchmarking, as well as streamlining maintenance. A unified implementation automatically weeds out clones.

Customability. Templates can produce optimal and custom elements not obtainable (or hard to obtain) through conventional methods.

A striking example of the latter is the UBOTP macroelement presented in Section A.3 of the Appendix. This concludes a three decade search for a four noded trapezoid insensitive to distortion and that passes the patch test [67]. To the writer's knowledge, this model cannot be obtained with conventional formulations.

Will the synthesis power translate into teaching changes in finite element courses? This is not presently likely. Two reasons can be cited.

First, advantages may show up only in advanced or seminar-level courses. Beginning calculus students are not taught Lebesgue integration and distribution theory despite their wider scope. Likewise, introductory FEM courses are best organized around a few specific methods. Students must be exposed to a range of formulations and hands-on work before they can appreciate the advantages of unified implementation.

Second, the theory has not progressed to the point where the configuration of a template can be written down from first principles in front of an audience. Only two general rules are presently known: the fundamental decomposition into basic and higher order components, and the method to get the matrix structure of the basic part. No general rules to construct the higher order component can be stated aside from orthogonality and definiteness constraints.

How far can templates go? As of this writing templates are only known for a few elements in one and two dimensions, such as beams and flat plates of simple geometry. What is the major technical obstacle to go beyond those? Symbolic power. One must rely on computer-aided symbolic manipulation because geometric, constitutive and fabrication properties must be carried along as variables. This can lead, and does, to a combinatorial tarpit as elements become more complicated.

The good news is that computer algebra programs are gradually becoming more powerful, and are now routinely available on laptops and personal computers. Over the next ten years PCs are expected to migrate to 64-bit multiple-CPUs capable of addressing hundreds of GBs of memory at over 10GHz speeds. As that happens the development of templates for 3D solid and shell elements in reasonable time will become possible.

Acknowledgements

Preparation of this paper has been partly supported by the Finite Elements for Salinas contract with Sandia National Laboratories, and partly by the Spanish Ministerio of Educación y Cultura through a faculty fellowship while visiting the Centro Internacional de Métodos Numéricos en Ingenería (CIMNE), in Barcelona, Spain, from April through June 2002.

References

[1] Turner, M. J., Clough, R. W., Martin, H. C., Topp, L. J., Stiffness and deflection analysis of complex structures, *J. Aero. Sci.*, **23**, 805–824, 1956.

[2] Argyris, J. H., Kelsey, S., *Energy Theorems and Structural Analysis*, London, Butterworth, 1960; Part I reprinted from *Aircr. Engrg.*, **26**, Oct-Nov 1954 and **27**, April-May 1955.

[3] Felippa, C. A., A historical outline of matrix structural analysis: a play in three acts, *Computers & Structures*, **79**, 1313–1324, 2001.

[4] Pestel, E. C., Leckie, F. A., *Matrix Methods in Elastomechanics*, McGraw-Hill, New York, 1963.

[5] Przemieniecki, J. S., *Theory of Matrix Structural Analysis*, McGraw-Hill, New York, 1968; Dover edition 1986.

[6] Gallaguer, R. H., *A Correlation Study of Methods of Matrix Structural Analysis*, Pergamon, Oxford, 1964.

[7] Melosh, R. J., Bases for the derivation of matrices for the direct stiffness method, *AIAA J.*, **1**, 1631–1637, 1963.

[8] Turner, M. J., The direct stiffness method of structural analysis, Structural and Materials Panel Paper, AGARD Meeting, Aachen, Germany, 1959.

[9] Turner, M. J., Dill, E. H., Martin, H. C., Melosh, R.J., Large deflection analysis of complex structures subjected to heating and external loads, *J. Aero. Sci.*, **27**, pp. 97-107, 1960.

[10] Turner, M. J., Martin, H. C., Weikel, R. C., Further development and applications of the stiffness method, in *AGARDograph 72: Matrix Methods of Structural Analysis*, ed. by B. M. Fraeijs de Veubeke, Pergamon Press, New York, 203–266, 1964.

[11] Melosh, R. J., Development of the stiffness method to define bounds on the elastic behavior of structures, *Ph.D. Dissertation*, University of Washington, Seattle, 1962.

[12] Fraeijs de Veubeke, B. M., Upper and lower bounds in matrix structural analysis, in *AGARDograph 72: Matrix Methods of Structural Analysis*, ed. by B. M. Fraeijs de Veubeke, Pergamon Press, New York, 174–265, 1964.

[13] Clough, R. W., The finite element method – a personal view of its original formulation, in *From Finite Elements to the Troll Platform – the Ivar Holand 70th Anniversary Volume*, ed. by K. Bell, Tapir, Norway, 89–100, 1994.

[14] Clough, R. W., The finite element method in plane stress analysis, *Proc. 2nd ASCE Conf. on Electronic Computation*, Pittsburgh, Pa, 1960.

[15] Clough, R. W., The finite element method in structural mechanics, in *stress Analysis*, ed. by O. C. Zienkiewicz and G. S. Holister, Wiley, London, 85–119, 1965.

[16] Fraeijs de Veubeke, B. M., Displacement and equilibrium models, in *Stress Analysis*, ed. by O. C. Zienkiewicz and G. Hollister, Wiley, London, 145–197, 1965; reprinted in *Int. J. Numer. Meth. Engrg.*, **52**, 287–342, 2001.

[17] Zienkiewicz, O. C., Cheung, Y. K., *The Finite Element Method in Engineering Science*, McGraw-Hill, London, 1967.

[18] Zienkiewicz, O. C., Cheung, Y. K., Finite elements in the solution of field problems, *The Engineer*, 507–510, 1965.

[19] Irons, B. M., Engineering application of numerical integration in stiffness methods, *AIAA J.*, **4**, pp. 2035–2037, 1966.

[20] Irons, B. M., Barlow, J., Comments on 'matrices for the direct stiffness method' by R. J. Melosh, *AIAA J.*, **2**, 403, 1964.

[21] Bazeley, G. P., Cheung, Y. K., Irons, B. M., Zienkiewicz, O. C., Triangular elements in plate bending – conforming and nonconforming solutions, in *Proc. 1st Conf. Matrix Meth. Struc. Mech.*, ed. by J. Przemieniecki et. al., AFFDL-TR-66-80, Air Force Institute of Technology, Dayton, Ohio, 1966, 547–576.

[22] Ergatoudis, J., Irons, B. M., Zienkiewicz, O. C., Curved, isoparametric, "quadrilateral" elements for finite element analysis, *Int. J. Solids Struc.*, **4**, 31–42, 1968.

[23] Irons, B. M., Ahmad, S., *Techniques of Finite Elements*, Ellis Horwood Ltd, Chichester, UK, 1980.

[24] Pian, T. H. H., Derivation of element stiffness matrices by assumed stress distributions, *AIAA J.*, **2**, 1333–1336, 1964.

[25] Pian, T. H. H., Element stiffness matrices for boundary compatibility and for prescribed boundary stresses, in *Proc. 1st Conf. on Matrix Methods in Structural Mechanics,* AFFDL-TR-66-80, Air Force Institute of Technology, Dayton, Ohio, 457–478, 1966.

[26] Pian, T. H. H., Tong, P., Basis of finite element methods for solid continua, *Int. J. Numer. Meth. Engrg.*, **1**, 3–29, 1969.

[27] Pian, T. H. H., Some notes on the early history of hybrid stress finite element method, *Int. J. Numer. Meth. Engrg.*, **47**, 2000, 419–425.

[28] Herrmann, L. R., Elasticity equations for nearly incompressible materials by a variational theorem, *AIAA Journal*, **3**, 1896–1900, 1965.

[29] Taylor, R. L., Pister, K. S., Herrmann, L. R., A variational principle for incompressible and nearly incompressible orthotropic elasticity, *Int. J. Solids Struc.*, **4**, 875-883, 1968.

[30] Strang, G., Fix, G., *An Analysis of the Finite Element Method.* Prentice-Hall, 1973.

[31] Strang, G., (1972). Variational crimes in the finite element method, in *The Mathematical Foundations of the Finite Element Method with Applications to Partial Differential Equations*, ed. by A. K. Aziz, Academic Press, New York, 689–710, 1972.

[32] Hughes, T. J. R., *The Finite Element Method: Linear Static and Dynamic Finite Element Analysis*, Prentice Hall, Englewood Cliffs, N. J., 1987.

[33] Atluri, S. N., Gallagher, R. N., Zienkiewicz, O. C. (eds.), *Hybrid and Mixed Finite Element Methods*, Wiley, New York, 1983.

[34] MacNeal, R. H., Derivation of element stiffness matrices by assumed strain distribution, *Nuclear Engrg. Design*, **70**, 3–12 (1978)

[35] Szabo, B., Babuska, I. , *Finite Element Analysis* Wiley, New York, 1991.

[36] MacNeal, R. H., The evolution of lower order plate and shell elements in MSC/NASTRAN, in T. J. R. Hughes and E. Hinton (eds.), *Finite Element Methods for Plate and Shell Structures, Vol. I: Element Technology*, Pineridge Press, Swansea, U.K., 1986, 85–127.

[37] MacNeal, R. H., *Finite Elements: Their Design and Performance*, Marcel Dekker, New York, 1994.

[38] Bergan, P. G., Finite elements based on energy orthogonal functions, *Int. J. Numer. Meth. Engrg.*, **15**, 1141–1555, 1980.

[39] Bergan, P. G., Nygård, M. K., Finite elements with increased freedom in choosing shape functions, *Int. J. Numer. Meth. Engrg.*, **20**, 643–664, 1984.

[40] Flanagan, D. P., Belytschko, T., A uniform strain hexahedron and quadrilateral with orthogonal hourglass control, *Int. J. Numer. Meth. Engrg.*, **17**, 679–706, 1981.

[41] Bathe, K. J., Dvorkin, E. N., A four-node plate bending element based on Mindlin-Reissner plate theory and a mixed interpolation, *Int. J. Numer. Meth. Engrg.*, **21**, 367–383, 1985.

[42] Huang, H. C., Hinton, E., A new nine node degenerated shell element with enhanced membrane and shear interpolation, *Int. J. Numer. Meth. Engrg.*, **22**, 73–92, 1986.

[43] Park, K. C., Stanley, G. M., A curved C^0 shell element based on assumed natural-coordinate strains, *J. Appl. Mech.*, **53**, 278–290, 1986.

[44] Stanley, G. M., Park, K. C., Hughes, T. J. R., Continuum based resultant shell elements, in T. J. R. Hughes and E. Hinton (eds.), *Finite Element Methods for Plate and Shell Structures, Vol. I: Element Technology*, Pineridge Press, Swansea, U.K., 1986, 1–45.

[45] Pian, T. H. H., Sumihara, K., Rational approach for assumed stress finite elements, *Int. J. Numer. Meth. Engrg.*, **20**, 1685–1695, 1984.

[46] Pian, T. H. H., Tong, P., Relations between incompatible displacement model and hybrid stress model, *Int. J. Numer. Meth. Engrg.*, **22**, 173-181, 1986.

[47] Punch, E. F., Atluri, S. N., Development and testing of stable, invariant, isoparametric curvilinear 2- and 3D hybrid stress elements, *Comp. Meths. Appl. Mech. Engrg.*, **47**, 331–356, 1984.

[48] Militello, C., Felippa, C. A., The First ANDES Elements: 9-DOF Plate Bending Triangles, *Comp. Meths. Appl. Mech. Engrg.*, **93**, 217–246, 1991.

[49] Felippa, C. A., Militello, C., Membrane triangles with corner drilling freedoms: II. The ANDES element, *Finite Elements Anal. Des.*, **12**, 189–201, 1992.

[50] Simo, J. C., Hughes, T. J. R., On the variational foundations of assumed strain methods, *J. Appl. Mech.*, **53**, 51–54, 1986.

[51] Simo, J. C., Rifai, M. S., A class of mixed assumed strain methods and the method of incompatible modes, *Int. J. Numer. Meth. Engrg.*, **29**, 1595–1638, 1990.

[52] Felippa, C. A., Militello, C., Developments in variational methods for high performance plate and shell elements, in *Analytical and Computational Models for Shells*, CED Vol. 3, Eds. A. K. Noor, T. Belytschko and J. C. Simo, The American Society of Mechanical Engineers, ASME, New York, 1989, 191–216.

[53] Fraeijs de Veubeke, B. M., Diffusive equilibrium models, in M. Geradin (ed.), *B. M. Fraeijs de Veubeke Memorial Volume of Selected Papers*, Sitthoff & Noordhoff, Alphen aan den Rijn, The Netherlands, 569–628, 1980.

[54] Bergan, P. G., Felippa, C. A., A triangular membrane element with rotational degrees of freedom, *Comp. Meths. Appl. Mech. Engrg.*, **50**, 25–69, 1985.

[55] Bergan, P. G., Felippa, C. A., Efficient implementation of a triangular membrane element with drilling freedoms, in T. J. R. Hughes and E. Hinton (eds.), *Finite Element Methods for Plate and Shell Structures, Vol. I: Element Technology*, Pineridge Press, Swansea, U.K., 1986, 128–152.

[56] Nygård, M. K., The Free Formulation for nonlinear finite elements with applications to shells, *Ph. D. Dissertation*, Division of Structural Mechanics, NTH, Trondheim, Norway, 1986.

[57] Felippa, C. A., Bergan, P. G., A triangular plate bending element based on an energy-orthogonal free formulation, *Comp. Meths. Appl. Mech. Engrg.*, **61**, 129–160, 1987.

[58] Felippa, C. A., Parametrized multifield variational principles in elasticity: II. Hybrid functionals and the free formulation, *Comm. Appl. Numer. Meth.*, **5**, 79–88, 1989.

[59] Felippa, C. A., The extended free formulation of finite elements in linear elasticity, *J. Appl. Mech.*, **56**, 609–616, 1989.

[60] Skeie, G., The Free Formulation: linear theory and extensions with applications to tetrahedral elements with rotational freedoms, *Ph. D. Dissertation*, Division of Structural Mechanics, NTH, Trondheim, Norway, 1991.

[61] Felippa, C. A., Clough, R. W., The finite element method in solid mechanics, in *Numerical Solution of Field Problems in Continuum Physics*, ed. by G. Birkhoff and R. S. Varga, SIAM–AMS Proceedings II, American Mathematical Society, Providence, R.I., 210–252, 1969.

[62] Taig, I. C., Kerr, R. I., Some problems in the discrete element representation of aircraft structures, in *Matrix Methods of Structural Analysis*, ed. by B. M. Fraeijs de Veubeke, Pergamon Press, London, 1964.

[63] Wilson, E. L., Taylor, R. L., Doherty, W. P., Ghaboussi, J., Incompatible displacement models, in *Numerical and Computer Models in Structural Mechanics*, ed. by S. J. Fenves, N. Perrone, A. R. Robinson and W. C. Schnobrich, Academic Press, New York, 43–57, 1973.

[64] Taylor, R. L., Wilson, E. L., Beresford, P. J., A nonconforming element for stress analysis, *Int. J. Numer. Meth. Engrg.*, **10**, 1211–1219, 1976.

[65] Belytschko, T., Liu, W. K., Engelmann, B. E., The gamma elements and related developments, in T. J. R. Hughes and E. Hinton (eds.), *Finite Element Methods for Plate and Shell Structures, Vol. I: Element Technology*, Pineridge Press, Swansea, U.K., 316–347, 1986.

[66] MacNeal, R. H., A simple quadrilateral shell element, *Computers & Structures*, **8**, 175–183, 1978.

[67] Lautersztajn-S, N., Samuelsson, A., Further discussion on four-node isoparametric elements in plane bending, *Int. J. Numer. Meth. Engrg.*, **47**, 129–140, 2000.

[68] Pian, T. H. H., Some notes on the early history of hybrid stress finite element method, *Int. J. Numer. Meth. Engrg.*, 419–425, 2000.

[69] Felippa, C. A., A survey of parametrized variational principles and applications to computational mechanics, *Comp. Meths. Appl. Mech. Engrg.*, **113**, 109–139, 1994.

[70] Felippa, C. A., Haugen, B., Militello, C., From the individual element test to finite element templates: evolution of the patch test, *Int. J. Numer. Meth. Engrg.*, **38**, 199–222, 1995.

[71] Felippa, C. A., Parametrized unification of matrix structural analysis: classical formulation and d-connected mixed elements, *Finite Elements Anal. Des.*, **21**, 45–74, 1995.

[72] Felippa, C. A., Recent developments in parametrized variational principles for mechanics, *Comput. Mech.*, **18**, 159–174, 1996.

[73] Felippa, C. A., Militello, C., Construction of optimal 3-node plate bending elements by templates, *Comput. Mech.*, **24**, 1–13 (1999).

[74] Felippa, C. A. Recent developments in basic finite element technologies, in *Computational Mechanics in Structural Engineering-Recent Developments*, ed. by F.Y. Cheng and Y. Gu, Elsevier, Amsterdam, 141–156, 1999.

[75] Felippa, C. A. Recent advances in finite element templates, in *Computational Mechanics for the Twenty-First Century*, ed. by B.J.V. Topping, Saxe-Coburn Publications, Edinburgh, U.K., 71–98, 2000.

[76] Bergan, P. G., Hanssen, L., A New Approach for Deriving 'Good' Finite Elements, in *The Mathematics of Finite Elements and Applications – Volume II*, ed. by J. R. Whiteman, Academic Press, London, 483–497, 1975.

[77] Hanssen, L., Bergan, P. G., Syversten, T. J., Stiffness derivation based on element convergence requirements, in *The Mathematics of Finite Elements and Applications – Volume III*, ed. by J. R. Whiteman, Academic Press, London, 83–96, 1979.

[78] Militello, C. and Felippa, C. A., The individual element patch revisited, in *The Finite Element Method in the 1990's — a book dedicated to O. C. Zienkiewicz*, ed. by E. Oñate, J. Periaux and A. Samuelsson, CIMNE, Barcelona and Springer-Verlag, Berlin, 554–564, 1991.

[79] Felippa, C. A., A study of optimal membrane triangles with drilling freedoms, submitted to *Comp. Meths. Appl. Mech. Engrg.*, 2002.

[80] Felippa, C. A., Customizing the mass and geometric stiffness of plane thin beam elements by Fourier methods, *Engrg. Comput.*, **18**, 286–303, 2001.

[81] Felippa, C. A., Customizing high performance elements by Fourier methods, *Trends in Computational Mechanics*, ed. by W. A. Wall, K.-U. Bleitzinger and K. Schweizerhof, CIMNE, Barcelona, Spain, 283-296, 2001.

[82] Doherty, W. P., Wilson, E. L., Taylor, R. L., Stress analysis of axisymmetric solids utilizing higher order quadrilateral finite elements, SESM Report 69-3, Department of Civil Engineering, University of California, Berkeley, 1969.

[83] Zienkiewicz, O. C., Taylor, R. L., Too, J. M., Reduced integration technique in general analysis of plates and shells, *Int. J. Numer. Meth. Engrg.*, **3**, 275–290, 1971.

[84] Pawsey, S. F., Clough, R. W., Improved numerical integration of thick shell finite elements, *Int. J. Numer. Meth. Engrg.*, **3**, 545–586, 1971.

[85] Kavanagh, K., Key, S. W., A note on selective and reduced integration techniques in the finite element method, *Int. J. Numer. Meth. Engrg.*, **4**, 148–150, 1972.

[86] Hughes, T. J. R., Generalization of selective integration procedures to anisotropic and nonlinear media, *Int. J. Numer. Meth. Engrg.*, **15**, 1413–148, 1980.

[87] Hughes, T. J. R., Malkus, D. S., Mixed finite element methods – reduced and selective integration techniques: a unification of concepts, *Comp. Meths. Appl. Mech. Engrg.*, bf 15, 63–81, 1978.

[88] Hughes, T. J. R., Malkus, D. S., A general penalty mixed equivalence theorem for anisotropic, incompressible finite elements, in *Hybrids and Mixed Finite Element Methods*, ed. by S. N. Atluri, R. H. Gallagher and O. C. Zienkiewicz, Wiley, London, 1983.

[89] Alvin, K., de la Fuente, H. M., Haugen, B., Felippa, C. A., Membrane triangles with corner drilling freedoms: I. The EFF element, *Finite Elements Anal. Des.*, **12**, 163–187, 1992.

[90] Felippa, C. A., Alexander, S., Membrane triangles with corner drilling freedoms: III. Implementation and performance evaluation, *Finite Elements Anal. Des.*, **12**, 203–239, 1992.

[91] Allman, D. J., Evaluation of the constant strain triangle with drilling rotations, *Int. J. Numer. Meth. Engrg.*, **26**, 2645–2655, 1988.

[92] Felippa, C. A., Refined finite element analysis of linear and nonlinear two-dimensional structures, *Ph.D. Dissertation*, Department of Civil Engineering, University of California at Berkeley, Berkeley, CA, 1966.

[93] Felippa, C. A., Optimal four noded membrane quadrilaterals, Report in preparation.

[94] Felippa, C. A., Fitting strains and displacements by minimizing dislocation energy, Report in preparation.

[95] Felippa, C. A., Park, K. C., The construction of free-free flexibility matrices for multilevel structural analysis, *Comp. Meths. Appl. Mech. Engrg.*, **191**, 2111-2140, 2002.

[96] MacNeal, R. H., Harder, R. L., A proposed standard set of problems to test finite element accuracy, *Finite Elements Anal. Des.*, **1**, 3–20, 1985.

[97] MacNeal, R. H., A theorem regarding the locking of tapered four noded membrane elements, *Int. J. Numer. Meth. Engrg.*, **24**, 1793–1799, 1987.

Appendix A. OTHER PANEL GEOMETRIES

The template framework of four noded membrane elements can be extended to more general geometries, at the cost of increased complexity in symbolic computations. This Appendix presents templates for parallelogram and trapezoidal geometries. The template for a general quadrilateral is the topic of a separate article [93].

The G1 direct elasticity methods of Sections 4–5 do not work beyond the parallelogram. The resulting "node collocation" elements fail the patch test and cannot be fitted in the template framework. Variational methods are required to get stress-assumed and strain-assumed elements that work. For stress elements the Hellinger-Reissner (HR) principle is used. For strain elements, a strain-fit method [94] in conjunction with de Veubeke's strain-displacement mixed functional is used.

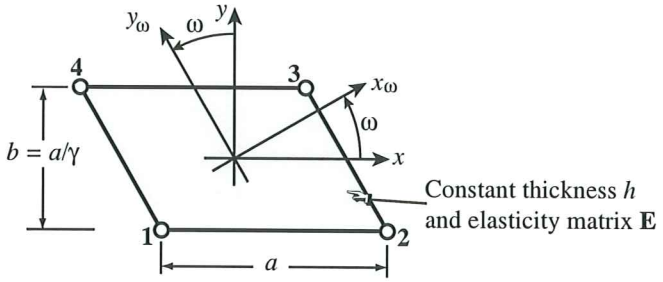

Figure 17. The 4-node parallelogram (swept) panel.

A.1 Parallelogram (Swept) Panel

The geometry of the parallelogram panel shown in Figure 17 is defined by the dimensions a, b and the skewangle ω, positive counterclockwise. The template again has the configuration (31) displayed in Figure 6. With $s = \tan\omega$ the matrices to be adjusted are

$$\mathbf{H}_c = \frac{1}{2ab}\begin{bmatrix} -b & 0 & b & 0 & b & 0 & -b & 0 \\ 0 & -a-bs & 0 & -a+bs & 0 & a+bs & 0 & a-bs \\ -a-bs & -b & -a+bs & b & a+bs & b & a-bs & -b \end{bmatrix}, \quad \mathbf{W} = \begin{bmatrix} \frac{1}{a} & 0 \\ -\frac{s}{b} & \frac{1}{b} \end{bmatrix}. \tag{63}$$

The higher order projector $\mathbf{H}_h$ is exactly as in (32), whereas $\mathbf{R}$ depends on the formulation, as explained below. For future use the compliance and elasticity in the median direction y_ω (see Figure 17) are denoted by

$$\begin{aligned} C^\omega_{22} &= C_{22}\cos^4\omega - 2C_{23}\cos^3\omega\sin\omega + (2C_{12}+C_{33})\cos^2\omega\sin^2\omega - 2C_{13}\cos\omega\sin^3\omega + C_{11}\sin^4\omega \\ &= \frac{C_{22} - 2C_{23}s + (2C_{12}+C_{33})s^2 - 2C_{13}s^3 + C_{11}s^4}{(1+s^2)^2}, \\ E^\omega_{22} &= E_{22}\cos^4\omega - 4E_{23}\cos^3\omega\sin\omega + (2E_{12}+4E_{33})\cos^2\omega\sin^2\omega - 4E_{13}\cos\omega\sin^3\omega + E_{11}\sin^4\omega \\ &= \frac{E_{22} - 4E_{23}s + (2E_{12}+4E_{33})s^2 - 4E_{13}s^3 + E_{11}s^4}{(1+s^2)^2}. \end{aligned} \tag{64}$$

Stress element. A 5-parameter stress element StressPP can be constructed either directly, as done by Gallagher [6, Ch. 3A], or by the HR principle, starting from the energy-orthogonal stress field

$$\begin{bmatrix} \sigma_{xx} \\ \sigma_{yy} \\ \sigma_{xy} \end{bmatrix} = \begin{bmatrix} 1 & 0 & 0 & y/b & \sin^2\omega\, x_\omega \\ 0 & 1 & 0 & 0 & \cos^2\omega\, x_\omega \\ 0 & 0 & 1 & 0 & -\sin\omega\cos\omega\, x_\omega \end{bmatrix} \begin{bmatrix} \mu_1 \\ \mu_2 \\ \mu_3 \\ \mu_4 \\ \mu_5 \end{bmatrix}, \tag{65}$$

in which $\sin\omega = s/\sqrt{1+s^2}$, $\cos\omega = 1/\sqrt{1+s^2}$, and $x_\omega = (x\cos\omega + y\sin\omega)/(a\cos\omega) = (x+ys)/a$. Both methods give the same stiffness. [Because (65) is an equilibrium field, an equilibrium stress hybrid formulation gives the same answer.] The stiffness is matched by the template with

$$R_{11} = \frac{1}{3C_{11}}, \quad R_{12} = 0, \quad R_{22} = \frac{1}{3C^\omega_{22}(1+s^2)^2}. \tag{66}$$

If the material is isotropic the diagonal entries are $R_{11} = \frac{1}{3}E$ and $R_{22} = \frac{1}{3}E/(1+s^2)^2$. The Q6 and QM6 elements continue to be clones of StressPP.

Strain element. A 5-parameter strain element StrainPP can be constructed by the direct elasticity method of Section 5, or by a variational strain-fitting method [94], starting from the companion of (65):

$$\begin{bmatrix} e_{xx} \\ e_{yy} \\ 2e_{xy} \end{bmatrix} = \begin{bmatrix} 1 & 0 & 0 & y/b & \sin^2\omega\, x_\omega \\ 0 & 1 & 0 & 0 & \cos^2\omega\, x_\omega \\ 0 & 0 & 1 & 0 & -2\sin\omega\cos\omega\, x_\omega \end{bmatrix} \begin{bmatrix} \chi_1 \\ \chi_2 \\ \chi_3 \\ \chi_4 \\ \chi_5 \end{bmatrix}. \tag{67}$$

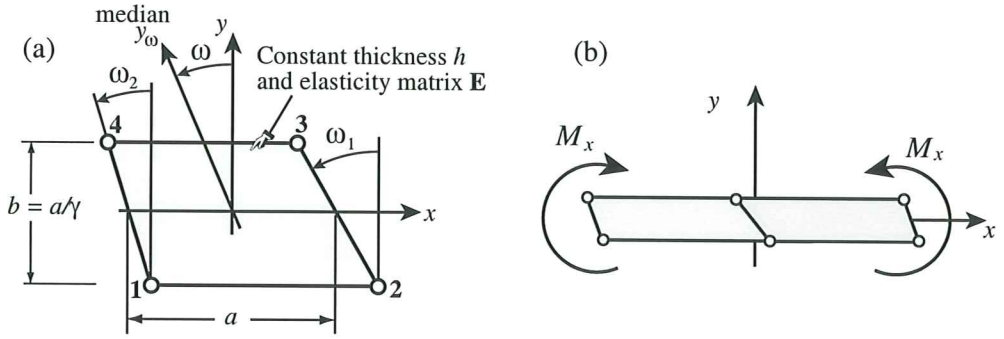

Figure 18. The four noded trapezoidal panel and a two-trapezoid repeatable macroelement.

Both methods give the same result. The stiffness is matched by setting

$$R_{11} = \tfrac{1}{3}E_{11}, \quad R_{12} = 0, \quad R_{22} = \frac{E^{\omega}_{22}}{3(1+s^2)^2}. \tag{68}$$

Displacement element. The conforming, exactly integrated isoparametric element DispPP is matched by setting

$$R_{11} = \frac{1}{3}\left(E_{11} + 4E_{13}s + (2E_{12}{+}4E_{33})s^2 + 4E_{23}s^3 + E_{22}s^4 + (E_{33} + 2E_{23}s + E_{22}s^2)\gamma^2\right),$$
$$R_{12} = \frac{1}{3\gamma}\left(E_{13} + (E_{12}{+}2E_{33})s + 3E_{23}s^2 + E_{22}s^3 + (E_{23}{+}E_{22}s)\gamma^2\right), \quad R_{22} = \frac{1}{3\gamma^2}(E_{33} + 2E_{23}s + E_{22}(s^2{+}\gamma^2)). \tag{69}$$

The StressPP element (as well as its clones Q6 and QM6) is again bending optimal along both x and y_ω (median) directions. The symbolic verification is far more involved than for the rectangular element because it requires the use of free-free flexibility methods [95], and is omitted.

A.2 Trapezoidal Panel

The geometry of the trapezoidal panel shown in Figure 18 is defined by the dimensions a, $b = a/\gamma$ and the two angles ω_1 and ω_2, both positive counterclockwise. Define

$$s_1 = \tan\omega_1, \quad s_2 = \tan\omega_2, \quad s = \tfrac{1}{2}(s_1 + s_2), \quad d = \tfrac{1}{2}(s_1 - s_2), \quad \phi = bd/a = d/\gamma. \tag{70}$$

The template is again given by the matrix form (34). Matrices $\mathbf{H}_c$ and $\mathbf{W}$ are as in (63), except that s has the new definition (70). The higher order projector matrix is

$$\mathbf{H}_h = \tfrac{1}{2}\begin{bmatrix} 1-\phi & 0 & -1+\phi & 0 & 1+\phi & 0 & -1-\phi & 0 \\ 0 & 1-\phi & 0 & -1+\phi & 0 & 1+\phi & 0 & -1-\phi \end{bmatrix}, \tag{71}$$

whereas $\mathbf{R}$ depends on the formulation, as detailed next.

Stress element. Element StressTP is generated by the 5-parameter stress assumption (65), with one change: the (1,4) entry y/b is replaced by $(y - y_C)/b$. If $y_C = -b^2(s_2 - s_1)/(12a) = -\frac{1}{6}ad/\gamma^2$ the bending stresses are energy orthogonal to constant stress fields. The stiffness matrix derived with the HR principle is matched by

$$R_{11} = \frac{1}{C_{11}(3 - d^2/\gamma^2)}, \quad R_{12} = 0, \quad R_{22} = \frac{1}{3C^{\omega}_{22}(1 + d^2/\gamma^2)(1+s^2)^2}, \tag{72}$$

in which C^{ω}_{22} is the compliance along the median y_ω (cf. Figure 18), given by (64).

QM6 element. The incompatible-mode element QM6 of [64] is no longer a clone of the stress element unless $d = 0$. Its stiffness is matched by

$$R_{11} = \frac{1}{C_{11}(3 - d^2/\gamma^2)}, \quad R_{12} = 0, \quad R_{22} = \frac{1}{C^{\omega}_{22}(3 - d^2/\gamma^2)(1+s^2)^2}. \tag{73}$$

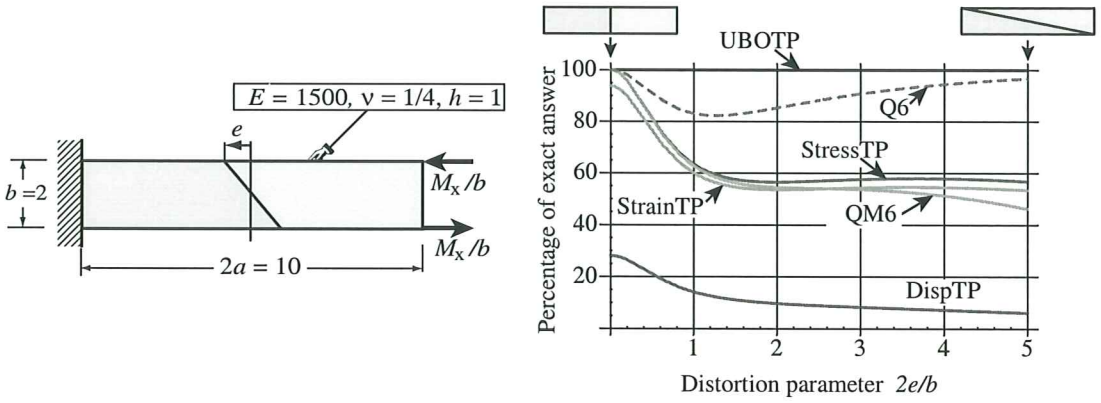

Figure 19. A well known distortion benchmark test. Dashed lines mark elements that fail the patch test (only Q6 in this plot). For additional results on other elements such as Pian-Sumihara and Enhanced Assumed Strain, see [67].

The only change is in R_{22}. The original incompatible-mode element Q6 of [63] fails the patch test if $d \neq 0$ and consequently cannot be matched by the template (31).

Strain element. Element StrainTP is generated by the 5-parameter strain assumption (67), with one change: the (1,4) entry y/b is replaced by $(y-y_C)/b$. Energy orthogonality is again obtained if $y_C = -b^2(s_2-s_1)/(12a) = -\frac{1}{6}ad/\gamma^2$. A strain-fitting variational formulation [94] yields a stiffness matched by

$$R_{11} = \frac{E_{11}}{3-d^2/\gamma^2}, \quad R_{12} = 0, \quad R_{22} = \frac{E^{\omega}_{22}}{3(1+d^2/\gamma^2)(1+s^2)^2}, \tag{74}$$

in which E^{ω}_{22} is the direct elasticity along the median y_ω direction, as given by (64).

Displacement element. The conforming isoparametric displacement element DispTP with 2×2 Gauss integration is matched by

$$\begin{aligned} R_{11} &= \frac{E_{11}+4E_{13}s+s^2(2E_{12}+4E_{33}+4E_{23}s+E_{22}s^2)+(E_{33}+2E_{23}s+E_{22}s^2)\gamma^2}{3-d^2/\gamma^2}, \\ R_{12} &= \frac{E_{13}+s(E_{12}+2E_{33}+3E_{23}s+E_{22}s^2)+(E_{23}+E_{22}s)\gamma^2}{\gamma(3-d^2/\gamma^2)}, \quad R_{22} = \frac{E_{33}+2E_{23}s+E_{22}(s^2+\gamma^2)}{\gamma^2(3-d^2/\gamma^2)} \end{aligned} \tag{75}$$

A.3 A Unidirectional-Bending-Optimal Trapezoidal Panel

Element StressTP is x-bending optimal (XBO) as an individual element, but far from it as a repeating macroelement. Consider the configuration of Figure 18(b): two mirror-image trapezoidal elements are put toghether to form a parallelogram macroelement. The macroelement shape is that of a swept panel, and is obviously repeatable along x.

If $a >> b$ and $s_1 \neq s_2$ the StressTP-fabricated macroelement rapidly becomes overstiff and overflexible in x- and y-bending, respectively. For example if $a/b = \gamma = 8$, $s_1 = 0$, $s_2 = 1/2$ and isotropic material with $\nu = 1/4$ the bending ratios are $r_x = 11.97$ and $r_y = 0.1414$. For the anisotropic elasticity matrix (61), $r_x = 6.93$ and $r_y = 0.0792$. If an elongated macroelement is supposed to model unidirectional x-bending correctly, the overstiffness caused by $s_1 \neq s_2$ is called *distortion locking*. This phenomenon has been widely studied since the MacNeal-Harder test suite gained popularity [96].

It is possible to construct a trapezoidal panel that is exact in unidirectional x bending when configured to form a repeatable macroelement as in Figure 18(b), for any aspect ratio γ as well as arbitrary side slopes s_1 and s_2. This template instance will be called UBOTP. A compact expression is obtained by taking the **R** matrix of StressTP,

generated by (72) and modifying the (2,1) entry of **W**:

$$\mathbf{W} = \begin{bmatrix} 1/a & 0 \\ -\dfrac{\left(C_{11}(3\gamma^2 - ds) + C_{13}\right)(s-d) - C_{12}d}{C_{11}(3\gamma^2 - d^2)b} & 1/b \end{bmatrix} \tag{76}$$

It would be equally possible to keep **W** of (63) and adjust the entries of **R**. However, the correction (76) points the way as to how to extend this result to arbitrary quadrilaterals [93].

It is not difficult to show that $\mathbf{W}^T\mathbf{R}\mathbf{W}$ for UBOTP is positive definite as long as the trapezoid is convex. Consequently the element stiffness is definite and has the proper rank.

Figure 19 presents results for a widely used mesh distortion test, which involves one macroelement of the type discussed. Results for six element types: UBOTP, StressTP, StrainTP, DispTP, Q6 and QM6 are shown. The percentage of the correct answer is of course $100/r_x$. Of these six models only Q6 fails the patch test, but otherwise works better than all others but UBOTP. StressTP, StrainTP and QM6 give similar results, as can be expected, whereas DispTP is way overstiff even for zero distortion. UBOTP gives the correct result for all distortion parameters from 0 through 5, since $r_x \equiv 1$. If the aspect ratio of the cantilever is changed to, say $2a/b = 10$, the differences between elements become more dramatic.

At first sight the existence of UBOTP contradicts a theorem by MacNeal [97], which says that four noded quadrilaterals cannot both pass the patch test and be insensitive to distortion. The escape hatch is that y-bending optimality (along the skew angular direction ω_1 of the macroelement) is not attempted. If one tries imposing $r_x = r_y = 1$, the solutions for $\{R_{11}, R_{12}, R_{22}\}$ become complex if $\gamma >> 1$ as soon as d deviates slightly from 0.